1/3.N88:25/4903/v.3

NUREG/CR-4903
Vol. 3

ORIGINAL

COMPLETED
17-7

Selection of Earthquake Resistant Design Criteria for Nuclear Power Plants - Methodology and Technical Cases

Dislocation Models of Near-Source Earthquake Ground Motion: A Review

Prepared by J. E. Luco

Structural and Earthquake Engineering Consultants, Inc.

Prepared for
U.S. Nuclear Regulatory Commission

19

NOTICE

This report was prepared as an account of work sponsored by an agency of the United States Government. Neither the United States Government nor any agency thereof, or any of their employees, makes any warranty, expressed or implied, or assumes any legal liability of responsibility for any third party's use, or the results of such use, of any information, apparatus, product or process disclosed in this report, or represents that its use by such third party would not infringe privately owned rights.

NOTICE

Availability of Reference Materials Cited in NRC Publications

Most documents cited in NRC publications will be available from one of the following sources:

1. The NRC Public Document Room, 1717 H Street, N.W.
   Washington, DC 20555
2. The Superintendent of Documents, U.S. Government Printing Office, Post Office Box 37082,
   Washington, DC 20013-7082
3. The National Technical Information Service, Springfield, VA 22161

Although the listing that follows represents the majority of documents cited in NRC publications, it is not intended to be exhaustive.

Referenced documents available for inspection and copying for a fee from the NRC Public Document Room include NRC correspondence and internal NRC memoranda; NRC Office of Inspection and Enforcement bulletins, circulars, information notices, inspection and investigation notices; Licensee Event Reports; vendor reports and correspondence; Commission papers; and applicant and licensee documents and correspondence.

The following documents in the NUREG series are available for purchase from the GPO Sales Program: formal NRC staff and contractor reports, NRC-sponsored conference proceedings, and NRC booklets and brochures. Also available are Regulatory Guides, NRC regulations in the *Code of Federal Regulations*, and *Nuclear Regulatory Commission Issuances*.

Documents available from the National Technical Information Service include NUREG-series reports and technical reports prepared by other federal agencies and reports prepared by the Atomic Energy Commission, forerunner agency to the Nuclear Regulatory Commission.

Documents available from public and special technical libraries include all open literature items, such as books, journal and periodical articles, and transactions. *Federal Register* notices, federal and state legislation, and congressional reports can usually be obtained from these libraries.

Documents such as theses, dissertations, foreign reports and translations, and non-NRC conference proceedings are available for purchase from the organization sponsoring the publication cited.

Single copies of NRC draft reports are available free, to the extent of supply, upon written request to the Division of Information Support Services, Distribution Section, U.S. Nuclear Regulatory Commission, Washington, DC 20555.

Copies of industry codes and standards used in a substantive manner in the NRC regulatory process are maintained at the NRC Library, 7920 Norfolk Avenue, Bethesda, Maryland, and are available there for reference use by the public. Codes and standards are usually copyrighted and may be purchased from the originating organization or, if they are American National Standards, from the American National Standards Institute, 1430 Broadway, New York, NY 10018.

NUREG/CR-4903
Vol. 3
RA

Selection of Earthquake Resistant Design Criteria for Nuclear Power Plants - Methodology and Technical Cases

Dislocation Models of Near-Source Earthquake Ground Motion: A Review

Manuscript Completed: September 1986
Date Published: May 1987

Prepared by
J. E. Luco*

Structural and Earthquake Engineering Consultants, Inc.
Arcadia, CA 91006

*University of California, San Diego

Prepared for
Division of Engineering
Office of Nuclear Regulatory Research
U.S. Nuclear Regulatory Commission
Washington, DC 20555
NRC FIN B8298
Under Contract No. NRC-04-83-022

COPY AVAILABLE

BLANK PAGE

ABSTRACT

The solutions available for a number of dynamic dislocation fault models are examined in an attempt at establishing some of the expected characteristics of earthquake ground motion in the near-source region. In particular, solutions for two-dimensional anti-plane shear and plane-strain models as well as for three-dimensional fault models in full space, uniform half-space and layered half-space media are reviewed.

BEST COPY AVAILABLE

BLANK PAGE

TABLE OF CONTENTS

		Page
1.	INTRODUCTION	1
	1.1 Objectives and Scope of the Study	1
	1.1 References	3
2.	TWO-DIMENSIONAL ANTI-PLANE SHEAR MODELS	4
	2.0 Introduction	4
	2.1 Steady-State Dislocation Models in a Uniform Full-Plane	7
	2.2 Starting Dislocation Models in a Uniform Full-Plane	13
	2.3 A Decomposition of the Near-Source Ground Motion	17
	2.4 Finite Fault Dislocation Models in a Uniform Full-Plane	25
	2.5 Dislocation Models with Nonuniform Slip and Variable Rupture Velocity	29
	2.6 Steady-State Dislocation Model in a Layered Full-Plane	32
	2.7 Anti-Plane Dislocation Models in a Uniform or Layered Half-Plane	37
	2.8 Conclusions	38
	2.9 References	41
3.	TWO-DIMENSIONAL PLANE-STRAIN MODELS	43
	3.0 Introduction	43
	3.1 Steady-State Dislocation Models in a Uniform Full-Plane	46
	3.2 Starting Dislocation Model in a Uniform Full-Plane	53
	3.3 Decomposition of the Near-Source Ground Motion	57
	3.4 Plane-Strain Dislocation Models in a Half-Plane	61
	3.5 Comparison of Two- and Three-Dimensional Models	80
	3.6 Conclusions	81
	3.7 References	83

BEST COPY AVAILABLE

4. THREE-DIMENSIONAL MODELS 85

4.0 Introduction 85

4.1 Steady-State Dislocation Model in a Full-Space 87

4.2 Three-Dimensional Dislocation Models in a Uniform Full-Space 96

4.3 Three-Dimensional Steady-State Dislocation Models in a Uniform Half-Space .. 104

4.4 Finite Three-Dimensional Dislocation Models in a Uniform Half-Space 111

4.5 Three-Dimensional Dislocation Models in a Layered Half-Space 112

4.6 Conclusions 117

4.7 References 119

5. SIMULATION OF NEAR-SOURCE RECORDS 124

5.0 Introduction 124

5.1 Parkfield 1966 Earthquake 127

5.2 Imperial Valley 1979 Earthquake 150

5.3 Conclusions 162

5.4 References 163

6. CLOSURE 169

BEST COPY AVAILABLE

FOREWORD

This report presents partial results of a four-task study on the development of methodology and technical bases for the selection of earthquake resistant design criteria for nuclear power plants. This research program was sponsored by the U. S. Nuclear Regulatory Commission (USNRC) under Contract NRC-04-83-022.

Volume 1 of this report presents the results of Task III which include:

IA) Attenuation of Modified Mercalli Intensity for small epicentral distance in California,

IB) Frequency dependent attenuation of strong earthquake ground motion,

IC) Preliminary empirical model for scaling Fourier amplitude spectra of strong ground acceleration in terms of earthquake magnitude, source to station distance, site intensity and recording site conditions,

ID) Preliminary empirical models for scaling pseudo relative velocity spectra of strong earthquake acceleration in terms of magnitude, distance, site intensity and recording site conditions.

Volume 2 of this report presents the results of Tasks I and IV which include:

IIA) A review of quantitative procedures to obtain earthquake occurrence from rates of geological processes: application to the eastern United States,

IIB) Uniform risk spectra of strong earthquake ground motion: NEQRISK.

Finally, Volume 3 of this report presents the results of Task II which correspond to a review of a number of theoretical fault models to establish some of the expected characteristics of earthquake ground motion in the near-source region.

Overall technical guidance and review was provided by A. Murphy, technical representative of the USNRC for this research project.

BEST COPY AVAILABLE

1. INTRODUCTION

1.0 Objectives and Scope of the Study.

Although a number of near-source earthquake ground motion records have been obtained in the last few years, the recorded data are not sufficient to derive a purely empirical description of the ground motion in the near-source region. The design and verification needs for facilities located in the near-source region of expected large earthquakes require that the empirical data be complemented by theoretical models so that extrapolation to other conditions (larger magnitudes, different source mechanism, different geological environment) can be conducted on a rational basis. The organization of the empirical data in the form of various correlations can also benefit from a better understanding of the characteristics of the near-source earthquake ground motion.

Since the pioneering work of Aki (1968) and Haskell (1969), kinematic dislocation fault models with various degrees of complexity have been used to synthesize near-source earthquake ground motion (for reviews refer to Aki, 1982; Luco and Anderson, 1985). Analytical and numerical solutions for some dynamic crack models which attempt to describe the stress release process are also available (for reviews refer to Rice, 1980; Swanger *et al.*, 1980). These solutions contain valuable qualitative information which has not been fully exploited.

In this report, we examine the solutions available for a number of theoretical fault models in an attempt at establishing some of the expected characteristics of the near-source earthquake ground motion. In particular, solutions for two-dimensional anti-plane shear and plane-strain models as well as three-dimensional models in full space, uniform half-space and layered half-space media are reviewed. The emphasis of the study is on the characterization of the near-source earthquake ground motion in terms of the various phases that could be found, on the relative importance of these phases, on the geometrical pattern of ground motion in the near-source region and on the types of attenuation of ground motion with distance to the fault. The emphasis of the review is on intermediate and low frequencies for which the effects of source and

BEST COPY AVAILABLE

path heterogeneities can be ignored. Some consideration is given to models for the generation of high frequencies by starting and stopping phases. No attempt is made at establishing absolute values for the amplitude of ground motion in the near-source region.

The various fault models considered in the literature can be classified according to the dimensionality of the model (two-and three-dimensional models), the extent of the model (full space, half space and layer over rigid rock models), the characterization of the assumed geologic structure (uniform and layered earth models), the type of prescribed condition on the fault area (kinematic dislocation and dynamic crack models), and according to the method of solution (Cagniard-de Hoop technique, synthesis of Green's functions in the time or frequency domains, discrete wave number representation, discrete finite element or finite different solutions). The solutions reviewed in this study correspond to kinematic dislocation models. Two-dimensional anti-plane shear and plane-strain models are reviewed in Chapters 2 and 3, respectively. Three-dimensional fault models are discussed in Chapter 4 and simulations of the Parkfield and Imperial Valley earthquakes are reviewed in Chapter 5. Conclusions are presented at the end of each chapter and some closing remarks are presented in Chapter 6.

BEST COPY AVAILABLE

1.1 References.

Aki, K. (1968). Seismic displacements near a fault, *J. Geophys. Res. 73*, 5359-5376.

Aki, K. (1982). Strong motion prediction using mathematical modeling techniques, *Bull. Seism. Soc. Am.* 72, S29-S41.

Haskell, N. A. (1969). Elastic displacements in the near-field of a propagating fault, *Bull. Seism. Soc. Am. 59*, 865-908.

Luco, J. E. and J. G. Anderson (1985). Near source earthquake ground motion from kinematic fault models in *Strong Ground Motion Simulation and Earthquake Engineering Applications: A Technological Assessment*, R. E. Scholl and J. L. King (Eds.), Publication No. 85-02, Earthquake Engineering Research Institute, Berkeley, California, 18.1 - 18.20.

Rice, J. R. (1980). The mechanisms of earthquake rupture, in *Physics of the Earth Interior* (Proc. of the International School of Physics Enrico Fermi, Course 78, 1979) ed. by A. M. Dziewonski and E. Boshi, Italian Physical Society (printed by North Holland Publishing Co.) 555-649.

Swanger, H. J., J. R. Murphy, J. J. Bennet and R. Guzman (1980). State-of-the-art study concerning near-field earthquake ground motion, NUREG/CR-1340, SSS-R-80-4217, August.

BEST COPY AVAILABLE

2. TWO-DIMENSIONAL ANTI-PLANE SHEAR MODELS

2.0 Introduction.

The simplest dislocation model corresponds to a two-dimensional anti-plane shear dislocation model in an unbounded plane in which a uniform dislocation starting from $x = -\infty$ at $t = -\infty$ propagates along the x-axis with constant rupture velocity (Fig. 2.0.1.a). The solution for this steady-state dislocation model has been obtained by Eshelby (1949), Frank (1949) and Liebfried and Dietze (1949) by elementary means. The case of an anti-plane shear dislocation which starts from $x = 0$ at $t = 0$ and then propagates with constant rupture velocity (Fig. 2.0.1.b) has been solved by Kiusalaas and Mura (1964), Mitra (1966) and Boore and Zoback (1974). The solution of Kiusalaas and Mura (1964) was obtained by specializing a representation due to Mura (1963) for the particle velocity of the medium in terms of a double integral of the slip and appropriate Green's functions over time and over the dislocation line (rupture front). The solution of Mitra (1966) and Boore and Zoback (1974) was obtained by use of the Cagniard-de Hoop technique. Integral representations for nonuniformly moving anti-plane shear dislocations have been presented by Eshelby (1953), Kiusalaas and Mura (1964), Geller (1974) and Markenscoff (1980). The relationship between the response for the steady-state and the suddenly starting dislocation models has been discussed by Aki and Richards (1980) and, in more detail, by Luco and Sotiropoulos (1985) and Lund (1985). The case of a steady-state antiplane shear dislocation in a medium consisting of two bonded half-planes with different elastic properties (Fig. 2.0.1.c) has been discussed by Luco and Sotiropoulos (1985).

Two-dimensional antiplane dislocation models in an elastic half-plane have been considered by several authors. Mitra (1966) obtained a solution for a strike-slip fault in a uniform elastic half-plane by considering two mirror-image faults in an unbounded plane (Fig. 2.0.1.d). Mal and Carriveau (1973) used an integral representation of the response in the frequency domain to obtain a solution for the same type of fault. In this solution, an elliptic slip function was used in an attempt at a better representation of the rupture mechanics. The same procedure was

BEST COPY AVAILABLE

used by Carriveau (1973) for the case of a two-dimensional strike-slip fault on a layered half-plane (Fig. 2.0.1.e). To complete the list of two-dimensional anti-plane solutions, we should mention the studies of Dravinski and Trifunac (1979, 1980) for a vertical strike-slip fault on a layered elastic slab supported on a rigid half-plane (Fig. 2.0.1.f).

From the point of view of application to faults on the earth, the two-dimensional anti-plane shear models mentioned above can be viewed, on the one hand, as simplified analogs from which qualitative information can be obtained. In some cases, however, these models are applicable to some realistic situations. Boore and Zoback (1974) have pointed out that the models shown in Figures 2.0.1a,b could represent in plan view the lateral propagation of a vertical dip-slip fault while the models shown in Figures 2.0.1d,e could represent in vertical section the propagation along the dip of a vertical or inclined strike-slip fault.

BEST COPY AVAILABLE

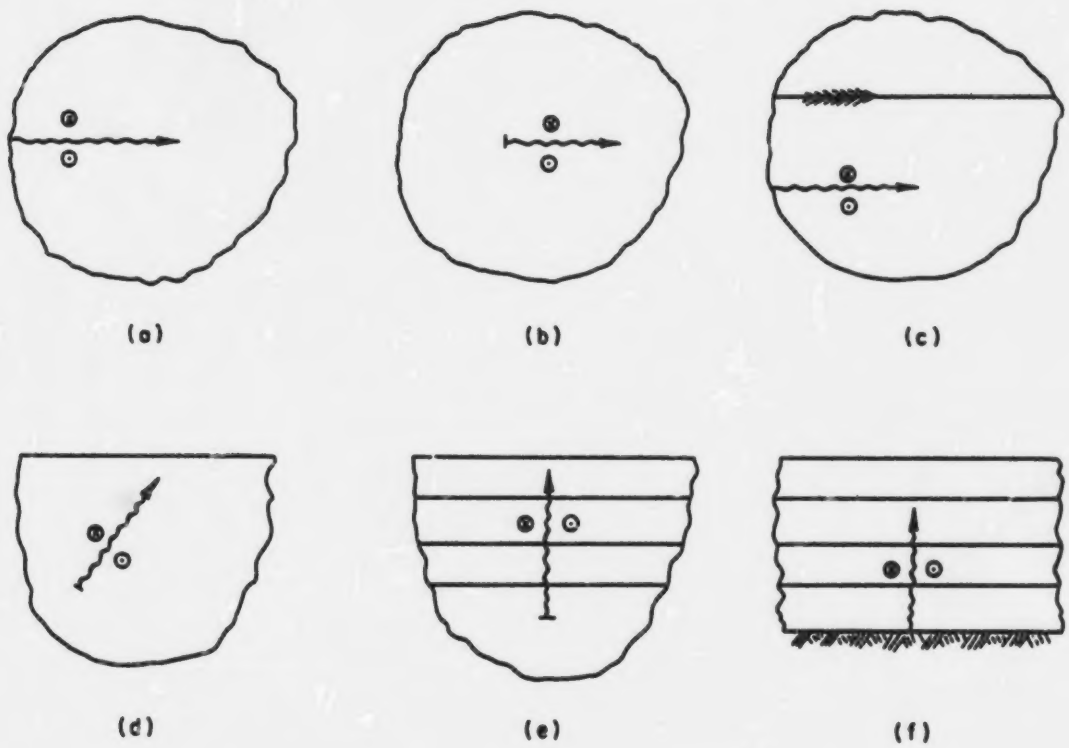

Fig. 2.0.1 **Two-dimensional antiplane shear dislocation models.**

BEST COPY AVAILABLE

2.1 Steady-State Dislocation Models in a Uniform Full-Plane.

To start consider a two-dimensional steady-state, anti-plane shear dislocation model in a uniform, elastic, isotropic, unbounded medium characterized by the shear wave velocity β. The rupture front corresponds to an infinite line parallel to the z-axis moving in the x- direction with uniform rupture velocity v (Fig. 2.1.1.a). In the steady-state dislocation model it is assumed that the rupture starts from $x = -\infty$ at time $t = -\infty$.

Assume first that the displacement discontinuity across the fault plane is given by

$$w(x,0^+,t) - w(x,0^-,t) = \Delta\bar{w}\ H(t - \frac{x}{v}) \tag{2.1.1}$$

where $w(x,y,t)$ is the z-component of the displacement field, $\Delta\bar{w}$ is the slip amplitude and $H(t)$ is the Heaviside step function. The particle velocity in the medium $\dot{w}(x,y,t)$ for the sub-sonic case ($v < \beta$), as resulting from the work of Eshelby (1949), Frank (1949) and Liebfried and Dietze (1949), is given in this case by

$$\dot{w}(x,y,t) = \frac{\partial w}{\partial t} = \frac{\Delta\bar{w}}{2\pi}\ \frac{vy\ \gamma}{(x - vt)^2 + y^2\gamma^2} \tag{2.1.2}$$

where $\gamma = [1 - (v/\beta)^2]^{1/2}$. The corresponding displacement and acceleration pulses are given by

$$w(x,y,t) = \frac{\Delta\bar{w}}{2\pi}\tan^{-1}[\gamma y/(x - vt)] \tag{2.1.3}$$

and

$$\ddot{w}(x,y,t) = \frac{\Delta\bar{w}}{2\pi}\ \frac{2v^2\gamma y(x - vt)}{[(x - vt)^2 + \gamma^2 y^2]^2} \tag{2.1.4}$$

respectively. In Eq. (2.1.3) $\tan^{-1}$ assumes values in the range $[0,\pi]$ for $y > 0$. The shapes of the displacement, velocity and acceleration pulses are shown in Fig. 2.1.2. The displacement pulse shows a permanent offset of $\Delta\bar{w}/2$. The particle velocity pulse is symmetric with respect

BEST COPY AVAILABLE

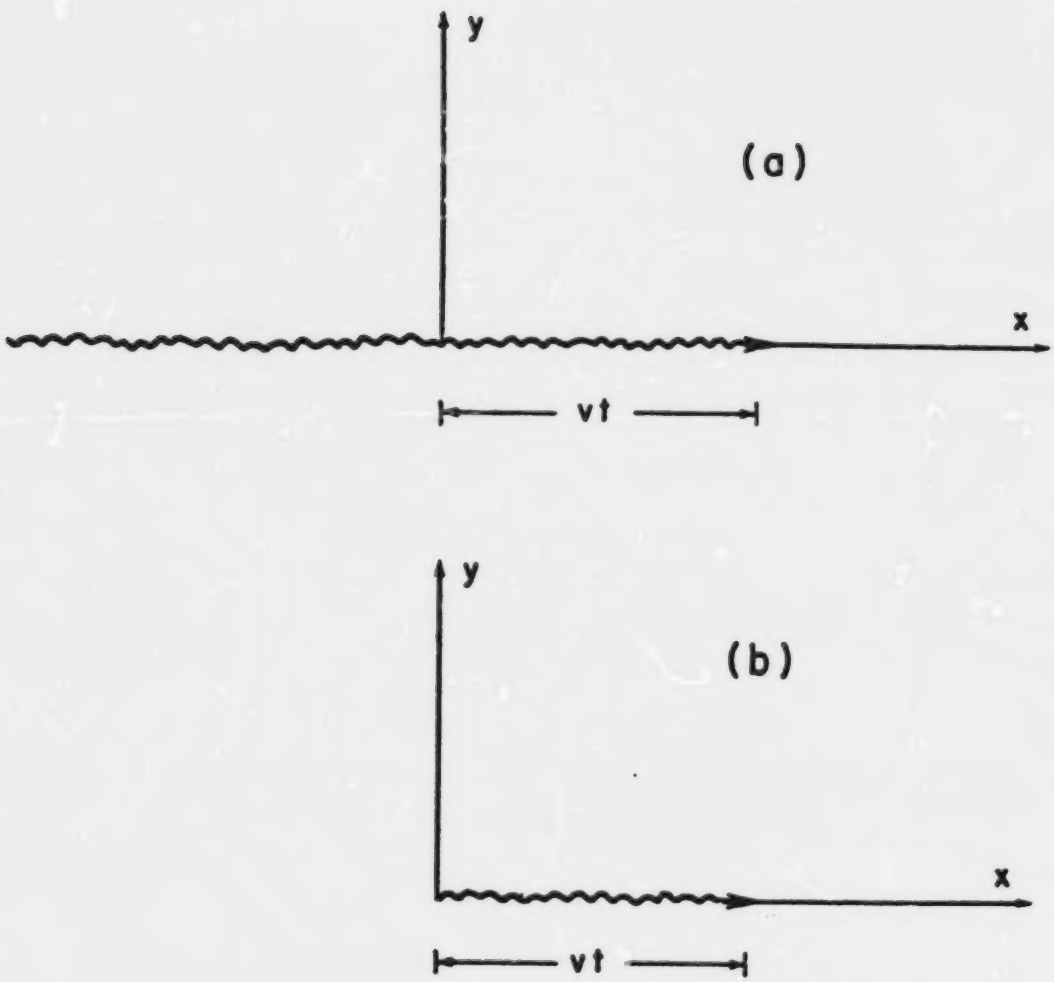

Fig. 2.1.1 Geometry of two-dimensional kinematic fault models, (a) Steady-state model, (b) Semi-finite model.

BEST COPY AVAILABLE

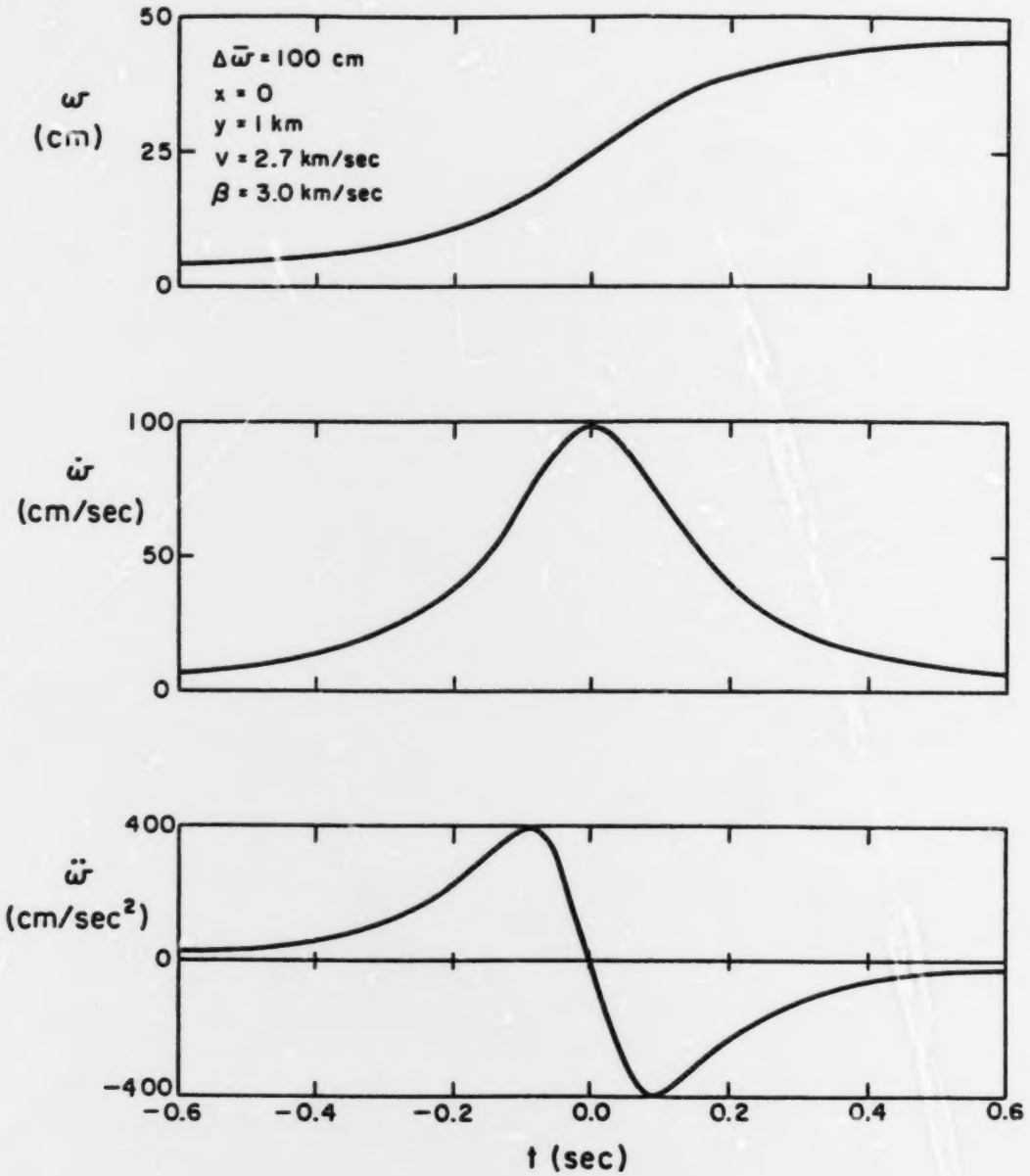

Fig. 2.1.2 Displacement, velocity and acceleration pulses for a steady-state step dislocation ($\Delta\bar{w}$ = 100 cm, x = 0, y = 1 km, v = 2.7 km/sec, β = 3.0 km/sec, r = 0).

BEST COPY AVAILABLE

to $t = x/v$. The peak value occurs at $t = x/v$ and is $(\Delta\bar{w}/2\pi)\,[v/y\gamma]$. The particle acceleration pulse is antisymmetric with respect to $t = x/v$ and takes peak values at $vt = x \pm (y\gamma/\sqrt{3})$. The peak acceleration is given by $(\Delta\bar{w}/2\pi)(9/8\sqrt{3})\,(v/\gamma\, y)^2$. Thus, the peak particle velocity decays with distance to the fault as y^{-1} while peak acceleration decays as y^{-2}. The peak acceleration and peak velocity are infinite on the plane of the fault and show a marked dependence on rupture velocity. In particular, as $v \to \beta$, $\gamma \to 0$ and the peak velocity and peak acceleration tend to infinity.

The Fourier transform of the particle velocity given by Eq. (2.1.2) is

$$\dot{w}\,(x,y,i\omega) = \frac{\Delta\bar{w}}{2}\, e^{-i(\omega x/v)}\, e^{-|\gamma\omega y/v|} \tag{2.1.5}$$

which shows a phase shift with position x along the fault and an exponential decay with frequency and distance to the fault (Aki and Richards, 1980, p. 835). The steady-state solution for $v < \beta$ corresponds then to a inhomogeneous plane wave trapped near the fault plane.

In the supersonic case ($v > \beta$) the character of the solution is completely different. In this case the particle velocity field for $y > 0$ is given by

$$\dot{w}\,(x,y,t) = \frac{\Delta\bar{w}}{2}\,\delta\,(t - x/v - \gamma^{*}\, y/v) \tag{2.1.6}$$

where $\delta(t)$ is the Dirac delta function and $\gamma^{*} = \sqrt{(v/\beta)^2 - 1}$. In the supersonic case there is no attenuation with distance to the fault and the particle velocity at any point in the medium has the same amplitude and form as the slip velocity (except for a factor of 1/2).

To illustrate the effects of the slip time-dependence on the particle velocity field it is convenient to consider a dislocation with time-dependence in the form of a finite ramp with rise time τ, i.e.

$$w\,(x,0^{+},t) - w\,(x,0^{-},t) = v_o\,(t - \frac{x}{v})[H(t - \frac{x}{v}) - H(t - \tau - \frac{x}{v})] \tag{2.1.7}$$

in which $v_o = \Delta\bar{w}/\tau$ is the slip velocity. The resulting particle velocity, in the subsonic case ($v < \beta$), is given by

BEST COPY AVAILABLE

$$\dot{w}(x,y,t) = \frac{v_o}{2\pi}\left(\tan^{-1}\frac{y\gamma}{x - vt} - \tan^{-1}\frac{y\gamma}{x - v(t-\tau)}\right) \qquad (2.1.8)$$

where $\tan^{-1}$ assumes values in the range $[0,\pi]$ for $y > 0$. The peak velocity, in this case, occurs at $t = x/v + \tau/2$ and the peak value is $(v_o/2)[1 - (2/\pi)\tan^{-1}(2y\gamma/v\tau)] = (v_o/\pi)\tan^{-1}(v\tau/2y\gamma)$. In this case, the particle velocity is finite throughout the medium. It is important to notice that the attenuation of peak velocity with distance to the fault is somewhat different from that for a step dislocation. For $y << (v\tau/\gamma)$, the peak velocity is approximately given by $(v_o/2)[1 - (4y\gamma/\pi v\tau)]$ indicating a linear decay with distance. For $y >> (v\tau/\gamma)$ the peak velocity can be approximated by $(v_o/\pi)(v\tau/2y\gamma) = (\Delta\bar{w}/2\pi)(v/y\gamma)$ which is the same expression obtained for a step dislocation. Thus the effects of rise time on the peak velocity can be felt only up to a distance of the order of $(v\tau/\gamma)$. The variation of $\dot{w}_{max}$ versus distance to the fault is shown in Fig. 2.1.3.

BEST COPY AVAILABLE

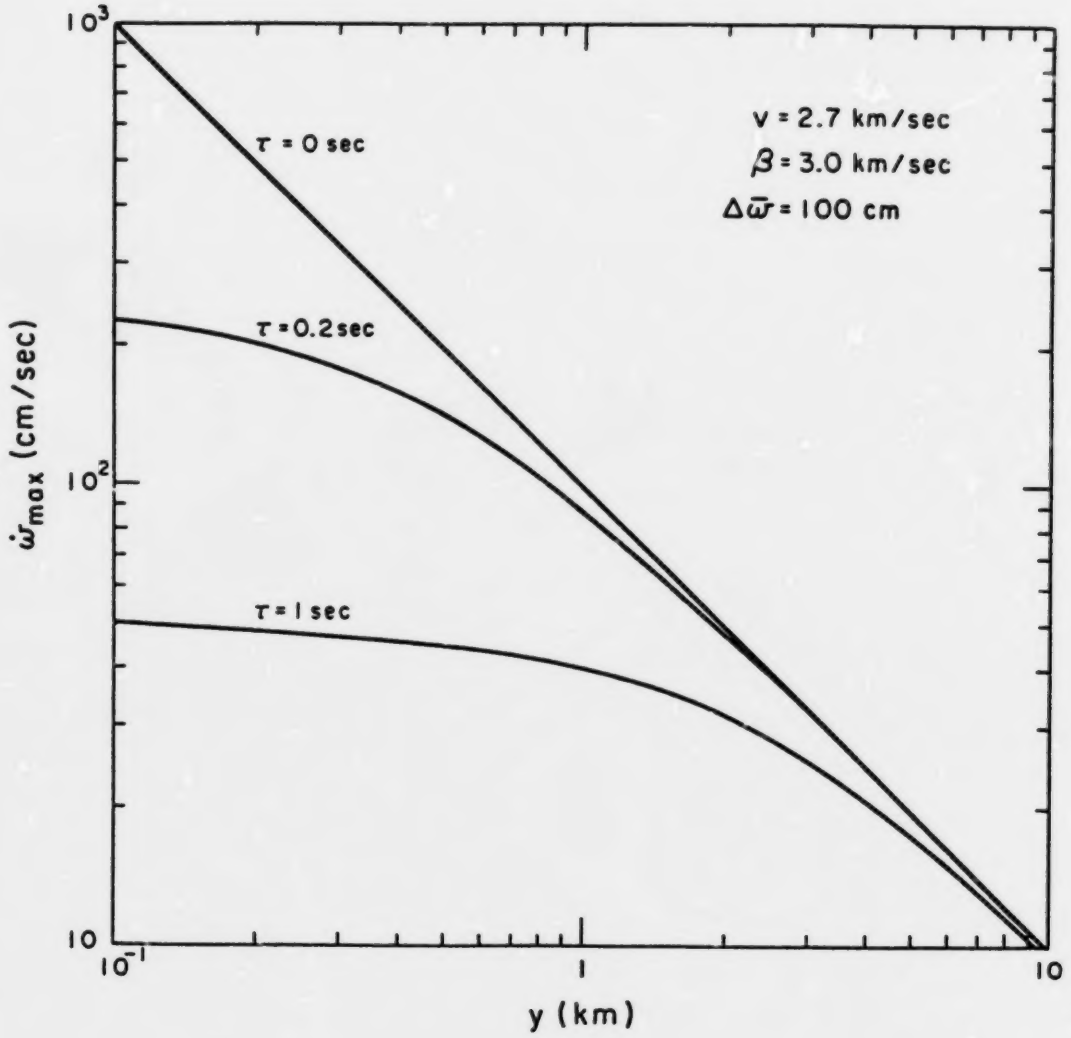

Fig. 2.1.3 Attenuation of peak velocity $\dot{w}_{max}$ with distance to the fault ($\Delta\bar{w}$ = 100 cm, v = 2.7 km/sec, β = 3.0 km/sec).

BEST COPY AVAILABLE

2.2 Starting Dislocation Models in a Uniform Full-Plane.

We consider next an anti-plane shear dislocation model in which the rupture starts from $x = 0$ at $t = 0$ and then propagates along the x-axis with constant rupture velocity v (Fig. 2.1.1.b). For a step dislocation the displacement discontinuity condition across the fault plane is

$$w(x,0^+,t) - w(x,0^-,t) = \Delta\bar{w}\ H\left(t - \frac{x}{v}\right) H(x) \tag{2.2.1}$$

and the resulting velocity field, as obtained by Kiusalaas and Mura (1964), Mitra (1966) and Boore and Zoback (1974) for the subsonic case ($v < \beta$), is given by

$$\dot{w}(x,t,t) = \frac{\Delta\bar{w}}{2\pi} \frac{vy\left(\beta t - x\frac{v}{\beta}\right)}{\left((x - vt)^2 + y^2\gamma^2\right)} \cdot \frac{H(\beta t - r)}{\sqrt{\beta^2 t^2 - r^2}} \tag{2.2.2}$$

where $r = \sqrt{x^2 + y^2}$.

Aki and Richards (1980, p. 837) have noted that Eq. (2.2.2) reduces to Eq. (2.1.2) for $t \sim x/v$ and $\theta = \tan^{-1}(y/x)$ small. Thus, the near-field ground motion for the fault which starts from $x = 0$ at $t = 0$ can be represented by the simpler steady-state solution for times in the vicinity of the arrival of the rupture front ($t = x/v$).

The most marked difference between the velocity field given by Eq. (2.2.2) for the starting fault and the velocity given by Eq. (2.1.1) for the steady-state dislocation model occurs in the vicinity of $t = r/\beta$ corresponding to the arrival time of the starting phase. For $t \sim r/\beta$ Eq. (2.2.2) reduces to

$$\dot{w}(x,y,t) \approx \frac{\Delta\bar{w}}{2\pi}\left(\frac{\sin\theta}{\frac{\beta}{v} - \cos\theta}\right)\sqrt{\frac{\beta}{2r}}\ \frac{H\left(t - \frac{r}{\beta}\right)}{\sqrt{t - \frac{r}{\beta}}} \tag{2.2.3}$$

Eq. (2.2.3) indicates that, for slip with a step time-dependence, the particle velocity associated with the starting phase exhibits a singularity at time $t = r/\beta$ of the type $(t - r/\beta)^{-1/2}$. The

BEST COPY AVAILABLE

velocity starting phase also reveals a radiation pattern ($\sin\theta$), a directivity factor $1/|(\beta/v) - \cos\theta|$ and a $r^{-1/2}$ decay with distance. The Fourier transform of the starting phase velocity pulse (for $\omega > 0$) is given by

$$\dot{w}(x,y,i\omega) = \frac{\Delta\bar{w}}{2\pi}\left(\frac{\sin\theta}{\frac{\beta}{v} - \cos\theta}\right)\sqrt{\frac{\pi\beta}{2\omega r}}\, e^{-i\omega r/\beta - i\pi/4} \qquad (2.2.4)$$

which reveals a $\omega^{-1/2}$ decay at high frequencies. The particle acceleration associated with the starting phase is also singular. In the time domain it exhibits a singularity of the type $(t - r/\beta)^{-3/2}$. In the frequency domain, it behaves as $\omega^{1/2}$ for high frequencies.

The velocity field for a slip with time dependence in the form of a finite ramp (rise time τ) for which the discontinuity condition is

$$w(x,0^+,t) - w(x,0^-,t) = v_o\,(t - \frac{x}{v})\left[H(t - \frac{x}{v}) - H(t - \tau - \frac{x}{v})\right] H(x) \quad (2.2.5)$$

is given in the subsonic case ($v < \beta$), by

$$\dot{w}(x,y,t) = \frac{v_o}{2\pi}\left\{\tan^{-1}\left(\frac{v}{\beta}\cdot\frac{y\sqrt{\beta^2t^2 - r^2}}{x(x - vt) + y^2}\right) H(\beta t - r)\right.$$

$$\left. - \tan^{-1}\left(\frac{v}{\beta}\cdot\frac{y\sqrt{\beta^2(t-\tau)^2 - r^2}}{x[x - v(t-\tau)] + y^2}\right) H[\beta(t-\tau) - r]\right\} \quad (2.2.6)$$

in which $v_o = \Delta\bar{w}/\tau$.

Again, as in the case of a step dislocation, Eq. (2.2.6) reduces to Eq. (2.1.8) for $t \sim x/v$ and $\theta = \tan^{-1}(y/x)$ small.

For $t \sim r/\beta$, Eq. (2.2.6) reduces to

$$\dot{w}(x,y,t) \approx \frac{v_o}{2\pi}\left(\frac{\sin\theta}{\frac{\beta}{v} - \sin\theta}\right)\sqrt{\frac{\beta t}{r} - 1}\; H(t - \frac{r}{\beta}) \;, \qquad (2.2.7)$$

which indicates that the velocity pulse associated with the starting phase for a ramp dislocation is non singular and behaves at $(t - r/\beta)^{1/2}$. In the frequency domain, the velocity starting

BEST COPY AVAILABLE

phase behaves as $\omega^{-3/2}$. The acceleration pulse associated with the starting phase is singular with behavior of the type $(t - r/\beta)^{-1/2}$ in the time domain and $\omega^{-1/2}$ in the frequency domain.

The previous discussion refers to a starting unilateral rupture. The case of a bilateral rupture, in which the rupture starts from $x = 0$ at $t = 0$ and then propagates in both the positive and negative x-directions with constant rupture velocity, can be obtained by superposition of the results for the case of unilateral rupture. In particular, for a subsonic ($v < \beta$) bilateral step dislocation

$$w(x,0^+,t) - w(x,0^-,t) = \Delta\bar{w}\ H(t - |x|/v) \tag{2.2.8}$$

the particle velocity in the medium is

$$\dot{w}(x,y,t) = \frac{\Delta\bar{w}}{2\pi}\left[\frac{\beta t - (xv/\beta)}{(x - vt)^2 + (\gamma y)^2} + \frac{\beta t + (xv/\beta)}{(x + vt)^2 + (\gamma y)^2}\right] \cdot \frac{vy\ H(\beta t - r)}{\sqrt{(\beta t)^2 - r^2}} \tag{2.2.9}$$

The starting phase for the bilateral rupture is obtained by setting to $t \sim r/\beta$ in Eq. (2.2.9) resulting in

$$\dot{w}(x,y,t) \simeq \frac{\Delta\bar{w}}{2\pi}\left[\frac{2\sin\theta}{1 - (v/\beta)^2\cos^2\theta}\right](\frac{v}{\beta})\sqrt{\frac{\beta}{2r}}\ \frac{H(t - \frac{r}{\beta})}{\sqrt{t - r/\beta}} \tag{2.2.10}$$

which differs from the starting phase for a unilateral rupture only by the factor $2/[1 + (v/\beta)\cos\theta)]$. Contours of equal amplitudes for the starting phases for unilateral (segmented lines) and bilateral (solid line) ruptures are compared in Fig. 2.2.1 for the case $v/\beta = 0.9$. A bilateral rupture appears to produce a stronger starting phase than the unilateral rupture.

BEST COPY AVAILABLE

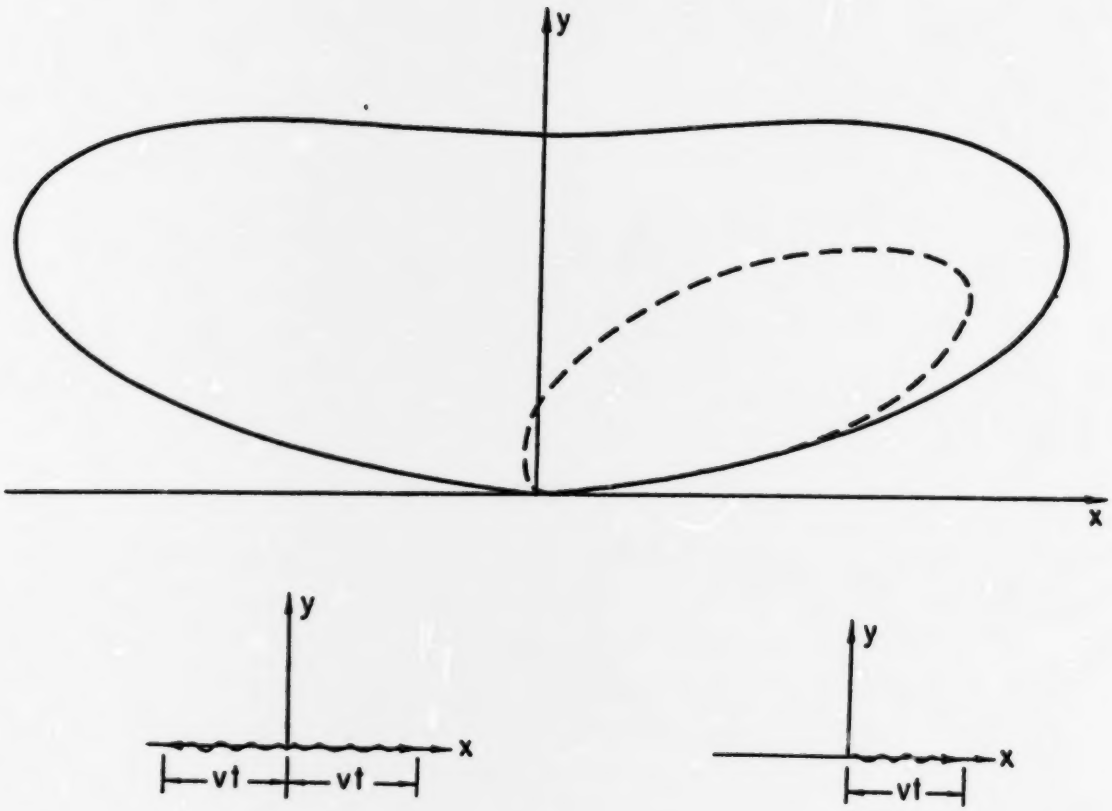

Fig. 2.2.1 Contours of equal amplitude for the starting phases for unilateral (segmented line) and bilateral (solid line) rupture for $v/\beta = 0.9$.

BEST COPY AVAILABLE

2.3 A Decomposition of the Near-Source Ground Motion.

A first glimpse into the character of the near source ground motion can be obtained by comparing the solution obtained for a starting dislocation with that for the steady-state model. The previous discussion suggests that, in the near-field, the total particle velocity for a starting dislocation may involve two important phases: the first phase corresponds to the starting phase, the second phase corresponds to the passage of the rupture front. The latter phase is essentially given by Eq. (2.1.2) for $\tau = 0$ and by Eq. (2.1.8) for $\tau = 0$ indicating that the rupture passage phase (RP phase) can be calculated by use of a simpler steady-state dislocation model. A condition for the existence of a RP pulse is that $x/v > \tau \neq \beta$ which is equivalent to $\theta < \cos^{-1}(v/\beta)$.

The relative importance of the starting and rupture passage phases has been studied by Sotiropoulos (1983) and Luco and Sotiropoulos (1985). Some typical numerical results are presented in Fig. 2.3.1 and 2.3.2. In Fig. 2.3.1 the total particle velocity for a starting fault is compared with the particle velocity for a steady-state dislocation model. The velocity pulses are plotted versus the reduced time $t - \tau/\beta$ for a model characterized by $\beta = 3.0$ km/sec, $v = 2.7$ km/sec and $\Delta\bar{w} = 100$ cm. The comparison in the upper portion of Fig. 2.3.1 is for a step dislocation ($\tau = 0$) while the comparison in the lower portion of Fig. 2.3.1 is for a finite ramp dislocation with a rise time $\tau = 0.2$ sec. The results in Fig. 2.3.1 are for observers at a distance $y = 1$ km from the plane of fault and at distances $x = 5$, 10 and 20 km from the point of initiation of the rupture. All of these observers are within the region $\theta < \cos^{-1}(0.9)$ for $v = 0.9\beta$. The results in Fig. 2.3.1 (upper) show that the velocity response for a starting step dislocation includes a singular starting phase and a very pronounced RP phase. For $y = 1$ km and $x \geq 10$ km, the RP phase is almost identical to the velocity pulse for the steady-state dislocation model (dashed line). The results in Fig. 2.3.1 (lower) show that for a ramp dislocation the starting phase velocity pulse is non singular and that for $y = 1$ km and $x \geq 10$ km the peak velocity is associated with the very pronounced RP pulse.

BEST COPY AVAILABLE

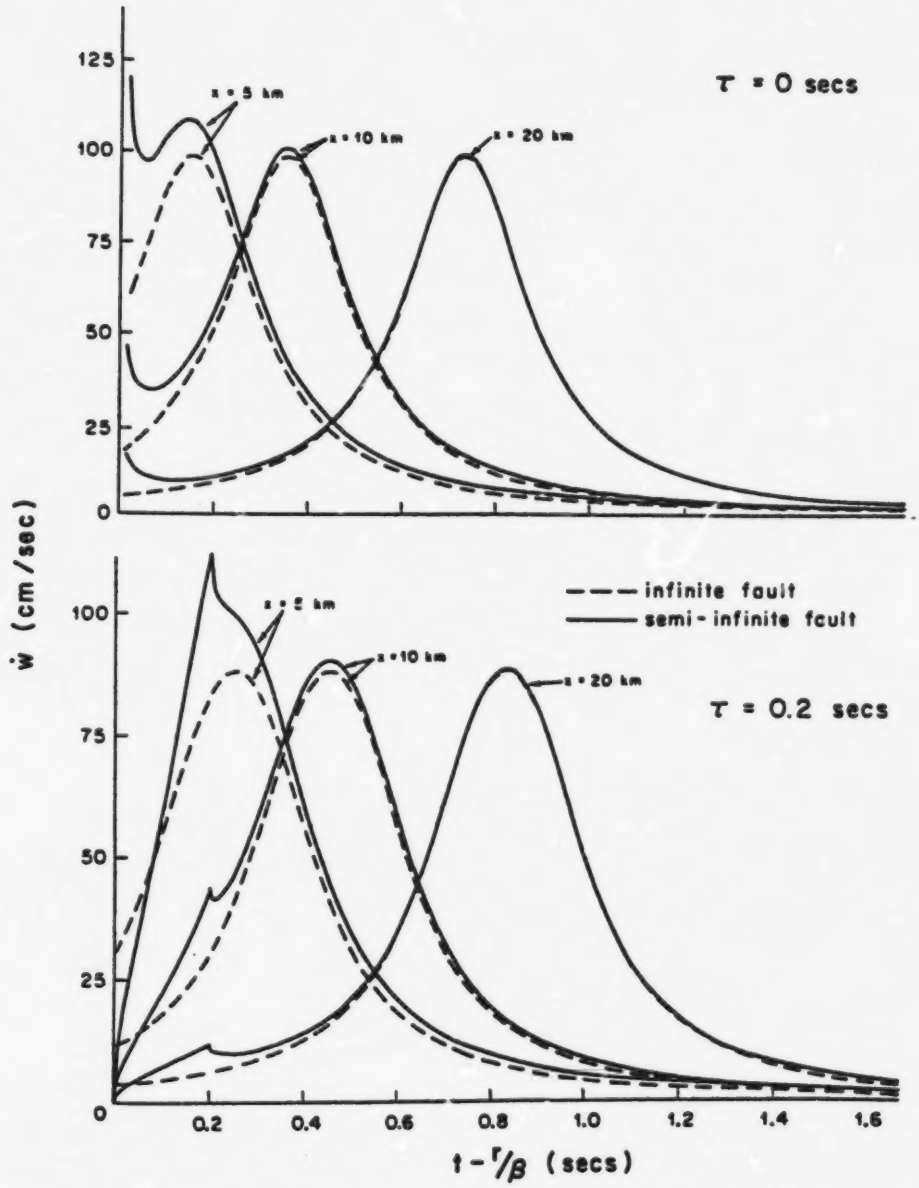

Fig. 2.3.1 Comparison of velocity pulses at y = 1 km and x = 5, 10, 20 km for steady-state (dashed line) and starting (solid line) anti-plane shear dislocation models. The top figure corresponds to a slip with zero rise time, while the bottom corresponds to a slip with a rise time of 0.2 secs (after Luco and Sotiropoulos, 1985).

BEST COPY AVAILABLE

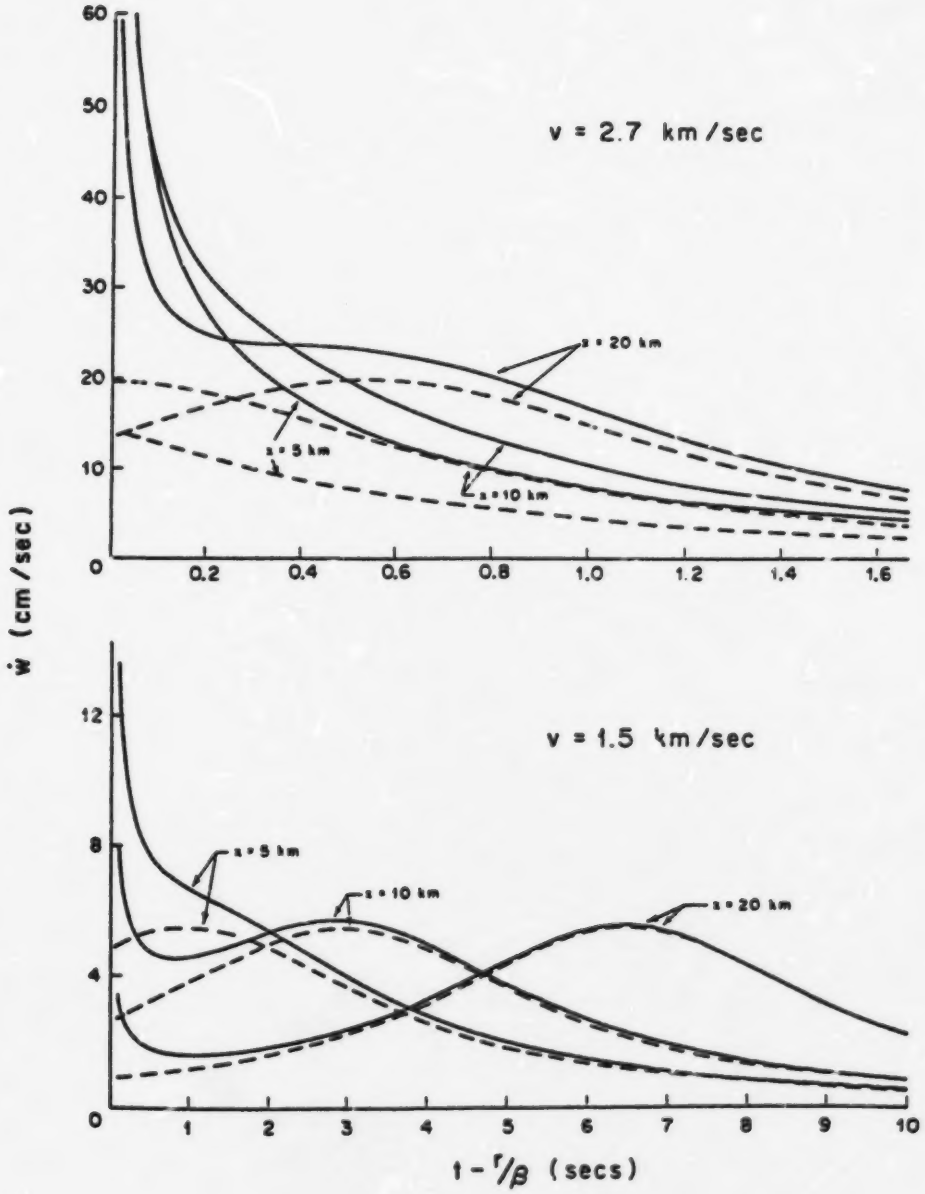

Fig. 2.3.2 Comparison of velocity pulses at y = 5 km and x = 5, 10, 20 km for steady-state (dashed line) and starting (solid line) anti-plane shear dislocation models. The top figure corresponds to a rupture velocity of 2.7 km/sec (β = 3.0 km/sec) while the bottom to a rupture velocity of 1.5 km/sec. In both cases the rise time is zero (Luco and Sotiropoulos, 1985).

BEST COPY AVAILABLE

Comparisons for observers at a distance $y = 5$ km from the plane of the fault and distances $x = 5$, 10, 20 km from the initiation of the rupture are shown in Fig. 2.3.2 (upper) for $\tau = 0$ and $v = 0.9\beta (v = 2.7$ km/sec). In this case, the observers are outside or close to the boundary of the region $\theta < \cos^{-1}(0.9)$ and the starting phase dominates the velocity pulse even at $x = 20$ km. The results in Fig. 2.3.2 (lower) for a lower rupture velocity of $v = 0.5\beta (v = 1.5$ km/sec) indicate that, in this case, the RP pulse becomes significant for $x = 10$ and 20 km at a distance $y = 5$ km. In this last case, all three observers are within the region $\theta < \cos^{-1}(0.5)$.

In summary, a condition for the existence of the rupture passage (RP) phase is that the observer be within the region defined by $\theta < \cos^{-1}(v/\beta)$. The smaller the angle θ, the larger the relative importance of the RP phase with respect to the starting phase. The ratio of the Fourier amplitude spectrum of the RP phase to that of the starting phase is given by $[(\beta/v - \cos\theta)/\sin\theta]\sqrt{2\pi\omega r/\beta}\exp(-|\gamma\omega y/v|)$ indicating that RP phase is significant at intermediate frequency while at sufficiently high frequencies the starting phase will become dominant. This behavior has been illustrated in Fig. 2.3.1 where the introduction of a rise time has increased the importance of the RP phase relative to the starting phase. Finally, the rupture passage pulse can be determined by considering a simpler steady-state dislocation model.

The total solution for the velocity field for a starting anti-plane shear dislocation given by Eq. (2.2.2) includes both the starting and the RP phases but these phases are not clearly separated. A method of solution which separates these two phases has been described by Sotiropoulos (1983) and Luco and Sotiropoulos (1985). The procedure relies on use of the integral representation of the Fourier transform $\dot{w}(x, y, i\omega)$ of the particle velocity $\dot{w}(x, y, t)$ given by

$$\dot{w}(x, y, i\omega) = -\frac{\Delta\bar{w}}{4\pi i}\int_{-\infty}^{\infty}\frac{e^{-ikx-\nu y}}{k-\frac{\omega}{v}}\,dk \qquad (2.3.1)$$

where $\nu = [k^2 - (\omega/\beta)^2]^{1/2}$. Modification of the contour of integration to the contour of

BEST COPY AVAILABLE

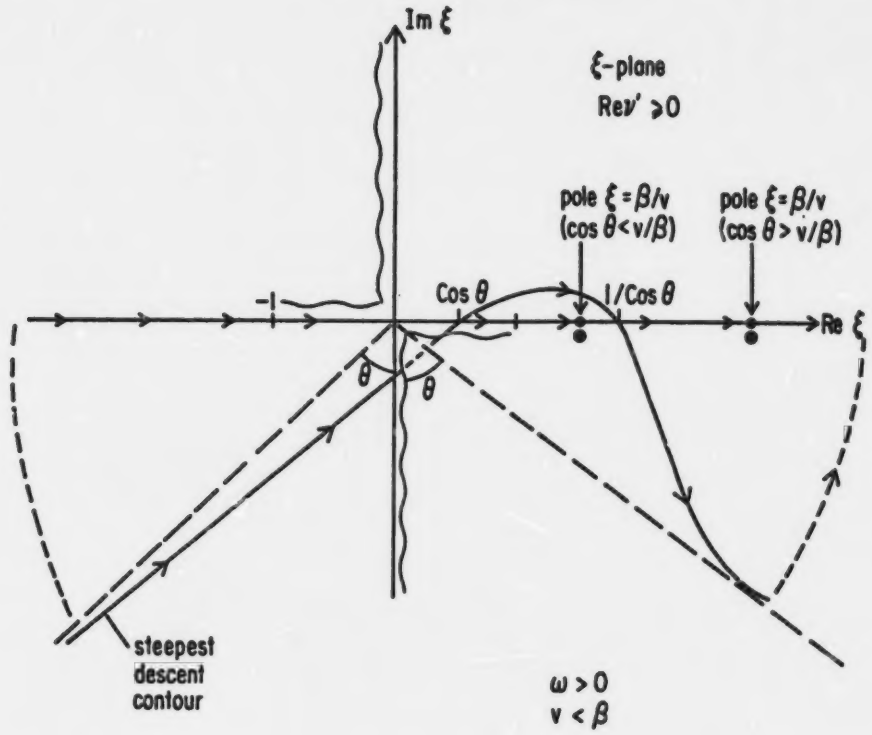

Fig. 2.3.3 Normalized ξ (wave number)-plane showing branch cuts, pole and contour of integration ($\omega > 0$, $v < \beta$).

BEST COPY AVAILABLE

steepest descent (Fig. 2.3.3) through the saddle point at $k = \omega\cos\theta/\beta$, $\theta = \cos^{-1}(x/\sqrt{x^2+y^2})$, and approximate evaluation of the resulting integral by the method of steepest descent leads to:

$$\dot{w}(x,y,i\omega) \approx \frac{\Delta\bar{w}}{2\pi}\,\frac{\sin\theta}{\frac{\beta}{v}-\cos\theta}\,\sqrt{\frac{\pi\beta}{2\omega r}}\,e^{-i\omega r/\beta - i\pi/4}$$

$$+\frac{\Delta\bar{w}}{2}\,e^{-|i\cos\theta+\gamma\sin\theta|(\omega r/v)}\,H(\cos\theta-\frac{v}{\beta}) \qquad (2.3.2)$$

valid for $\omega > 0$, $v < \beta$ and $\omega r/\beta >> 1$. The corresponding result for $\omega < 0$ is given by the complex conjugate of Eq. (2.3.2). The first term in Eq. (2.3.2) corresponds to the saddle point contribution while the second term corresponds to the contribution of a pole which has to be included if $\cos\theta > v/\beta$. Inverting to the time domain leads to

$$\dot{w}(x,y,t) \approx \frac{\Delta\bar{w}}{2\pi}\,\frac{\sin\theta}{\frac{\beta}{v}-\cos\theta}\,\sqrt{\frac{\beta}{2r}}\,\frac{H(t-\frac{r}{\beta})}{\sqrt{t-\frac{r}{\beta}}}$$

$$+\frac{\Delta\bar{w}}{2\pi}\,\frac{vy\gamma}{(x-vt)^2+y^2\gamma^2}\,H(\cos\theta-\frac{v}{\beta}) \qquad (2.3.3)$$

The first term in Eq. (2.3.3) corresponds to the starting phase given by Eq. (2.2.3) while the second term corresponds exactly to the rupture passage phase given by Eq. (2.1.2). This phase can only be observed within the region, $\theta < \cos^{-1}(v/\beta)$. The approximate procedure just described effectively separates the two phases.

An alternative derivation of the decomposition of the near-source ground motion has been presented by Lund (1985). The derivation is based on the integral representation presented by Eshelby (1953) and Mura (1963) for a uniform anti-plane shear dislocation with arbitrary rupture velocity $v(t) = dx_R(t)/dt$ in which $x_R(t)$ gives the position of the rupture front at time t. The representation for the particle velocity is

BEST COPY AVAILABLE

$$\dot{w}(x,y,t) = -\frac{\partial}{\partial y}\left[\left(\frac{\Delta\bar{w}}{2\pi}\right)\int_{-\infty}^{\tau_\rho}\frac{v(\tau)}{F(\tau)}\,d\tau\right] \tag{2.3.4}$$

in which

$$F(\tau) = \left[(t-\tau)^2 - \beta^{-2}\left\{[x - x_R(\tau)]^2 + y^2\right\}\right]^{1/2} \tag{2.3.5}$$

and τ_ρ, the retarded time, is the solution of

$$\beta^2(t-\tau)^2 = [x - x_R(\tau)]^2 + y^2 \tag{2.3.6}$$

The particle velocity for a starting dislocation for which $v(t) = v\,H(t)$, $x_R(t) = vt\,H(t)$ is given by

$$\dot{w}(x,y,t) = -\frac{\partial}{\partial y}\left[\left(\frac{v\,\Delta\bar{w}}{2\pi}\right)\int_{0}^{\tau_\rho}\frac{d\tau}{F(\tau)}\,H(\beta t - \tau)\right] \tag{2.3.7}$$

Lund (1985) noted that Eq. (2.3.7) can be written in the form

$$\dot{w}(x,y,z) = (\dot{w}_I + \dot{w}_{II})H(\beta t - \tau) \tag{2.3.8}$$

where

$$\dot{w}_I(x,y,t) = -\frac{\partial}{\partial y}\left[\left(\frac{v\,\Delta\bar{w}}{2\pi}\right)\int_{-\infty}^{\tau_\rho}\frac{d\tau}{F(\tau)}\right] \tag{2.3.9}$$

and

$$\dot{w}_{II}(x,y,t) = \frac{\partial}{\partial y}\left[\left(\frac{v\,\Delta\bar{w}}{2\pi}\right)\int_{-\infty}^{\bullet}\frac{d\tau}{F(\tau)}\right] \tag{2.3.10}$$

in which $x_R(t) = vt$. The term $\dot{w}_I$ corresponds to the particle velocity for the steady-state dislocation for $v(t) = v$ and $x_R(t) = vt$. After performing the integration and differentiation indicated in Eq. (2.3.9) it can be shown that (for $v < \beta$) $\dot{w}_I$ is given by Eq. (2.1.2). The term

BEST COPY AVAILABLE

$-\dot{w}_{II}$ corresponds to a dislocation which starts from $x = -\infty$ at $t = -\infty$ and stops at $x = 0$ at time $t = 0$. Performing the operations indicated in Eq. (2.3.10) leads to

$$\dot{w}_{II}(x,y,t) = \frac{\Delta\bar{w}}{2\pi} \frac{vy}{\gamma(\beta^2 t^2 - r^2) - (xv - \beta^2 t)(t^2 - r^2/\beta^2)^{1/2}} \tag{2.3.11}$$

which when combined with $\dot{w}_I$ gives for the total particle velocity the result expressed by Eq. (2.2.2). For $t \sim r/\beta$, $\dot{w}_{II}$ reduces to the starting phase given by Eq. (2.2.3).

BEST COPY AVAILABLE

2.4 Finite Fault Dislocation Models in a Uniform Full-Plane.

To illustrate the behavior of the ground motion in the vicinity of a fault of finite length we refer to the two-dimensional anti-plane shear fault model shown in Fig. 2.4.1. The solution for the velocity field $\dot{w}_F(x,y,t)$ for the finite fault can be obtained by superposition of the results $\dot{w}(x,y,t)$ for semi-infinite faults. In particular,

$$\dot{w}_F(x,y,t) = \dot{w}(x,y,t) - \dot{w}(x - L, y, t - L/v) \tag{2.4.1}$$

where L is the length of the fault. Based on the previous results we expect that the starting phase will be dominant in the region identified in Fig. 2.4.1 as zone III. The stopping phase will be dominant in region I while in region II, and, close to the plane of the fault, we expect that the rupture passage phase will be the most pronounced pulse. This behavior is illustrated in Fig.. 2.4.2 which shows contours of equal peak velocity for an anti-plane shear fault which starts at $x = 0$, $y = 0$ and propagates with constant rupture velocity towards $x > 0$ stopping at $x = 30$ km, $y = 0$. The other characteristics of the model are $\beta = 3.0$ km/sec, $v = 2.7$ km/sec, $\Delta\bar{w} = 100$ cm and $\tau = 0.2$ sec. The amplitudes shown in the contours in Fig. 2.4.2 are normalized by $\Delta w/2\pi\tau = 79.58$ cm/sec. The pattern shown in Fig. 2.4.2 indicates that the regions in the vicinity of (0,0) and (30, 0) are dominated by the starting and stopping phases, respectively. In these regions the radiation patterns of the starting and stopping phases defined by Eqs. (2.2.7) are clearly visible. In the region defined by $10 < x < 30$ km and $0 < y < 3$ km, the peak velocity is essentially independent of x indicating that, in this region, the RP phase is predominant. For a longer rise time or at lower frequencies, the region in which the RP phase is dominant would be larger than that shown in Fig. 2.4.2.

The distribution of peak velocities with distance y to the plane of the fault is shown in Fig. 2.4.3 for different values of x. The resulting scatter of the data involving factors of the order of 2 for $y = 5$ km may explain some of the scatter of the observed near-source velocity data.

BEST COPY AVAILABLE

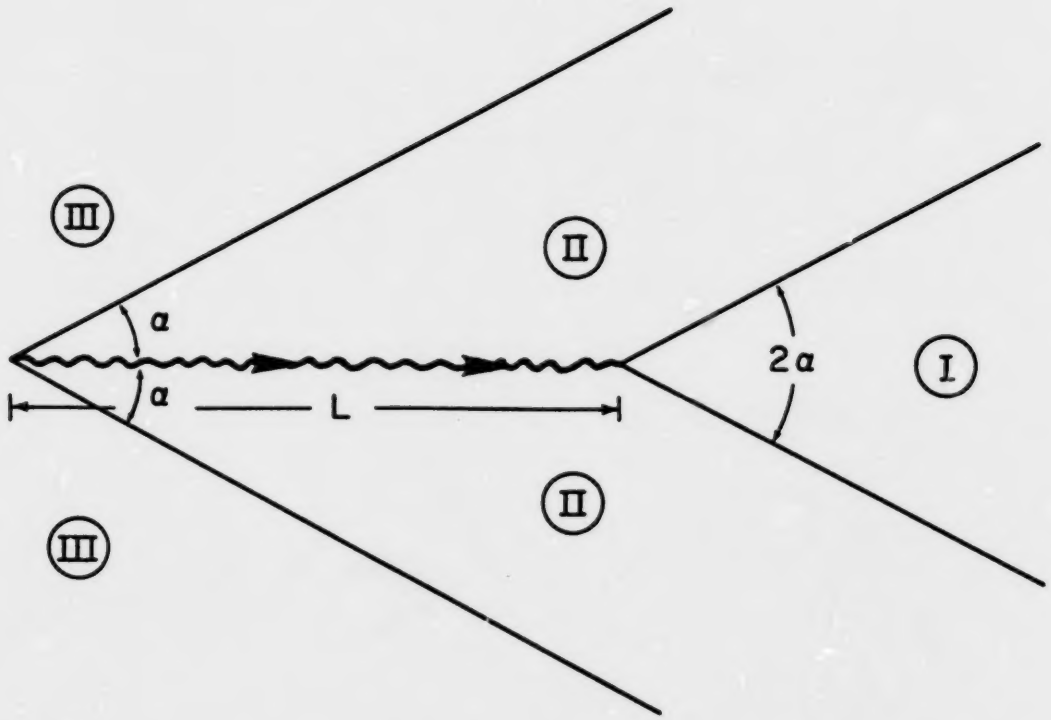

$$\alpha = \cos^{-1}\left(v/\beta\right)$$

Fig. 2.4.1 Schematic presentation of areas in which starting, stopping and passage-of-the-rupture-front phases are predominant.

BEST COPY AVAILABLE

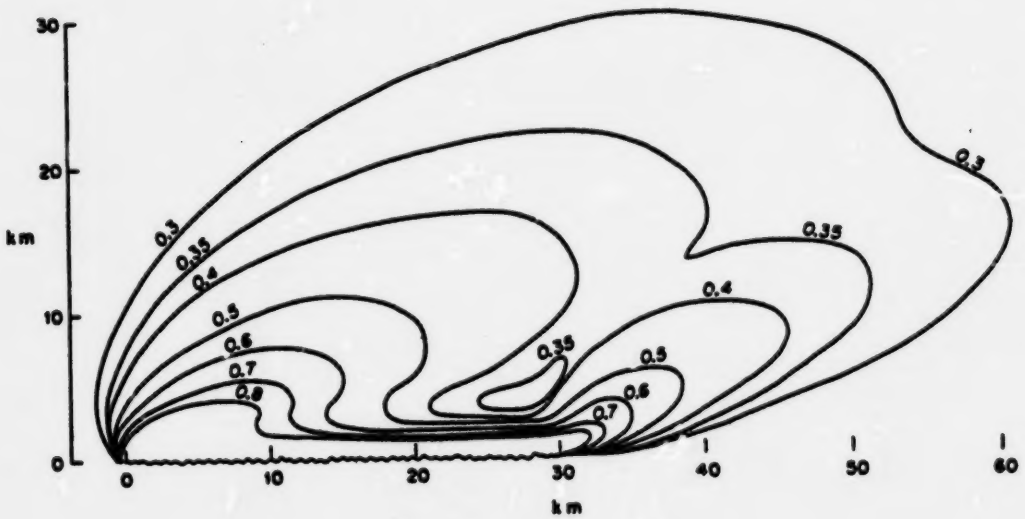

Fig. 2.4.2 Contours of equal amplitude peak velocities for an anti-plane shear dislocation model of finite length L = 30 km, $\Delta\bar{w}$ = 100 cm, τ = 0.2 secs, v = 2.7 km/sec, β = 3.0 km/sec. (Amplitudes shown in the contours are normalized by 79.58 cm/sec) (Luco and Sotiropoulos, 1985).

BEST COPY AVAILABLE

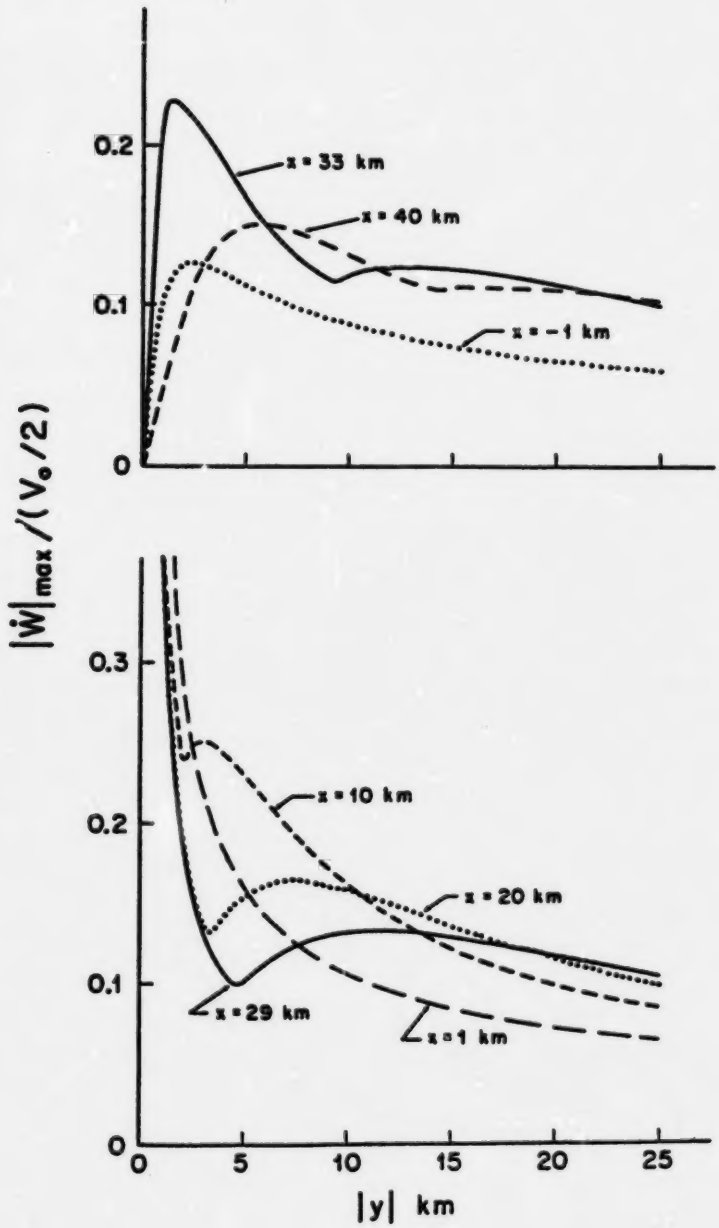

Fig. 2.4.3 Dependence of peak velocities on distance y from the fault. The model considered has a fault length of 30 km, slip of 100 cm with a rise time of 0.2 secs, and v = 2.7 km/sec = 0.9β (Luco and Sotiropoulos, 1985).

BEST COPY AVAILABLE

2.5 Dislocation Models with Nonuniform Slip and Variable Rupture Velocity.

The dislocation models considered in the previous sections were characterized by constant rupture velocity and uniform slip. To illustrate the effects of non-uniform rupture velocity we consider the case of a uniform step dislocation with rupture velocity given by

$$v(t) = \begin{cases} V_o\, t/\tau_o & 0 \leqslant t \leqslant \tau_o \\ V_o & t \geqslant \tau_o \end{cases} \qquad (2.5.1)$$

in which τ_o is the duration of the acceleration of the rupture front and V_o the constant rupture velocity after time $t = \tau_o$. An approximation to the starting phase for this case has been given by Kiusalaas and Mura (1964) in the form

$$\dot{w}(x,y,t) \approx \frac{\Delta\bar{w}}{2\pi}\left(\frac{\sin\theta}{r}\right)\left(\frac{V_o}{\tau_o}\right)\left[\sqrt{t^2 - r^2/\beta^2}\, H\,(t - r/\beta)\right.$$

$$\left. - \sqrt{(t-\tau_o)^2 - r^2/\beta^2}\, H(t - \tau_o - r/\beta)\right] . \qquad (2.5.2)$$

Eq. (2.5.2) indicates that the starting phase is non-singular in this case. The peak velocity associated with the starting phase occurs at $t = r/\beta + \tau_o$ and it is given by

$$\dot{w}\left(x,y,\frac{r}{\beta} + \tau_o\right) \approx \frac{\Delta\bar{w}}{2\pi}\,\frac{\sin\theta}{(\beta/V_o)}\sqrt{\frac{\beta}{2r}}\,\frac{2}{\sqrt{\tau_o}} \qquad (2.5.3)$$

for $\tau_o < r/\beta$. Comparison of Eq. (2.5.3) with Eq. (2.2.3) for $t = r/\beta + \tau_o$ indicates that the approximation to the starting phase for the accelerating rupture includes a factor β/V_o instead of the directivity factor $(\beta/V_o) - \cos\theta$. This suggests that the approximation is valid only for $|\cos\theta| << \beta/V_o$. In addition, the peak amplitude of the starting phase for an accelerating rupture is approximately twice the velocity at $t = r/\beta + \tau_o$ for a dislocation with constant rupture velocity.

A comparison of the starting phase for a uniform step dislocation with constant rupture velocity with that for an accelerating rupture is presented in Fig. 2.5.1.

BEST COPY AVAILABLE

Sotiropoulos and Nair (1985) have discussed the conditions on the spatial and temporal variation of the slip such that the starting phase (or, shear wave-front more generally) has a non-singular particle velocity field. The assumed form of the slip on the fault is of the type

$$\Delta w(x,t) = A\ x^p H(x)[t - t_R(x)]^q\ H[t - t_R(x)] \qquad (2.5.4)$$

in which $t_R(x)$ denotes the time of arrival of the rupture at point x. If $(dt_R/dx)_{x=0} \neq \infty$, the conditions for a non-singular velocity in the shear-wave front are

$$p + q \geq 1/2\ ,\ p \geq 0\ ,\ q \geq 0 \qquad (2.5.5)$$

In particular, for a step dislocation for which $q = 0$, p must satisfy the condition $p \geq 1/2$ implying that $\Delta w(0^+,t) = 0$.

To study the situation $(dt_R/dx)_{x=0} = \infty$, Sotiropoulos and Nair (1985) have considered the case $t_R(x) \sim x^\rho$ $(0 < \rho < 1)$. In this case, the conditions for a non-singular velocity field are

$$\frac{p+1}{\rho} + q \geq \frac{3}{2}\ ,\ p \geq 0\ ,\ q \geq 0\ ,\ 0 < \rho < 1\ . \qquad (2.5.6)$$

For a uniform $(p=0)$ step $(q=0)$ dislocation with constant acceleration of the rupture front $(\rho = 1/2)$ these conditions are satisfied and the resulting starting velocity pulse is non-singular as already discussed.

BEST COPY AVAILABLE

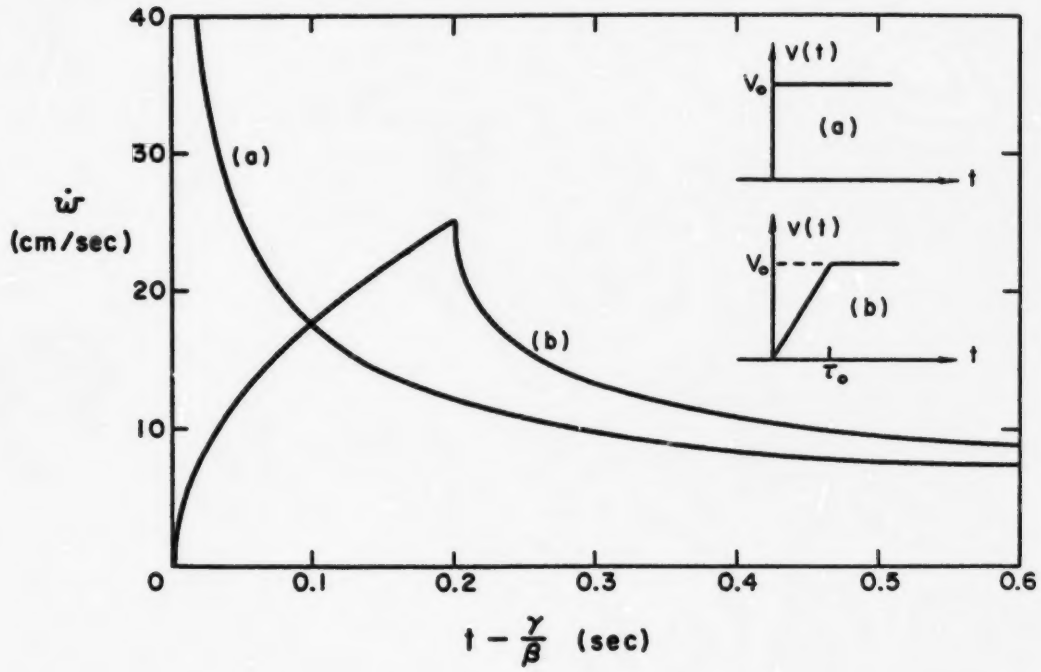

Fig. 2.5.1 Comparison of starting phases for a uniform step dislocation with (a) constant rupture velocity and (b) accelerating rupture (r = 10 km, $\theta = 90^\circ$, β = 3.0 km/sec, V_o = 2.7 km/sec, τ_o = 0.2 sec, $\Delta\bar{w}$ = 100 cm) (modified from Kiusalaas and Mura, 1964).

BEST COPY AVAILABLE

2.6 Steady-State Dislocation Model in a Layered Full-Plane.

To illustrate the effects of a low-velocity surficial sedimentary layer on the near source ground motion we consider the simple two-dimensional model shown in Fig. 2.6.1a. The model corresponds to a steady-state anti-plane shear dislocation which starts from $x = -\infty$ at $t = -\infty$ and propagates along the x-axis with constant velocity v so that at time $t = 0$ the rupture front is at $x = 0$. The medium in which the rupture develops consists of a half-space $y < h$ characterized by a S-wave velocity β_1 and density ρ_1, bonded to a half-space $y > h$ characterized by S-wave velocity β_2 and density ρ_2. The fault plane $y = 0$ is at a distance h from the interface between the two media.

The displacement fields $w_j(x,y,t)$ $(j=1,2)$ in both media must satisfy the corresponding equation of motion with $\beta = \beta_j$. On the fault plane $(y = 0)$ the conditions are

$$w_1(x,0^+,t) - w_1(x,0^-,t) = \Delta\bar{w}\ H(t - \frac{x}{v}) \tag{2.6.1}$$

and

$$\mu_1(\partial w_1/\partial y)_{y=0^+} = \mu_1(\partial w_1/\partial y)_{y=0^-} \tag{2.6.2}$$

where $\Delta\bar{w}$ is the slip on the fault and $\mu_j = \beta_j^2\,\rho_j$ is the shear modulus of the jth material. The continuity conditions at the interface $y = h$ are

$$w_1(x,h,t) = w_2(x,h,t) \tag{2.6.3}$$

and

$$\mu_1(\partial w_1/\partial y)_{y=h} = \mu_2(\partial w_2/\partial y)_{y=h} \tag{2.6.4}$$

for all x and t. Radiation conditions as $y \to -\infty$ and ∞ are also imposed on the displacement fields w_1 and w_2, respectively.

By use of Fourier integral transforms with respect to time and with respect to the x-coordinate it can be shown (Luco and Sotiropoulos, 1985) that the Fourier transforms with respect to time of the particle velocity fields in the two media are given by

BEST COPY AVAILABLE

$$\dot{w}_1(x,y,i\omega) = \frac{\Delta\bar{w}}{2}\left[sign\,(y)\; e^{-\tilde{\nu}_1|y|} + \tilde{R}_{11}\, e^{-\tilde{\nu}_1(2h-y)}\right] e^{-i\omega x/v} \quad , \; y \leqslant h \qquad (2.6.5)$$

$$\dot{w}_2(x,y,i\omega) = \frac{\Delta\bar{w}}{2}\,\tilde{T}_{12}\, e^{-\left|\tilde{\nu}_2(y-h)+\tilde{\nu}_1 h + i\frac{\omega x}{v}\right|} \quad , \; y \geqslant h \qquad (2.6.6)$$

in which

$$\tilde{R}_{11} = 2\mu_1\tilde{\nu}_1/(\mu_1\tilde{\nu}_1 + \mu_2\tilde{\nu}_2) \qquad (2.6.7)$$

$$\tilde{T}_{12} = (\mu_1\tilde{\nu}_1 - \mu_2\tilde{\nu}_2)/(\mu_1\tilde{\nu}_1 + \mu_2\tilde{\nu}_2) \qquad (2.6.8)$$

and

$$\tilde{\nu}_j = \left[(\omega/v)^2 - (\omega/\beta_j)^2\right]^{1/2} \quad , \; (j=1,2) \qquad (2.6.9)$$

are determined by the conditions $Re\;\tilde{\nu}_j \geqslant 0$.

We consider first the subsonic case $v < \beta_2 < \beta_1$. In this case

$$\nu_j = \frac{|\omega|\,\gamma_j}{v} \quad (j=1,2) \qquad (2.6.10)$$

in which $\gamma_j = \sqrt{1-(v/\beta_j)^2}$ are real quantities and Eqs. (2.6.5) and (2.6.6) indicate that the Fourier transform of the particle velocities in both media decay exponentially with frequency and with distance from the fault. The particle velocity in medium 2 ($y > h$) obtained by inversion of Eq. (2.6.6) is given by

$$\dot{w}_2(x,y,t) = \frac{\Delta\bar{w}}{2\pi}\left(\frac{2\mu_1\gamma_1}{\mu_1\gamma_1+\mu_2\gamma_2}\right)\frac{[\gamma_1 h + \gamma_2(h-y)]v}{(x-vt)^2 + [\gamma_1 h + \gamma_2(h-y)]^2} \qquad (2.6.11)$$

and in particular, the peak velocity $\dot{w}_{max}$ is

$$\dot{w}_{2max} = \frac{\Delta\bar{w}}{2\pi}\left(\frac{2\mu_1\gamma_1}{\mu_1\gamma_1+\mu_2\gamma_2}\right)\frac{v}{\gamma_1 h + \gamma_2(y-h)} \qquad (2.6.12)$$

which must be compared with $(\Delta\bar{w}/2\pi)(v/\gamma_1 y)$ for a uniform medium with properties equal to those of the first medium. The amplification of the peak particle velocity is given by the factor

BEST COPY AVAILABLE

$$\frac{\dot{w}_{2max}}{(\Delta\bar{w}/2\pi)(v/\gamma_1 y)} = \left(\frac{2\mu_1\gamma_1}{\mu_1\gamma_1 + \mu_2\gamma_2}\right)\frac{\gamma_1 y}{\gamma_1 h + \gamma_2(y - h)} \tag{2.6.13}$$

As illustration, in the case v = 2.1 km/sec, β_2 = 2.5 km/sec, β_1 = 3.0 km/sec, h = 0.5 km and y = 2 km, the amplification factor is 1.596. If $\beta_2 = v$ ($\gamma_2 = 0$) then the amplification factor is $(2y/h)$ which corresponds to a factor of 8 for h = 0.5 km and y = 2 km. Thus, a large amplification can be obtained if the rupture velocity is similar to the velocity in the softer medium.

We consider next the case $\beta_2 < v < \beta_1$ in which the rupture velocity is subsonic with respect to the characteristics of medium 1 but supersonic with respect to the S-wave velocity in the softer medium 2. In this case,

$$\tilde{\nu}_1 = |\omega|\gamma_1/v \quad , \quad \tilde{\nu}_2 = i\omega\gamma_2^*/v \tag{2.6.14}$$

where $\gamma_1 = \sqrt{1 - (v/\beta_1)^2}$ and $\gamma_2^* = \sqrt{(v/\beta_2)^2 - 1}$.

Equations (2.6.5) and (2.6.6) indicate that the Fourier transforms of the particle velocities also decay exponentially with frequency. For the particle velocity in medium 2, however, the decay depends only on the distance h and not on the full distance $y (y > h)$ Inversion of Eq. (2.6.6) to the time domain leads to

$$\dot{w}_2(x,y,t) = \frac{\Delta\bar{w}}{2\pi}\left(\frac{v}{\gamma_1 h}\right)\frac{2}{1 + (\mu_2\gamma_2^*/\mu_1\gamma_1)^2}\cdot\frac{1 + (\mu_2\gamma_2^*/\mu_1\gamma_1)[v(t-\tau)/\gamma_1 h]}{1 + [v(t-\tau)/\gamma_1 h]^2} \quad , \; y > h \tag{2.6.15}$$

where

$$\tau = [x + \gamma_2^*(y - h)]/v \tag{2.6.16}$$

The peak particle velocity in medium 2 occurs at

$$t - \tau = \frac{h\gamma_1}{v\kappa}\left(\sqrt{1 + \kappa^2} - 1\right) \tag{2.6.17}$$

BEST COPY AVAILABLE

in which $\kappa = \mu_2\gamma_2/\mu_1\gamma_1$. The amplitude of the peak velocity is

$$\dot{w}_{2max} = \frac{\Delta\bar{w}}{2\pi}\left(\frac{v}{\gamma_1 h}\right)\frac{\sqrt{1+\kappa^2}+1}{(1+\kappa^2)} \tag{2.6.18}$$

which is independent of the distance to the fault $(y - h)$.

A measure of the amplification resulting by the presence of medium 2 is obtained by comparing $\dot{w}_{2max}$, with the peak velocity at the same distance y for the case of a uniform medium with the properties of medium 1, i.e. $(\Delta\bar{w}/2\pi)(v/\gamma_1 y)$. The amplification ratio is

$$\frac{\dot{w}_{2max}}{(\Delta\bar{w}/2\pi)(v/\gamma_1 y)} = \left(\frac{y}{h}\right)\frac{\sqrt{1+\kappa^2}+1}{1+\kappa^2}\ , \quad y > h \tag{2.6.19}$$

which depends on the distance h from the fault to the interface. For κ in the range from 0 to 1, the amplification factor ranges from $2y/h$ to $1.207\ y/h$. In particular, for $\beta_1 = 3.0$ km/sec, $\beta_2 = 1$ km/sec, $v = 2.7$ km/sec, $\rho_1 = \rho_2$, $y = 2$ km and $h = 0.5$ km, the amplification factor given by Eq. (2.5.19) is 6.22. Clearly, the shock wave generated in the softer medium leads to large amplifications as first suggested by Aki (1968) and as verified by Bouchon (1979). An example of the effects introduced by the presence of a softer material is shown in Fig. 2.6.1b in which the velocity pulse given by Eq. (2.6.15) (solid line) is compared with the velocity pulse for a uniform medium with properties β_1 and ρ_1 (segmented line). In addition to the large amplification effect already mentioned, there is a change in pulse shape and a delay of $\tau - \frac{x}{v} = 1.42$ sec of the peak amplitude with respect to the passage of the rupture front below the station.

BEST COPY AVAILABLE

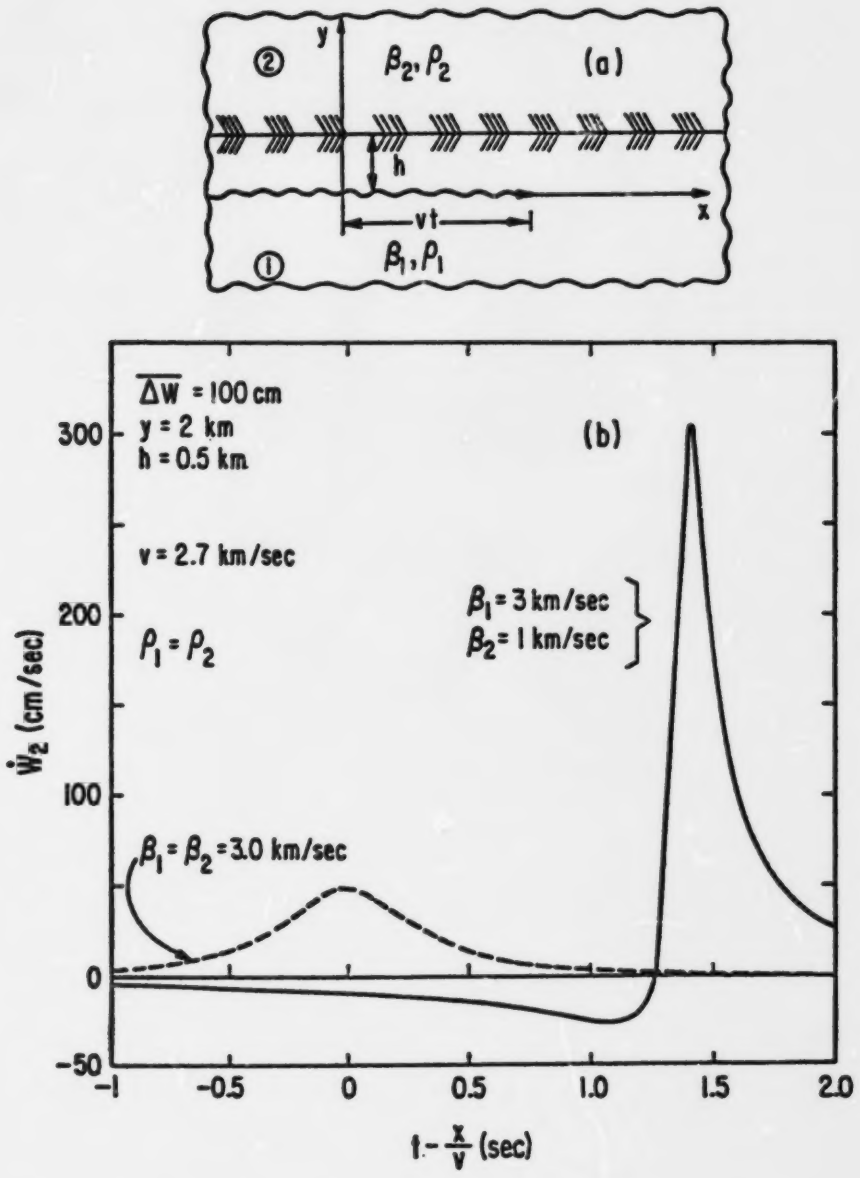

Fig. 2.6.1 (a) Description of the steady-state anti-plane dislocation model in a two-material medium. (b) Comparison of particle velocities at a distance $y = 2$ km from the fault for a uniform medium (segmented line) and a two-material medium (solid line) (Luco and Sotiropoulos, 1985).

BEST COPY AVAILABLE

2.7 Anti-Plane Dislocation Models in a Uniform or Layered Half-Plane.

Two-dimensional antiplane dislocation models in an elastic half-space have been considered by various authors. Mitra (1966) obtained a solution for an infinitely long strike-slip fault in a uniform elastic half-space by considering two mirror-image faults in an unbounded medium. Mal and Carriveau (1973) used an integral representation of the response in the frequency domain to obtain a solution for an infinitely long strike-slip fault in a uniform half-space and modelled the horizontal component of the displacement recorded at Pacoima Dam in a direction parallel to the trace of the fault as resulting from slip along the strike of the fault. In this solution, an elliptic slip function was used in an attempt at a better representation of the rupture mechanics. The same procedure was used by Carriveau (1973) for the case of an infinitely long strike-slip fault on a layered half-space.

Boore and Zoback (1974) corrected some errors in the Cagniard-de Hoop solution of Mitra (1966) for a two-dimensional anti-plane shear fault in an elastic half-space and used the model to show that peak displacements and velocities for an inclined fault are greater on the upper block than on the lower block.

To complete the review of two-dimensional anti-plane solutions, we should mention the studies of Dravinski and Trifunac (1979, 1980) for a vertical strike-slip fault on a layered elastic slab supported on a rigid half-space. In particular, Dravinski and Trifunac (1980) found that the response of an elastic layer bonded to a rigid half-space and including a vertical infinitely long strike-slip fault can be written, for a given frequency, as a sum of a finite number of progressing modes and an infinite number of locally standing modes. The amplitudes of the locally standing modes decay exponentially with distance to the fault plane and the contribution of these standing modes to the total response is significant only within a distance of the order of the thickness of the layer.

BEST COPY AVAILABLE

2.8 Conclusions

Analysis of the solutions available for a number of two-dimensional anti-plane shear dislocation models leads to the following characterization of the resulting motion:

1(i) The motion in the vicinity of a two-dimensional anti-plane shear fault model follows a two-dimensional pattern in which three regions can be distinguished. In the regions close to the geometrical beginning and end of the fault starting and stopping phases, respectively, dominate the velocity and acceleration pulses. In the region between the beginning and end of the fault and close to the plane of the fault, the velocity and acceleration fields show three pulses corresponding to starting rupture passage and stopping phases. Under some general conditions, the particle velocity in this region is dominated by the rupture passage phase.

1(ii) At distances of several fault dimensions the motion follows a simpler pattern than closer to the fault.

1(iii) Given the two-dimensional pattern of the motion, the variation of peak response amplitudes with distance to the fault does not follow simple monotonically decreasing functions. In addition, the variation of peak amplitudes with distance along a line perpendicular to the fault depends on the location of this line with respect to the fault. When peak amplitudes are plotted versus distance to the fault without consideration of location within the 2-D pattern, the resulting diagrams show scatter of amplitudes by factors of the order of 2.

2(i) The starting and stopping phases show a distance decay of the type $r^{-1/2}$, a radiation pattern of the form $\sin\theta$ and a directivity factor $1/|(\beta/v) - \cos\theta|$.

2(ii) Bilateral ruptures appear to have a stronger starting phase than unilateral ruptures.

2(iii) The time-dependence of the starting phase is highly dependent on the spatial and temporal description of the slip on the fault and on the variation of rupture velocity with

BEST COPY AVAILABLE

position. For a uniform step dislocation which starts at a point and then moves with constant rupture velocity, the velocity starting phase shows a singularity of the type $(t - r/\beta)^{1/2}$. The introduction of a finite rise time, a gradual spatial variation of the slip or a non instantaneous acceleration of the rupture, eliminates the singularity of the velocity pulse.

2(iv) The higher the ratio of rupture velocity to shear wave velocity ($v/\beta < 1$) the more pronounced the importance of the starting and stopping phases vis a vis the rupture passage phase.

3(i) The rupture passage phase in the subsonic case ($v/\beta < 1$) is represented by a wide and pronounced pulse of width proportional to ($y\gamma/v$). In the supersonic case ($v/\beta > 1$) the shape of the rupture passage pulse is identical to the slip on the fault and has amplitude equal to half the slip on the fault.

3(ii) The peak amplitudes of the velocity and acceleration rupture passage pulses in the subsonic case are dependent on the ratio of rupture velocity to shear wave velocity through the factors $1/\gamma$ and $1/\gamma^2$, respectively. The effect of the ratio v/β on peak amplitude is stronger for peak acceleration. In the supersonic case ($v/\beta > 1$), the amplitude of the rupture passage pulse is independent of v/β; only the arrival time of the pulse is affected by the value of v.

3(iii) In the subsonic case, the peak velocities and peak accelerations associated with the rupture passage pulse decay with distance to the fault as $1/y$ and $1/y^2$, respectively. These distance attenuation factors apply for distances larger than $v\tau/\gamma$ where τ is the rise time. In the supersonic case, there is no attenuation with distance.

3(iv) The amplitude of the rupture passage pulse is strongly affected by propagation through low-velocity layers on which the rupture velocity is equal or higher than the propagation velocity ($v \geq \beta_2$). Amplifications of the order of $(1 \div 2)y/h$ with respect to the case of a

BEST COPY AVAILABLE

uniform medium with $\beta_1 > v$ are obtained (y is the total distance to the fault and h is the distance travelled in the medium for which $\beta_1 > v$).

S(v) The Fourier amplitude spectrum of the rupture passage velocity pulse has an exponential decay with frequency (for $v/\beta < 1$). The exponential decay depends on the factor $(\gamma y/v)$.

BEST COPY AVAILABLE

2.9 References

Aki, K. (1968). Seismic displacements near a fault, *J. Geophys. Res.* 73, 5359-5376.

Aki, K. and P. G. Richards (1980). *Quantitative seismology: Theory and methods*, Vol. II, W. H. Freeman and Co., San Francisco.

Boore, D. M. and M. D. Zoback (1974). Near-field motions from kinematic models of propagating faults, *Bull. Seism. Soc. Am.* 64, 321-342.

Bouchon, M. (1979). Predictability of ground displacement and velocity near an earthquake fault: an example: the Parkfield earthquake of 1966, *J. Geophys. Res.* 84, 6149-6156.

Carriveau, A. R. (1973). Ground motion due to strike-slip faulting, *Ph.D. Thesis*, Dept. of Mechanics and Structures, University of California, Los Angeles, CA.

Dravinski, M. and M. D. Trifunac (1979). Static, dynamic and rotational components of strong earthquake shaking near faults, Dept. of Civil Engineering Report No. CE79-06, University of Southern California, Los Angeles, CA.

Dravinski, M. and M. D. Trifunac (1980). Response of a layer to strike-slip vertical fault, *J. Engrg. Mech. Div. ASCE* 106, 609-621.

Eshelby, J. D. (1949). Uniformly moving dislocations, *Proc. Phys. Soc.* A62, 307-314.

Eshelby, J. D. (1953). The equation of motion of a dislocation, *Physical Review, 90*, 248-255.

Frank, F. C. (1949). On the equations of motion of crystal dislocations, *Proc. Phys. Soc.* A62, 131-134.

Geller, R. J. (1974). Representation theorems for an infinite shear fault, *Geophys. J. R. astr. Soc.* 39, 123-131.

Kiusalaas, J. and T. Mura (1964). On the motion of a screw dislocation, in A. C. Eringen, ed., *Recent Advances in European Science*, Gordon Beach, New York, p. 543.

Luco, J. E. and D. A. Sotiropoulos (1985). On a decomposition of near-source earthquake ground motion, *Soil Dynamics and Earthquake Engineering, 4*, 210-220.

BEST COPY AVAILABLE

Liebfried, G. and H. D. Die[illegible] (1949). Zur theorie der Schraufenversetzung, *Zeitschr. für Geophys.* 126, 790-808.

Lund, F. (1985). A note on the synthesis of near field ground motion (submitted for publication).

Mal, A. K. and A. R. Carriveau (1973). Earthquake ground motion near the source, *Proc. 5th World Conf. on Earthquake Engrg.*, Rome Italy.

Markenscoff, X. (1980). The transient motion of a nonuniformly moving dislocation, *J. Elasticity* 10, 183-201.

Mitra, M. (1966). Surface displacement produced by an underground fracture, *Geophysics* 31, 204-213.

Mura, T. (1963). Continuous distribution of moving dislocations, *Phil. Mag.* *8*, 843-857.

Sotiropoulos, D. A. (1983). On synthesis of ground motions from earthquakes, *Ph.D. Thesis*, University of California, San Diego, La Jolla, CA.

Sotiropoulos, D. A. and S. Nair (1985). Shear wave-front motion from a nonuniform dislocation (submitted for publication).

BEST COPY AVAILABLE

3. TWO-DIMENSIONAL PLANE-STRAIN MODELS

3.0 Introduction.

The simplest two-dimensional plane-strain model in an unbounded medium corresponds to a line shear dislocation with slip perpendicular to the rupture front (gliding edge dislocation) which starts from $x = -\infty$ at $t = -\infty$ and propagates towards $x > 0$ with constant rupture velocity (Fig. 3.0.1.a). Solutions for this steady-state dislocation model have been obtained by Eshelby (1949) and by Boore, Aki and Todd (1971). The two-dimensional problem of a suddenly starting shear (gliding edge) dislocation which then propagates with constant speed in an unbounded medium (Fig. 3.0.1.b) has been solved by Niazy (1973) and Boore and Zoback (1974a) by use of the Cagniard-de Hoop technique. The corresponding two-dimensional problem of a suddenly starting opening dislocation which then propagates with constant rupture velocity in an unbounded medium has been studied by Ang and Williams (1959) also by use of the Cagniard-de Hoop technique. Kiusalaas and Mura (1964) and Gelier (1974) have derived alternative representations for the solution of these two-dimensional plane-strain dislocation problems. The representation obtained by Geller (1979), given in terms of a line integral of temporal convolutions over the width of the fault, are obtained by analytical integration of the full-space Green's function over the direction of infinite length. The relation between the response for the steady-state and the starting gliding dislocation models has been investigated by Boore and Zoback (1974a) and Luco and Sotiropoulos (1985).

The response of a uniform half-space to an infinitely long thrust fault (Fig. 3.0.1.c) has been studied by Mal (1972), Schafer (1973), Niazy (1975), Litehiser (1976), Bouchon and Aki (1977), Bouchon (1978a,b) and Madariaga (1980).

As in the case of the two-dimensional anti-plane shear dislocation models discussed in Chapter 2, the plane-strain gliding edge dislocation models shown in Fig. 3.0.1 can be used both as generalized analogs or as actual models. Boore and Zoback (1974a) have suggested that the gliding edge models shown in Figs. 3.0.1a,b when considered as plan views could represent the

BEST COPY AVAILABLE

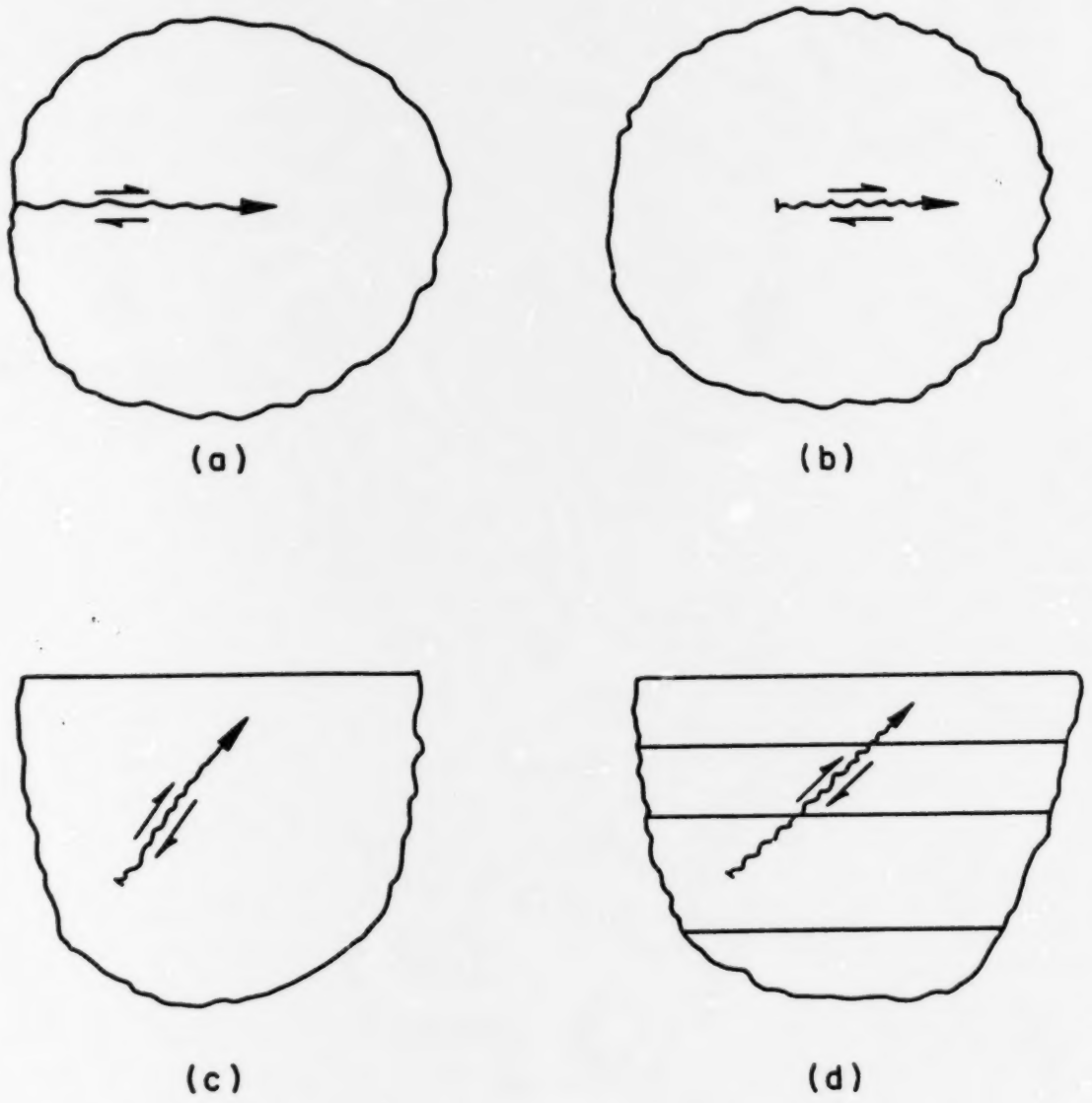

Fig. 3.0.1 Two-dimensional plane-strain (gliding edge) dislocation models.

BEST COPY AVAILABLE

lateral propagation of a vertical strike-slip fault while the models shown in Figs. 3.0.1c,d when viewed as vertical sections could represent propagation along the dip of an inclined fault with dip-slip motion. In fact, two-dimensional plane-strain gliding edge fault models in a full space have been used to model the Parkfield 1966 earthquake (Boore *et al.* 1971; Niazy, 1973; Boore and Zoback, 1974a) and the San Fernando 1971 earthquake (Niazy, 1973; Boore and Zoback, 1974b). Niazy (1975), Bouchon and Aki (1977) and Bouchon (1978b) have used two-dimensional plane-strain fault models in a half-space to analyze near-source records obtained during the San Fernando earthquake of 1971.

BEST COPY AVAILABLE

3.1 Steady-State Dislocation Models in a Uniform Full-Plane.

As already mentioned, one of the simplest two-dimensional plane-strain models in an unbounded medium corresponds to a line shear dislocation with slip perpendicular to the rupture front (gliding edge dislocation) which starts from $x = -\infty$ at $t = -\infty$ and propagates towards $x > 0$ with constant rupture velocity (Fig. 3.1.1a). Solutions for this steady-state dislocation model have been obtained by Eshelby (1949) and by Boore, Aki and Todd (1971).

To illustrate some of the characteristics of the solution we consider a model defined by displacement discontinuity condition across the fault plane:

$$u_x(x,0^+,t) - u_x(x,0^-,t) = \Delta\bar{u}\ H\left(t - \frac{x}{v}\right) \tag{3.1.1}$$

where u_x is the x-component of the displacement vector and $\Delta\bar{u}$ is the slip. The y-component of displacement, u_y, and the traction on the fault plane are continuous across $y = 0$. The solution of Eshelby (1949) for $v < \beta$ gives for $y > 0$:

$$u_x = \frac{\Delta\bar{u}}{\pi}\left(\frac{\beta}{v}\right)^2\left[\tan^{-1}\left(\frac{\gamma_\alpha y}{x'}\right) - \left(\frac{1+\gamma_\beta^2}{2}\right)\tan^{-1}\left(\frac{\gamma_\beta y}{x'}\right)\right] \tag{3.1.2a}$$

$$u_y = \frac{\Delta\bar{u}}{\pi}\left(\frac{\beta}{v}\right)^2\left\{\gamma_\alpha \ln\left[\frac{(x')^2+\gamma_\alpha^2 y^2}{a^2}\right]^{1/2} - \left(\frac{1+\gamma_\beta^2}{2\gamma_\beta}\right)\ln\left[\frac{(x')^2+\gamma_\beta^2 y^2}{a^2}\right]^{1/2}\right\} \tag{3.1.2b}$$

$$\dot{u}_x = \frac{v\,\Delta\bar{u}}{\pi}\left(\frac{\gamma_\alpha}{(x')^2+\gamma_\alpha^2 y^2} - \left(\frac{1+\gamma_\beta^2}{2}\right)\frac{\gamma_\beta}{(x')^2+\gamma_\beta^2 y^2}\right) y\left(\frac{\beta}{v}\right)^2 \tag{3.1.3a}$$

$$\dot{u}_y = -\frac{v\,\Delta\bar{u}}{\pi}\left(\frac{\gamma_\alpha}{(x')^2+\gamma_\alpha^2 y^2} - \left(\frac{1+\gamma_\beta^2}{2\gamma_\beta^2}\right)\frac{\gamma_\beta}{(x')^2+\gamma_\beta^2 y^2}\right) x'\left(\frac{\beta}{v}\right)^2 \tag{3.1.3b}$$

$$\ddot{u}_x = \frac{\Delta\bar{u}}{\pi}\beta^2\left\{\frac{2\gamma_\alpha}{[(x')^2+\gamma_\alpha^2 y^2]^2} - \left(\frac{1+\gamma_\beta^2}{2}\right)\frac{2\gamma_\beta}{[(x')^2+\gamma_\beta^2 y^2]^2}\right\} x'y \tag{3.1.4a}$$

$$\ddot{u}_y = -\frac{\Delta\bar{u}}{\pi}\beta^2\left\{\frac{[(x')^2-\gamma_\alpha^2 y^2]\gamma_\alpha}{[(x')^2+\gamma_\alpha^2 y^2]^2} - \left(\frac{1+\gamma_\beta^2}{2\gamma_\beta^2}\right)\frac{[(x')^2-\gamma_\beta^2 y^2]\gamma_\beta}{[(x')^2+\gamma_\beta^2 y^2]^2}\right\} \tag{3.1.4b}$$

BEST COPY AVAILABLE

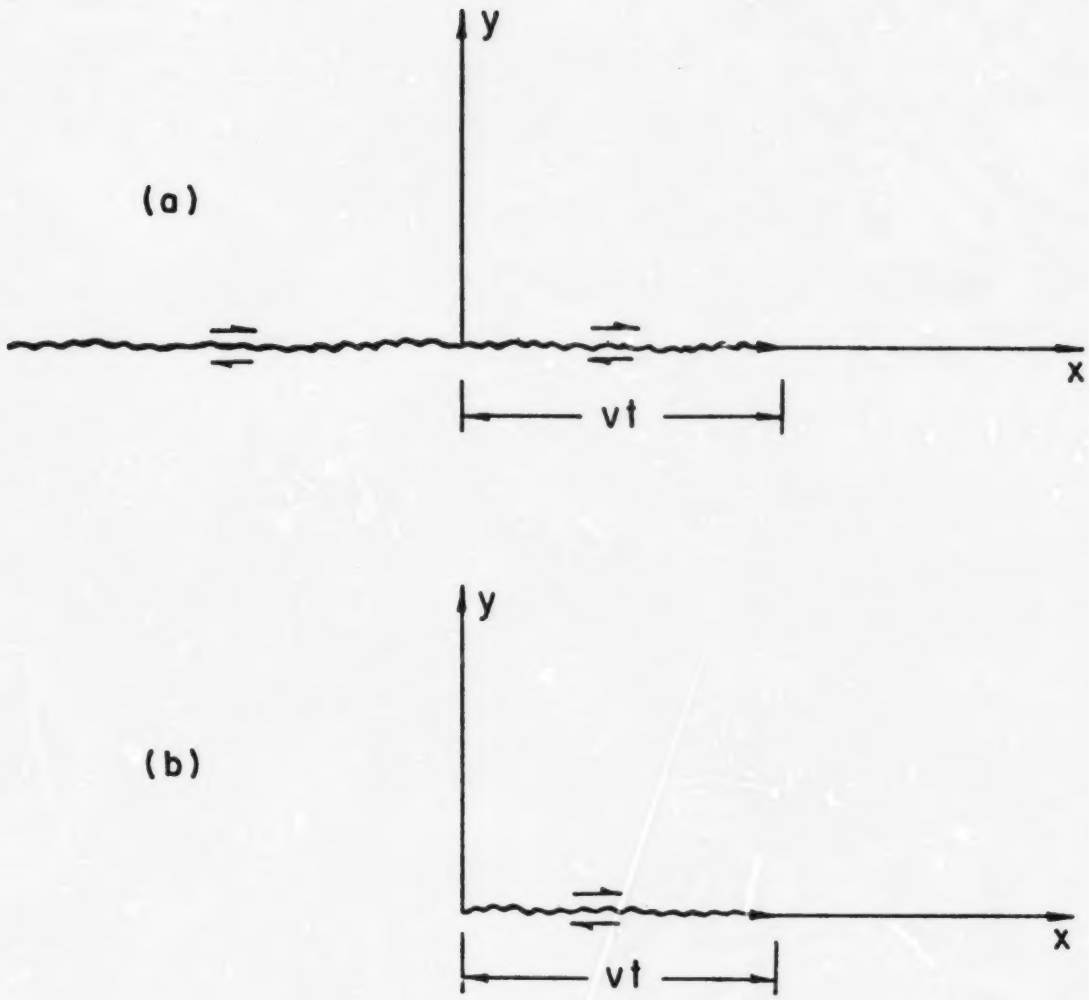

Fig. 3.1.1 Steady-state (a) and starting (b) gliding edge dislocation models.

BEST COPY AVAILABLE

where β is the shear wave velocity in the medium, α denotes the P-wave velocity, $x' = x - vt$, $\gamma_\alpha = \sqrt{1 - (v/\alpha)^2}$ and $\gamma_\beta = \sqrt{1 - (v/\beta)^2}$. In Eq. (3.1.3b), the symbol a stands for an arbitrary constant with dimensions of length.

The forms of the displacement, velocity and acceleration pulses for $x = 0$ $y = 1$ km, $\alpha = 6.0$ km/sec, $\beta = 3.464$ km/sec, $v = 2.5$ km/sec and $\Delta\bar{u} = 100$ cm are shown in Fig. 3.1.2. The most pronounced features of the response shown in Fig. 3.1.2 are the large acceleration, velocity and displacement pulses associated with the perpendicular (y) component of motion. It must be noted that u_y becomes infinite as $t \to \pm \infty$. Eqs. (3.1.3) and (3.1.4) indicate that the peak values of the velocity and acceleration components decay as y^{-1} and y^{-2}, respectively.

On the plane of the fault ($y = 0$)

$$u_x(x,0^+,t) = \frac{\Delta\bar{u}}{2} H\left(t - \frac{x}{v}\right) \tag{3.1.5a}$$

$$u_y(x,00^+,t) = \frac{\Delta\bar{u}}{2} \left(\frac{\beta}{v}\right)^2 \left(\frac{2\gamma_\alpha\gamma_\beta - 1 - \gamma_\beta^2}{2\gamma_\beta}\right) \ln\left|\frac{x'}{a}\right| \tag{3.1.5b}$$

$$\dot{u}_x(x,0^+,t) = \frac{\Delta\bar{u}}{2} \delta\left(t - \frac{x}{v}\right) \tag{3.1.6a}$$

$$\dot{u}_y(x,0^+,t = - v \frac{\Delta\bar{u}}{\pi} \left(\frac{\beta}{v}\right)^2 \left(\frac{2\gamma_\alpha\gamma_\beta - 1 - \gamma_\beta^2}{2\gamma_\beta}\right) \frac{1}{x'} \tag{3.1.6b}$$

$$\ddot{u}_x(x,0^+,t) = \frac{\Delta\bar{u}}{2} \dot{\delta}\left(t - \frac{x}{v}\right) \tag{3.1.7a}$$

$$\ddot{u}_y(x,0^+,t) = \frac{\Delta\bar{u}}{\pi} \beta^2 \left(\frac{2\gamma_\alpha\gamma_\beta - 1 - \gamma_\beta^2}{2\gamma_\beta}\right) \frac{1}{(x')^2} \tag{3.1.7b}$$

which indicate that with the exception of $u_x(x,0^+,t)$ all other response components on $y = 0$ are singular for $x' = x - vt = 0$.

Boore *et al.* (1971) were the first to use a steady-state two-dimensional dislocation model in an attempt at modelling the perpendicular displacement pulse inferred from the acceleration record obtained at station No. 2 during the Parkfield 1966 earthquake. Boore *et al.* (1971)

BEST COPY AVAILABLE

considered a number of smeared-out or finite-length steady-state dislocation models in an attempt at removing the singularities of the perpendicular displacement pulse at $x' = 0$.

The effects of a finite rise time (τ) can be analyzed by considering a finite ramp dislocation

$$u_x(x,0^+,t) - u_x(x,0^-,t) = \left(\frac{\Delta\bar{u}}{\tau}\right)\left[t\ H(t - \frac{x}{v}) - (t - \tau)H(t - \tau - \frac{x}{v})\right] \quad (3.1.8)$$

where $\Delta\bar{u}$ is the final slip. In this case, the velocity response is given by

$$\dot{u}_x = \frac{\Delta\bar{u}}{\pi\tau}\left(\frac{\beta}{v}\right)^2\left\{\left[\tan^{-1}\left(\frac{\gamma_\alpha y}{x'}\right) - \tan^{-1}\left(\frac{\gamma_\alpha y}{x''}\right)\right] - \left(\frac{1+\gamma_\beta^2}{2}\right)\left[\tan^{-1}\left(\frac{\gamma_\beta y}{x'}\right) - \tan^{-1}\left(\frac{\gamma_\beta y}{x''}\right)\right]\right\} \quad (3.1.9a)$$

$$\dot{u}_y = \frac{\Delta\bar{u}}{\pi\tau}\left(\frac{\beta}{v}\right)^2\left\{\gamma_\alpha \ln\left[\frac{(x')^2+\gamma_\alpha^2 y^2}{(x'')^2+\gamma_\alpha^2 y^2}\right]^{1/2} - \left(\frac{1+\gamma_\beta^2}{2\gamma_\beta}\right)\ln\left[\frac{(x')^2+\gamma_\beta^2 y^2}{(x'')^2+\gamma_\beta^2 y^2}\right]^{1/2}\right\} \quad (3.1.9b)$$

in which $x' = x - vt$, $x'' = x - vt + v\tau$ and $\tan^{-1}$ is in the range from 0 to π. The effects of τ on the shape and amplitude of the perpendicular velocity pulse near the fault ($y = 0.1$ km) are shown in Fig. 3.1.3. The effect of rise time on the distribution of peak velocity with distance to the fault is illustrated in Fig. 3.1.4 for the perpendicular velocity component.

BEST COPY AVAILABLE

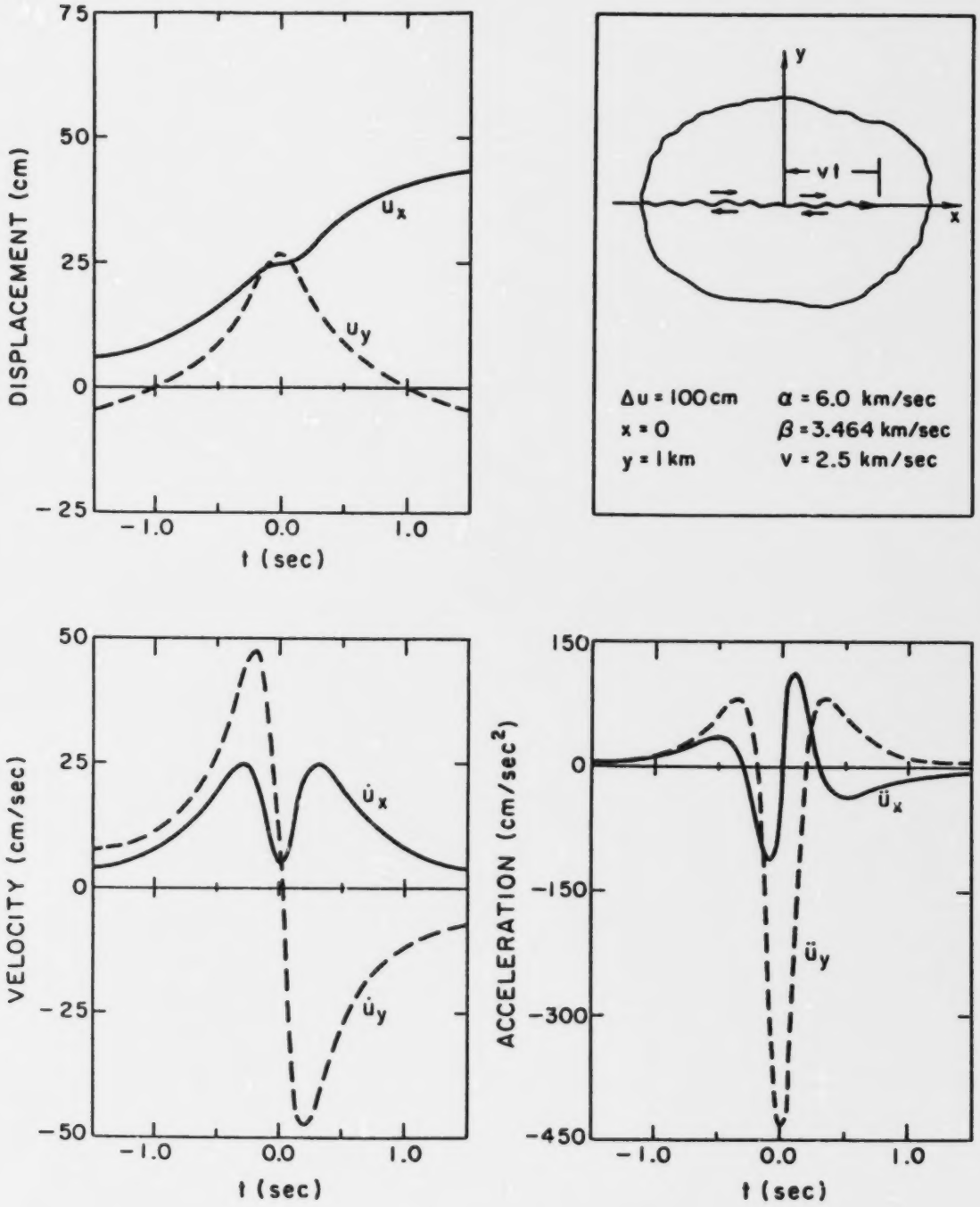

Fig. 3.1.2 Displacement, velocity and acceleration pulses for a step ($\tau = 0$) gliding edge dislocation model ($\Delta\bar{u} = 100$ cm, $x = 0$, $y = 1$ km, $\alpha = 6.0$ km/sec, $\beta = 3.464$ km/sec, $v = 2.5$ km/sec). The arbitrary additive constant affecting u_y has been selected such that $u_y = 0$ for $t = 1$ sec.

BEST COPY AVAILABLE

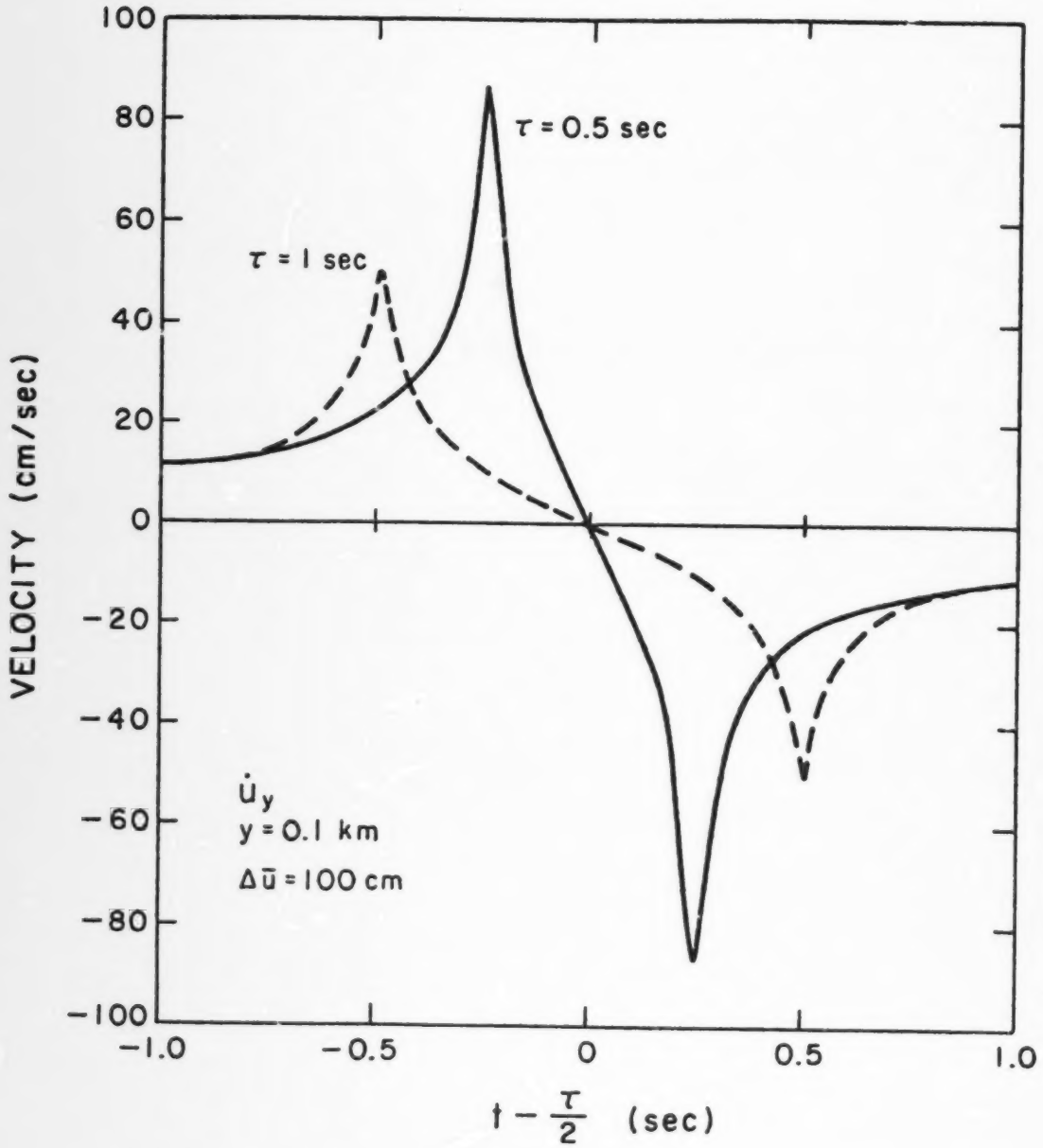

Fig. 3.1.3 Effect of rise time on the perpendicular velocity component ($\dot{u}_y$) ($\Delta\bar{u}$ = 100 cm, x = 0, y = 0.1 km, α = 6.0 km/sec, β = 3.464 km/sec, v = 2.5 km/sec).

BEST COPY AVAILABLE

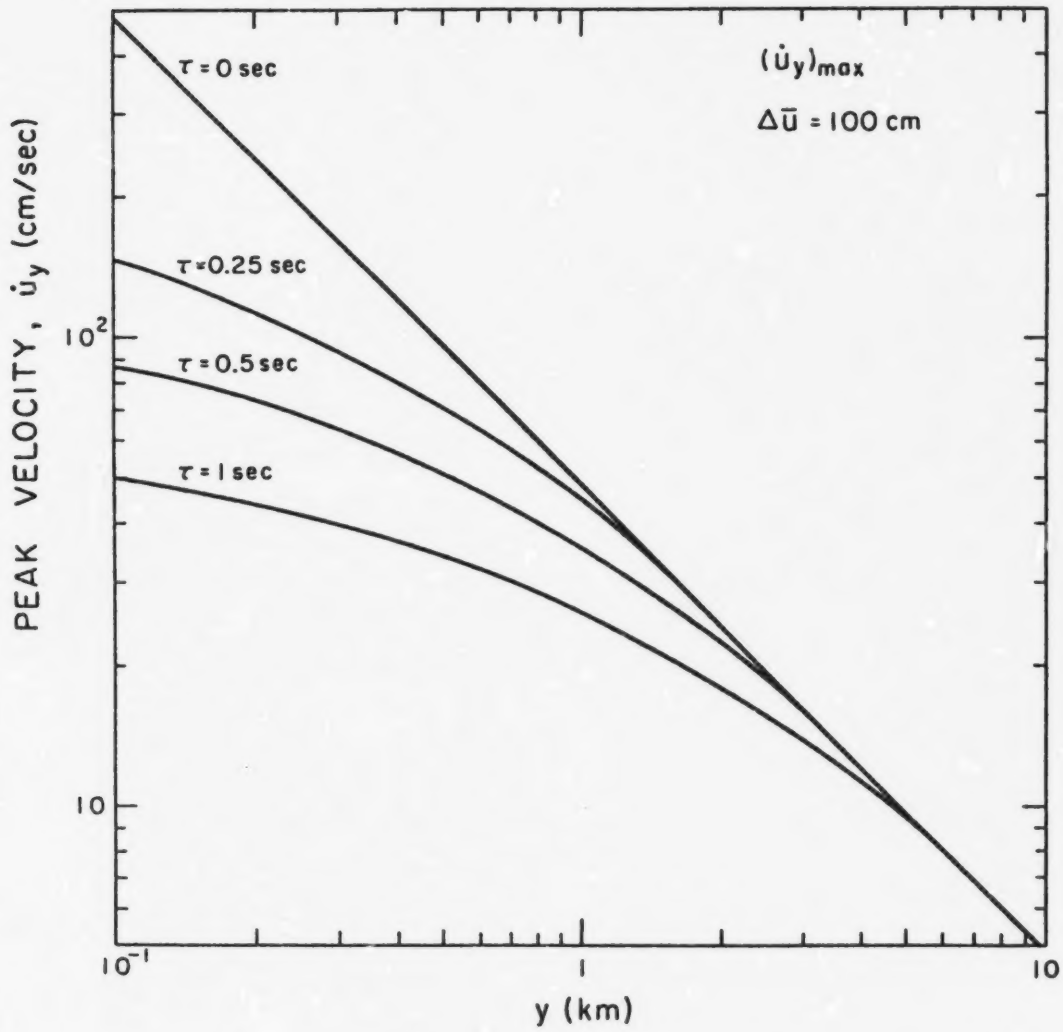

Fig. 3.1.4 Effect of rise time on the variation of peak perpendicular velocity $\dot{u}_y$ with distance to the fault ($\Delta\bar{u}$ = 100 cm, x = 0, α = 6.0 km/sec, β = 3.464 km/sec, v = 2.5 km/sec).

BEST COPY AVAILABLE

3.2 Starting Dislocation Model in a Uniform Full-Plane.

The two-dimensional problem of a suddenly starting shear (gliding edge) dislocation which then propagates with constant speed in an unbounded medium (Fig. 3.1.1.b) has been solved by Niazy (1973) and Boore and Zoback (1974a). Niazy (1973) used the Cagniard-de Hoop technique to obtain first the response for a suddenly appearing line dislocation and then proceeded to integrate analytically to obtain the response for a moving dislocation. On the other hand, Boore and Zoback (1974a) obtained directly the solution for a moving dislocation by application of the Cagniard-de Hoop technique. The corresponding two-dimensional problem of a suddenly starting opening dislocation which then propagates with constant rupture velocity in an unbounded medium has been studied by Ang and Williams (1959) by use of the Cagniard-de Hoop technique. Kiusalaas and Mura (1964) and Geller (1974) have derived alternative representations for the solution of these two-dimensional plane-strain dislocation problems. The representation obtained by Geller (1974), given in terms of a line integral of temporal convolutions over the width of the fault, are obtained by analytical integration of the full-space Green's function over the direction of infinite length.

To compare with the solution for the steady-state case, we consider the case of a two-dimensional edge dislocation which starts from $x = 0$ at $t = 0$ and propagates in the positive x direction with constant velocity v. The discontinuity condition across the fault plane in this case is given by

$$u_x(x,0^+,t) - u_x(x,0^-,t) = \Delta\bar{u}\ H(t - x/v)\ H(x) \qquad (3.2.1)$$

The displacement u_y and the stresses σ_{xy} and σ_{yy} are continuous across the plane $y = 0$. The particle velocities as resulting from the work of Ang and Williams (1959) and Boore and Zoback (1974a) are:

BEST COPY AVAILABLE

$$\dot{u}_x(x,y,t) = \frac{\beta^2 \Delta\bar{u}}{\pi} \left\{ \mathrm{Im} \left(\frac{p_1^2 \left[t \sin\theta + i \cos\theta \left(t^2 - r^2/\alpha^2 \right)^{1/2} \right]}{i/v - p_1} \right) \frac{H(t - r/\alpha)}{r\left(t^2 - r^2/\alpha^2 \right)^{1/2}} \right.$$

$$\left. - \mathrm{Im} \left(\left(\frac{1}{2\beta^2} + p_2^2 \right) \frac{\left[t \sin\theta + i \cos\theta \left(t^2 - r^2/\beta^2 \right)^{1/2} \right]}{i/v - p_2} \right) \frac{H(t - r/\beta}{r\left(t^2 - r^2/\beta^2 \right)^{1/2}} \right\} \qquad (3.2.2)$$

$$\dot{u}_y(x,y,t) = \frac{\beta^2 \Delta\bar{u}}{\pi} \left\{ Re \left(\frac{(1/\alpha^2 + p_1^2) p_1}{i/v - p_1} \right) \frac{H(t - r/\alpha)}{\left(t^2 - r^2/\alpha^2 \right)^{1/2}} \right.$$

$$\left. - \mathrm{Re} \left(\frac{\left(\frac{1}{2\beta^2} + p_2^2 \right) p_2}{i/v - p_2} \right) \frac{H(t - r/\beta)}{\left(t^2 - r^2/\beta^2 \right)^{1/2}} \right\} \qquad (3.2.3)$$

where $x = r\cos\theta$, $y = r\sin\theta$, $p_1 = [(t^2 - r^2/\alpha^2)^{1/2} \sin\theta + i\ t\ \cos\theta]/r$, and $p_2 = [(t^2 - r^2/\beta^2)^{1/2} \sin\theta + i\ t\ \cos\theta]/r$

Equations (3.2.2) and (3.2.3) indicate that the P- and S- starting phases arriving at $t = r/\alpha$ and $t = r/\beta$, respectively, are singular. In particular, the starting phases are given by

$$\begin{Bmatrix} \dot{u}_x \\ \dot{u}_y \end{Bmatrix} = \frac{\Delta\bar{u}}{\pi} \left(\frac{\beta}{\alpha} \right)^2 \frac{\sin 2\theta}{(\alpha/v - \cos\theta)} \frac{H(t - r/\alpha)}{(2r/\alpha)^{1/2} (t - r/\alpha)^{1/2}} \begin{Bmatrix} \cos\theta \\ \sin\theta \end{Bmatrix}$$

$$+ \frac{\Delta\bar{u}}{\pi} \frac{\cos 2\theta}{2(\beta/v - \cos\theta)} \frac{H(t - r/\beta)}{(2r/\beta)^{1/2} (t - r/\beta)^{1/2}} \begin{Bmatrix} -\sin\theta \\ \cos\theta \end{Bmatrix} \qquad (3.2.4)$$

which show singularities of the type $(t - r/\alpha)^{-1/2}$ and $(t - r/\beta)^{-1/2}$. The high-frequency components of the velocity spectra show a $\omega^{-1/2}$ decay with frequency.

The radial and transverse components of the starting phases

$$\dot{u}_r = \dot{u}_x \cos\theta + \dot{u}_y \sin\theta$$

$$\dot{u}_\theta = -\dot{u}_x \sin\theta + \dot{u}_y \cos\theta \qquad (3.2.5)$$

are given by

BEST COPY AVAILABLE

$$\dot{u}_r = \frac{\Delta\bar{u}}{\pi}\left(\frac{v}{\beta}\right)\left(\frac{\beta}{\alpha}\right)^{5/2}\frac{\sin 2\theta}{1-\left(\frac{v}{\alpha}\right)\cos\theta}\cdot\frac{H(t-r/\alpha)}{(2r/\beta)^{1/2}(t-r/\alpha)^{1/2}} \tag{3.2.6}$$

$$\dot{u}_\theta = \frac{\Delta\bar{u}}{\pi}\left(\frac{v}{\beta}\right)\frac{\cos 2\theta}{1-\left(\frac{v}{\beta}\right)\cos\theta}\cdot\frac{H(t-r/\beta)}{(2r/\beta)^{1/2}(t-r/\beta)^{1/2}} \tag{3.2.7}$$

which indicate that the radial component of the starting phase corresponds to the P-wave while the transverse component corresponds to the S-wave. Contours of equal velocity defined by

$$r_s = \frac{1}{A_\theta^2}\left[\frac{\cos 2\theta}{1-\left(\frac{v}{\beta}\right)\cos\theta}\right]^2 \tag{3.2.8}$$

$$r_p = \frac{1}{A_r^2}\left[\frac{\sin 2\theta}{1-\left(\frac{v}{\alpha}\right)\cos\theta}\right]^2\left(\frac{\beta}{\alpha}\right)^5 \tag{3.2.9}$$

where A_r and A_θ are proportional to the amplitudes of $\dot{u}_r$ and $\dot{u}_\theta$, respectively, are shown in Figs. 3.2.1a and 3.2.1b for α = 6.0 km/sec, β = 3.464 km/sec, v = 2.5 km/sec. The contour for the radial component (P-wave) has been drawn for an amplitude $A_r = A_\theta/10$; the contour for $A_r = A_\theta$ when plotted to the same scale as that for the transverse component would have a maximum radial coordinate of 1/100 of (r_s)max. The smaller amplitude of the P-wave results, in part, from the factor $(\beta/\alpha)^{5/2}$ affecting $\dot{u}_r$. The contours of equal velocity shown in Figs. 3.2.1a and 3.2.1b illustrate the radiation pattern and the directivity effects. The directivity effect is more pronounced for the transverse component (S-wave).

The relative importance of the starting phase with respect to the total response is examined in the following section.

Two-dimensional gliding edge fault models in a full space have been used to model the Parkfield 1966 earthquake (Niazy, 1973; Boore and Zoback, 1974a) and the San Fernando 1971 earthquake (Niazy, 1973; Boore and Zoback, 1974b).

BEST COPY AVAILABLE

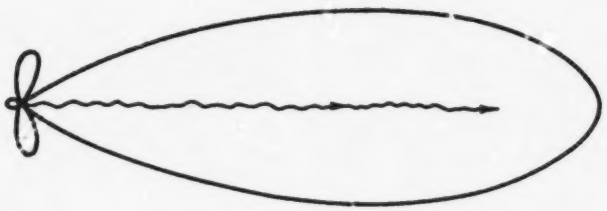

(a) $\dot{u}_\theta$ (S - wave)

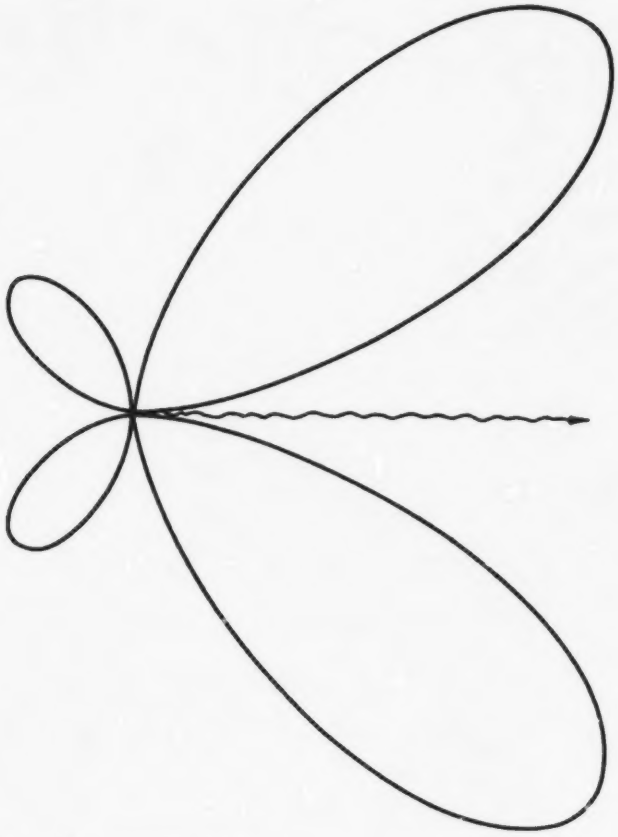

(b) $\dot{u}_r$ (P - wave)

Fig. 3.2.1 Contours of equal velocity for the transverse (S-wave) and radial (P-wave) components. The contour for the P-wave corresponds to an amplitude for $\dot{u}_r$ equal to 1/10 of $\dot{u}_\theta$ (α = 6.0 km/sec, β = 3.464 km/sec, v = 2.5 km/sec).

BEST COPY AVAILABLE

3.3 Decomposition of the Near-Source Ground Motion.

Aki and Richards (19800, p. 846) have noted that for small θ and for $t \sim x/v$ Eqs. (3.2.2) and (3.2.3) giving the total response for a starting dislocation reduce to the steady-state velocity field given by Eqs. (3.1.2a) and (3.1.2b), respectively. Thus, in the near-field region, the motion at the time of the passage of the rupture front is approximately given by the steady-state solution. On the other hand, for $t \sim r/\alpha$ and $t \sim r/\beta$ the total response reduces to the starting P- and S-phases. The relative importance of the starting P- and S- phases with respect to the passage-of-the-rupture front phase has been investigated by Niazy (1973), Boore and Zoback (1974a) and Luco and Sotiropoulos (1985). Niazy (1973), as part of a test of a solution for a two-dimensional gliding edge dislocation model of finite length, studied the effect of rupture velocity on the perpendicular component of displacement at a station at mid-length and essentially on the fault plane. He found that, in the subsonic case, the peak amplitude of the normal displacement component occurred at the time of passage of the rupture front. The results obtained by Zoback also indicate that the starting and stopping phases had amplitudes significantly lower than that of the pulse associated with passage of the rupture front. Boore and Zoback (1974a) studied the ground motion in the vicinity of a two-dimensional dipping fault model and concluded that the calculated phases could be grouped into starting and stopping phases and on a phase due to the accumulated effect of the propagating rupture. This phase would be distinguished by its relatively low-frequency content and by the lack of a specific arrival time.

Some typical results presented by Luco and Sotiropoulos (1985) for the comparison of the starting and steady-state dislocation models are illustrated in Figs. 3.3.1 and 3.3.2 for observers at locations x = 10 km, y = 1 km and x = 20 km, y = 1 km, respectively. In each Figure, the parallel $\dot{u}_x$ (bottom) and perpendicular $\dot{u}_y$ (top) velocity components for a starting (solid line) and a steady-state dislocation model (dashed line) are shown versus the reduced time $t - r/\alpha$. The characteristics of the model employed in the calculations are α = 6.0 km/sec, β = 3.464 km/sec, v = 2.5 km/sec and $\Delta\bar{u}$ = 100 cm. The starting P-phase is singular but characterized

BEST COPY AVAILABLE

by low strength. For $\theta = 0$ the starting P-phase is nodal in both components. The starting S-wave arriving at $t - r/\alpha = 1.23$ sec in Fig. 3.3.1 and at $t - r/\alpha = 2.44$ sec in Fig. 3.3.2 reveals a singularity of the type $(t - r/\beta)^{-1/2}$. The parallel u_z component of the starting S-wave is nodal at $\theta = 0$ explaining the relatively lower importance of the starting phase in that component. The rupture passage (RP) pulse is symmetric in the parallel u_z component and anti-symmetric in the perpendicular u_y component. The passage of the rupture occurs at time $t - r/\alpha = 2.33$ sec in Fig. 3.3.1 and at time $t - r/\alpha = 4.66$ sec in Fig. 3.3.2. The RP pulse is quite pronounced relative to the starting phases particularly at $\alpha = 20$ km, $y = 1$ km. Consideration of a non-instantaneous slip in the fault would further reduce the importance of the starting phases relative to the RP phase. Figs. 3.3.1 and 3.3.2 reveal that for $y = 1$ km and $x \geqslant 10$ km the RP phase can be calculated by use of the simpler steady-state dislocation model.

The studies of Zoback (1973), Boore and Zoback (1974a) and Luco and Sotiropoulos (1985) illustrate the importance and characteristics of the rupture passage phase and show that the motion in the near-source region can be written in the form

$$\begin{Bmatrix} \dot{u}_x \\ \dot{u}_y \end{Bmatrix} \approx \begin{Bmatrix} \dot{u}_{x1} \\ \dot{u}_{y1} \end{Bmatrix} + \begin{Bmatrix} \dot{u}_{x2} \\ \dot{u}_{y2} \end{Bmatrix} H\left(\cos\theta - \frac{v}{\beta}\right) \tag{3.3.1}$$

in which $(\dot{u}_{x1}, \dot{u}_{y1})$ corresponds to the starting phases given by Eq. (3.2.4) while $(\dot{u}_{x2}, \dot{u}_{y2})$ represents the rupture passage pulse given by Eqs. (3.1.3a) and (3.1.3b). The rupture passage pulse would be felt only within the wedge $\theta < \cos^{-1}(v/\beta)$.

A formal derivation of the approximate decomposition given by Eq. (3.3.1) can be obtained by a procedure similar to that used by Luco and Sotiropoulos (1985) for the corresponding anti-plane shear dislocation problem. An exact decomposition has been presented by Lund (1985).

BEST COPY AVAILABLE

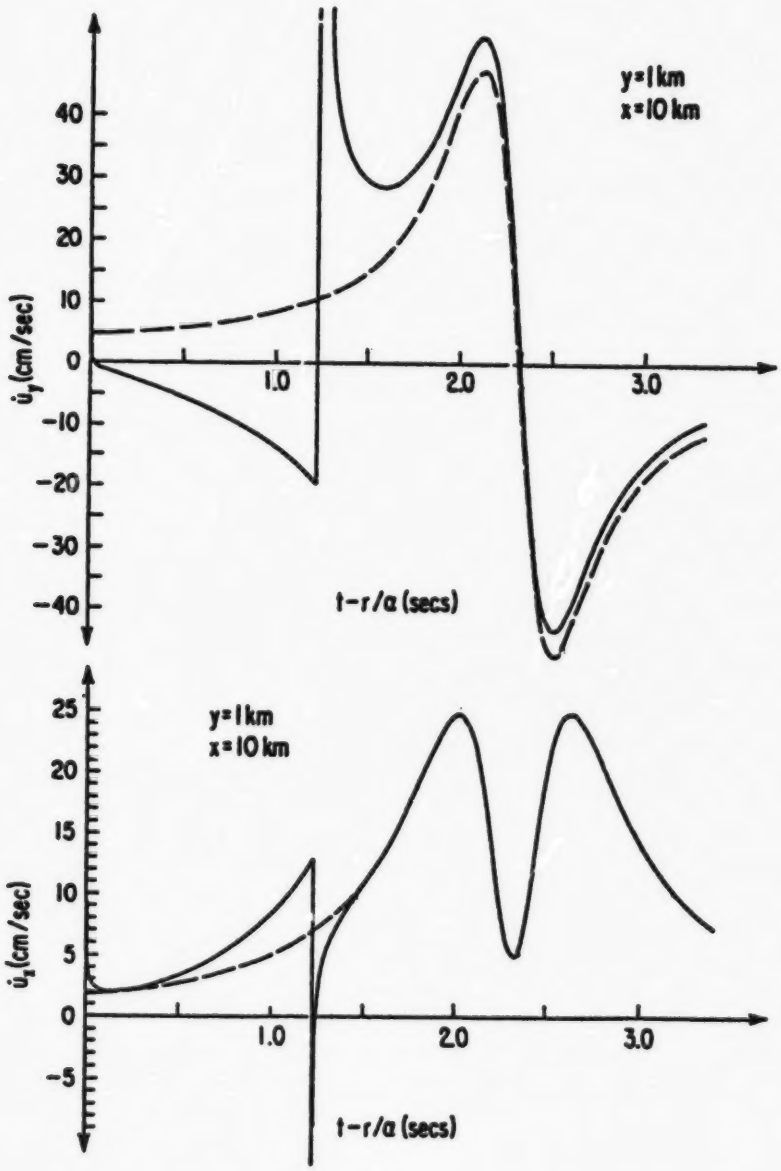

Fig. 3.3.1 Comparison of velocity pulses at y = 1 km and x = 10 km for steady-state (dashed lines) and starting (solid lines) gliding dislocation models. ($\Delta\bar{u}$ = 100 cm, α = 6.0 km/sec, β = 3.464 km/sec, ν = 2.5) km/sec (Luco and Sotiropoulos, 1985).

BEST COPY AVAILABLE

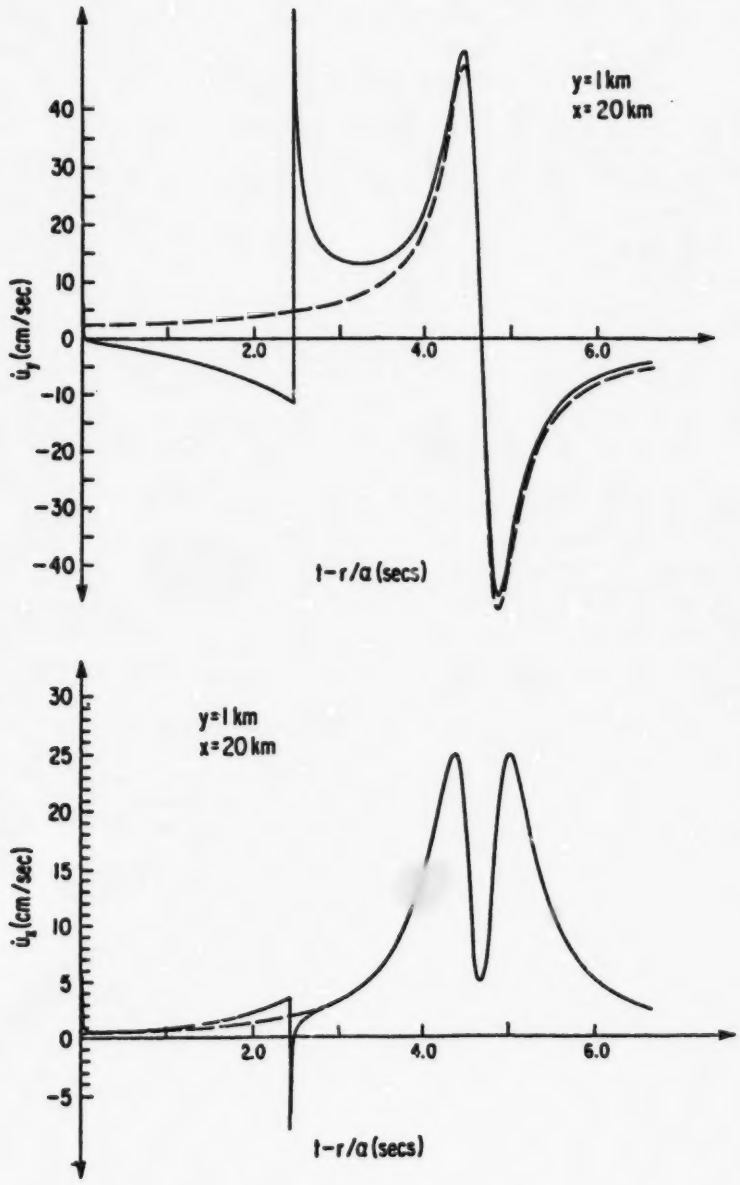

Fig. 3.3.2 Comparison of velocity pulses at $y = 1$ km and $x = 20$ km for the same models as in Fig. 3.3.1 (Luco and Sotiropoulos, 1985).

BEST COPY AVAILABLE

3.4 Plane-Strain Dislocation Models in a Half-Plane.

The earlier attempts at estimating the response of an elastic half-space to an infinitely long dipping thrust fault were based on the use of the solutions for a full space modified by a factor of two to approximately account for the free-surface effects. Boore and Zoback (1974a) tested this free-surface approximation by comparing the static two-dimensional solution for a dipping thrust fault in a half-space with that for a full space multiplied by a factor of two. The agreement was found to be encouraging, particularly for locations on the upper block. Based on such approximation, Boore and Zoback (1974a) studied the motion in the vicinity of a dipping thrust fault and concluded that the calculated phases could be associated with starting and stopping phases from the ends of the fault and to a phase due to the accumulated effect of the propagating rupture. This phase is characterized by a relatively low frequency content and by the lack of a specific arrival time; the best characteristic time appears to be the time of closest approach of the rupture front to the observation point. Boore and Zoback (1974a) found that the rupture passage phase is more critical on the hanging-wall side of the fault. They also found that the amplitude of the parallel component of motion (with respect to the fault) is somewhat larger on the upper block than at the same distance on the lower block. The amplitude of the normal component of motion shows less difference in amplitude with respect to side of the fault.

The response of a half-space to an infinitely long thrust fault with proper account of the free-surface effects has been studied by Mal (1972), Schafer (1973), Niazy (1975), Litehiser (1976), Bouchon and Aki (1977), Bouchon (1978a,b) and Madariaga (1980). Mal (1972) obtained the Rayleigh waves produced by a moving dip-slip fault of finite width and arbitrary dip embedded in a uniform half-space. Schafer (1973) used an integral representation in the frequency domain to obtain a complete solution. A closed-form solution for a step dislocation function was obtained by Niazy (1975) by use of the Cagniard-de Hoop method. Litehiser (1976) used the Cagniard-de Hoop method to obtain a closed-form solution for a fixed-line dislocation in a half-space and calculated the response for an extended thrust fault by numerical integration of the solution for a line source. Madariaga (1980), also using the Cagniard-de Hoop

BEST COPY AVAILABLE

technique, was able to obtain a simpler solution by representing a fault of finite width as the combination of two semi-infinite faults. Bouchon and Aki (1977) and Bouchon (1978a,b) utilized a discrete wavenumber representation to obtain the response of an infinitely long fault of finite width embedded in a layered half-space. In this method, the solution in the frequency domain is obtained as a series of waves propagating with discrete wavenumbers. The discretization of the solution is accomplished by assuming that the source is spatially periodic.

To gain some insight into the characteristics of the ground motion in the vicinity of an infinitely long thrust fault of finite width buried in an elastic half-space it is necessary to review in some detail the results obtained by the authors listed above. To start, we consider the work of Mal (1972) who studied the Rayleigh waves generated by a uniform dislocation moving on the fault model shown in Fig. 3.4.1. The rupture starts at the focus S and propagates with constant velocity on an inclined plane forming the angle δ with the horizontal plane until it intersects the free surface at S.

In particular, Mal (1972) found that for $x_1 \geq d$, the total Rayleigh wave motion corresponds to a forward-traveling wave of constant amplitude. For $x_1 \leq 0$, the situation is reversed and a backward-traveling Rayleigh wave of constant amplitude is obtained. For $\theta \neq 90°$, the amplitudes of the forward and backward traveling waves are not equal. Interference between forward and backward traveling surface waves is obtained at points of observation in the epicentral region OA. In particular, Mal (1972) wrote the horizontal component of the surface displacement in the form

$$U_1(x_1,0) = \begin{cases} \alpha_s\, e^{i\omega x_1/C_R} + \alpha_A\, e^{i\omega[l/c + (x_1 - d)/C_R]}, & x_1 > d \qquad (3.4.1) \\ \beta_s\, e^{-i\omega x_1/C_R} + \beta_A\, e^{i\omega[l/c + (d - x_1)/C_R]}, & x_1 < 0 \qquad (3.4.2) \\ \alpha_s\, e^{i\omega x_1/C_R} + \beta_A\, e^{i\omega[l/c + (d - x_1)/C_R]} + g(d - x_1)e^{i\omega x_1/c\cos\theta} & \qquad (3.4.3) \\ \qquad\qquad 0 < x_1 < d \end{cases}$$

BEST COPY AVAILABLE

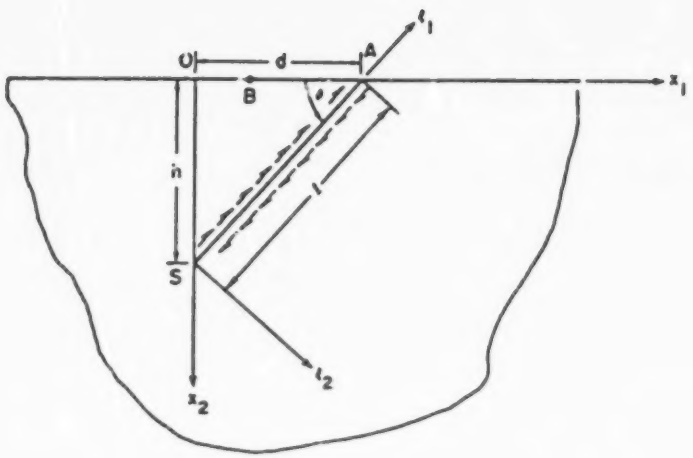

Fig. 3.4.1 Geometry of the two-dimensional thrust fault model considered by Mal (1972).

BEST COPY AVAILABLE

where

$$\alpha_s = -\alpha_1 e^{-\omega\eta_1 h} + \alpha_2 e^{-\omega\eta_2 h}$$

$$\beta_s = \beta_1 e^{-\omega\eta_1 h} - \beta_2 e^{-\omega\eta_2 h} \qquad (3.4.4)$$

$$\alpha_A = \alpha_1 - \alpha_2$$

$$\beta_A = -\beta_1 + \beta_2$$

$$g(x) = (\alpha_1 + \beta_1)e^{-\omega\eta_1 x\tan\theta} - (\alpha_2 + \beta_2)e^{-\omega\eta_2 x\tan\theta}$$

in which C_R is the Rayleigh wave speed, $\eta_1 = \sqrt{1/C_R - 1/\alpha^2}$, $\eta_2 = \sqrt{1/C_R^2 - 1/\beta^2}$ and α_1, α_2, β_1 and β_2 are functions of the frequency ω, the rupture velocity c, the dip angle θ and the slip on the fault. Mal (1972) points out that the terms associated with α_s and β_s correspond to waves generated at $t = 0$ at the focus S whereas the terms associated with α_A and β_A correspond to waves generated at the fault break A at $t = l/C$. The third term in the epicentral region $0 < x_1 < d$ is attributed by Mal (1972) to a virtual source located at the free-surface directly above the moving source.

Eqs. (3.4.4) indicate that at high frequencies ($\omega h/C_R >> 1$) the contributions from the focus are small. For $\omega(d - x_1)/c_R >> 1$ the contribution of the third term in Eq. (3.4.3) is also small. In summary, at high frequencies, the motion on the free surface, with the exception discussed next, is mainly produced by the fault break. The only exception is a zone above the fault and next to the fault break where the second and third terms in Eq. (3.4.3) contribute and interfere with each other. In this area severe modulation can exist. Mal (1972) also found that, at high frequency, the Rayleigh wave motion ahead of the fault ($x_1 > d$) is larger than that behind the epicentral region ($x_1 < 0$). The observed amplification depends on the orientation of the fault and on the rupture velocity.

Niazy (1975) obtained an extensive set of numerical results for the two-dimensional fault model shown in 3.4.2. The rupture starts at a depth of 14 km, propagates with constant rupture velocity on a fault plane inclined 52° with respect to the free surface and stops after

BEST COPY AVAILABLE

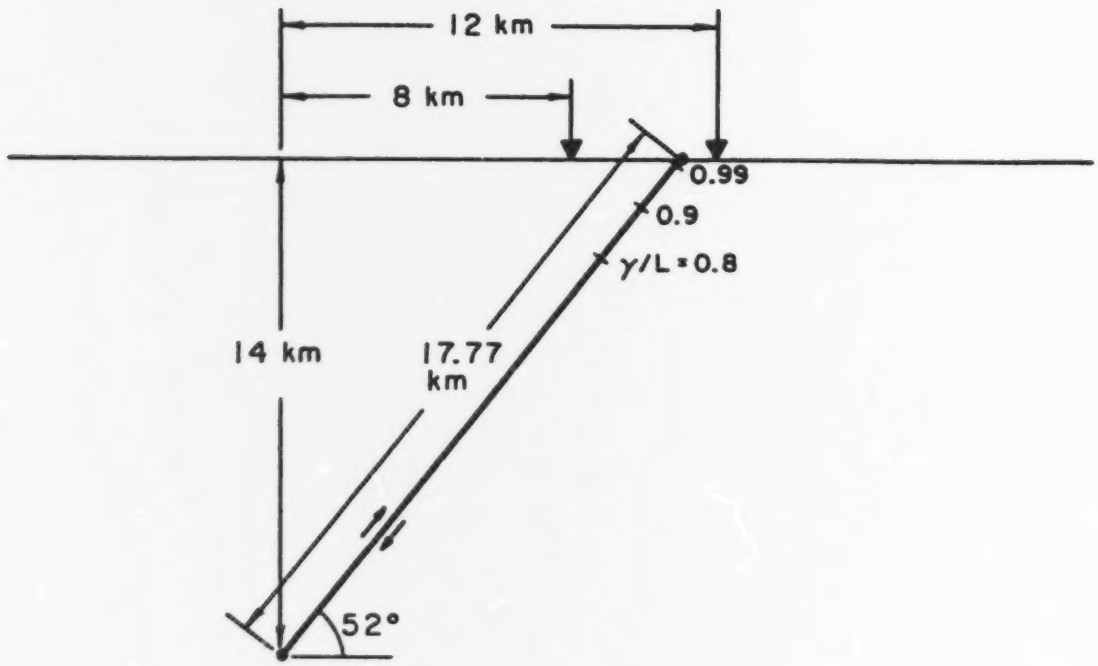

Fig. 3.4.2 Geometry of the two-dimensional thrust fault model considered by Niazy (1975).

BEST COPY AVAILABLE

having ruptured a length γ. Numerical results are presented for $\gamma = 0.8L = 14.22$ km, $\gamma = 0.9L = 15.99$ km and $\gamma = 0.99L = 17.59$ km where $L = 17.78$ km is the length of a fault which intersects the free surface. The half-space is characterized by $\alpha = 5.6$ km/sec and $\beta = 3.2$ km/sec and observers are located at $x = 8$ km and $x = 12$ km. Rupture velocities of $v = 2.5$ and 2.94 km/sec are considered. Some typical results obtained by Niazy (1975) illustrating a comparison of the response for a half-space (top two frames) with that for a full-space (lower two frames) are shown in Fig. 3.4.3 for $x = 8$ km, $\gamma = 0.99L$ and $v = 2.5$ km/sec. A first observation is that the long-period displacement amplitudes for the half-space are approximately twice as large as those for the full-space. To assist in the interpretation of the results we have added in the figures the arrival times P_o, S_o, P_1 and S_1 corresponding to the direct P- and S-waves from the starting (subscript zero) and stopping (subscript 1) points. In addition, we have also included a time designated RP corresponding to the time of passage of the rupture through the point on the fault closest to the station. The importance of the direct S-phase from the hypocenter (S_o) and of the rupture passage phase (RP) is clear in both the half- and full-space results. Niazy (1975) noted that for $\gamma > 0.9L$ a surface P (critically reflected SP) wave from the end point of the fault arrives at the station at $x = 8$ km. Also, the end of the records must include a Rayleigh wave emanating from the stopping end of the fault. Some of the high-frequency components appearing in the half-space results, such as the pulses arriving 1 and 4 sec after P_o, cannot be easily interpreted on the basis of the nominal values given for α and β, and, may be questionable. Niazy (1975) also found that increasing the rupture velocity shortens the length of the signal and increases the amplitudes of both components.

Numerical results for the two-dimensional fault model shown in Fig. 3.4.4 have been obtained by Niazy (1975) and Bouchon and Aki (1977). In this case, the rupture starts at a depth of 14 km, propagates with velocity $v_1 = 2.5$ km/sec on a plane forming an angle of 52° with the horizontal until it has ruptured a length of 11 km. At this point the rupture continues with velocity v_2 on a plane forming an angle of 40° with the horizontal. Niazy (1975) considered values of $v_2 = 1.5$ and 2.0 km/sec. Niazy (1975) stopped the rupture at about 120 m

BEST COPY AVAILABLE

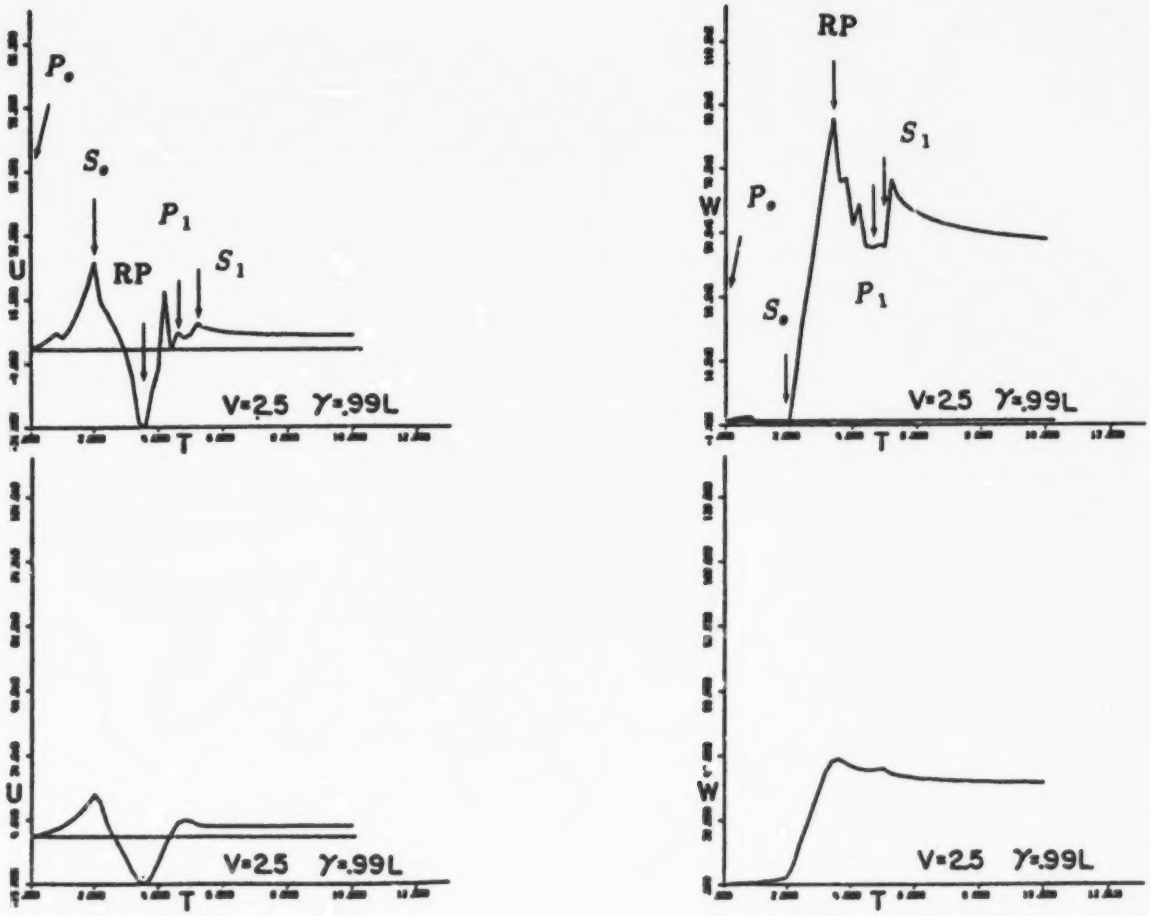

Fig. 3.4.3 Horizontal (left) and vertical (right) displacements for the configuration in Fig. 3.4.2. The upper frames correspond to a half-space, the lower frames to a full-space (v = 2.5 km/sec, γ = 0.99L) (after Niazy, 1975).

BEST COPY AVAILABLE

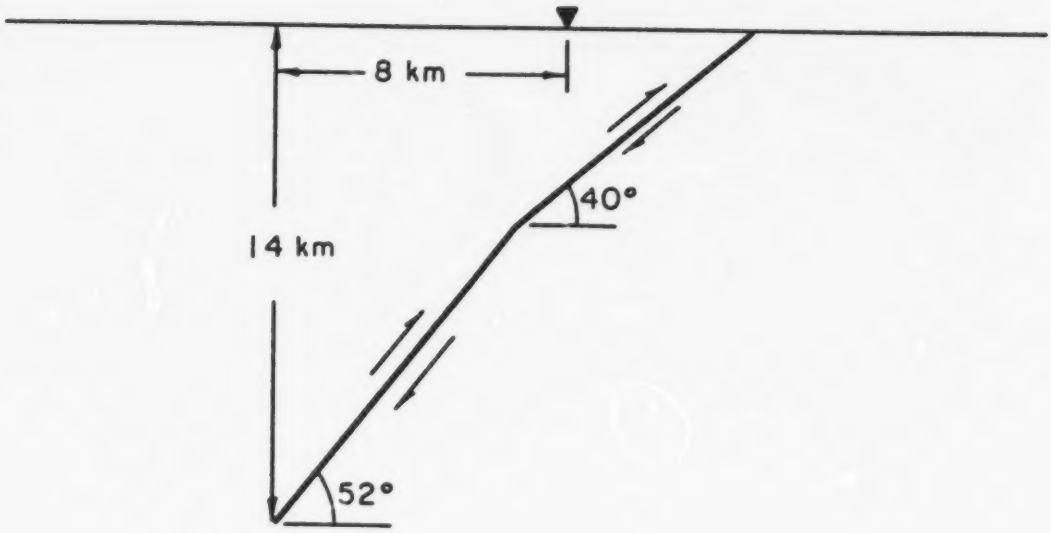

Fig. 3.4.4 Geometry of a two-dimensional fault model considered by Niazy (1975) and Bouchon and Aki (1977)

BEST COPY AVAILABLE

below the surface; Bouchon and Aki (1977) considered, in addition, the case in which the fault cuts the free surface. Some results obtained by Bouchon and Aki (1977) for a step dislocation with slip amplitude of 1 m in a medium characterized by α = 5.6 km/sec and β = 3.2 km/sec are shown in Fig. 3.4.5. The displacements shown include the cases of a full-space (left two frames) and a half-space (two frames on the right) for v_2 = 1.5 km/sec and for the rupture not intersecting the free-surface. The calculations include frequencies up to 10 Hz. Bouchon and Aki (1977) conclude that the vertical displacement waveform for the half-space bears much resemblance to the infinite medium solution and its amplitude is about twice as large. The horizontal component is comparatively more affected by the presence of the free surface, particularly around the time of arrival of the S wave from the break point of the fault (S_2). The solutions show strong S-waves from the hypocenter (S_1) and from the break point of the fault S_2 and also a Rayleigh wave from the upper end of the fault. The results obtained by Niazy (1975) for the same half-space geometry contain high-frequency pulses not apparent in the solution of Bouchon and Aki (1977). These authors attribute the differences to errors in the exact solution of Niazy (1975).

The accelerations calculated by Bouchon and Aki (1977) for the configuration shown in Fig. 3.4.4 for v_2 = 2.0 km/sec and the fault intersecting the free surface are shown in Fig. 3.4.6. The computed accelerations have been convolved with an instrument response and with a ramp source function with a rise time of 0.25 sec. The results obtained show strong acceleration pulses at the arrival of S-waves from the hypocenter (S_1) and breakpoint (S_2) of the fault and at the time of arrival of the Rayleigh wave from the point at which the fault intersects the free surface (R).

As part of a study on the importance of the surface P wave, Bouchon (1978a) calculated the motion in the vicinity of the two-dimensional thrust fault model shown in Fig. 3.4.7. The model which corresponds to the lower portion of the San Fernando earthquake fault model shown in Fig. 3.4.4 involves a rupture which starts at a depth of 14 km and propagates with a rupture velocity of v = 2.5 km/sec on a plane forming an angle of 52° with the horizontal

BEST COPY AVAILABLE

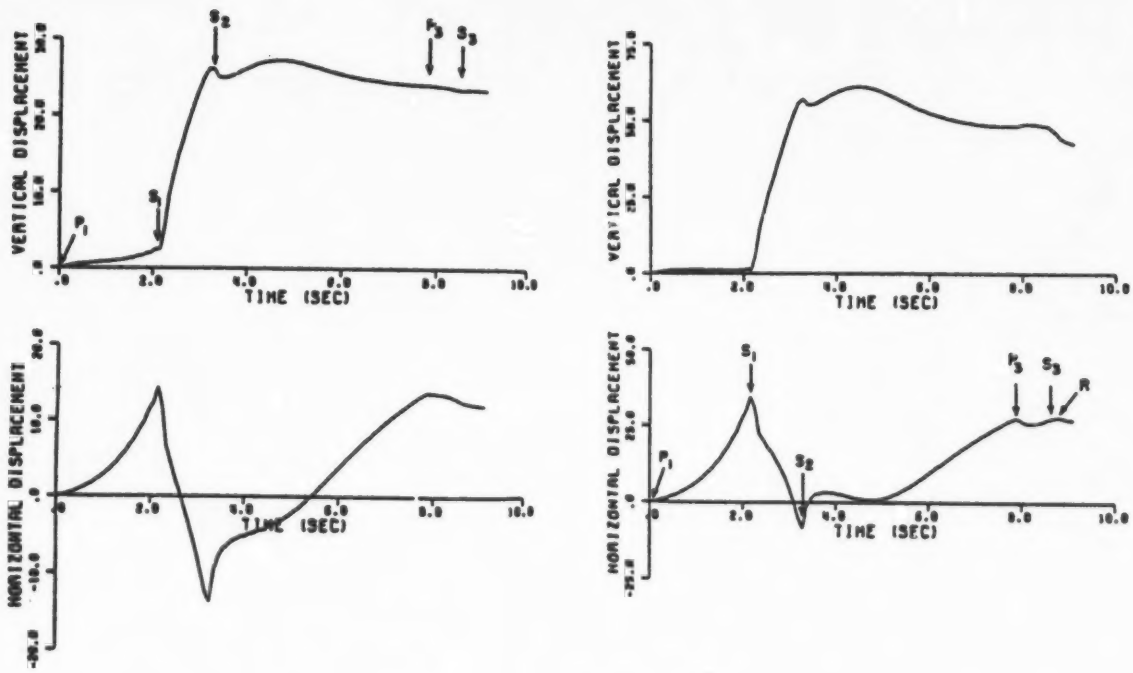

Fig. 3.4.5 Displacements (in centimeters) for a full-space (left) and a half-space (right) in the configuration shown in Fig.3.4.4. P_i, S_i indicate arrivals of P- and S-waves from the hypocenter (1), breakpoint of the fault (2) and upper tip (3). R denotes arrival of the Rayleigh wave from the upper tip of the fault. The fault does not extend to the free-surface and v = 1.5 km/sec (after Bouchon and Aki, 1977).

BEST COPY AVAILABLE

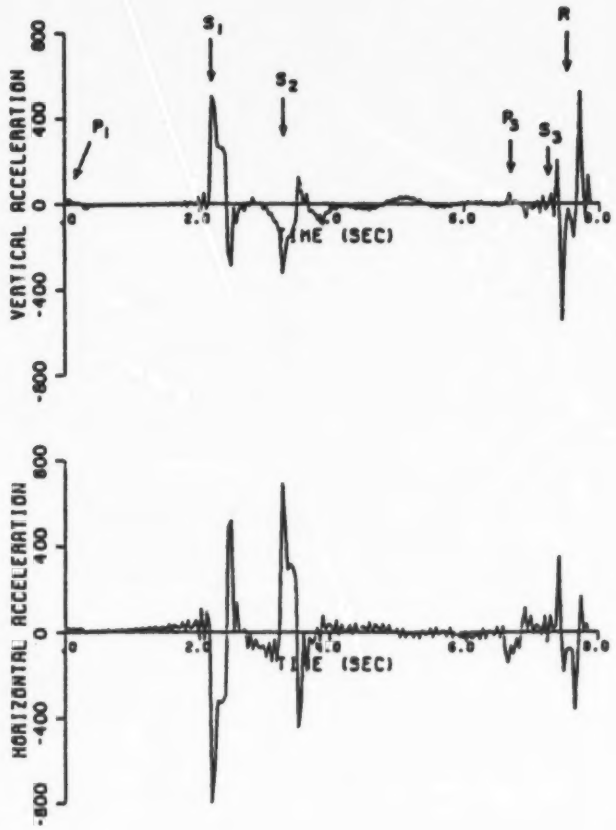

Fig. 3.4.6 Computed accelerations (in cm/sec^2) for the configuration in Fig. 3.4.4. The fault intersects the free surface and v = 2.0 km/sec. The response has been convolved with an instrument response and with a ramp source function with a rise time of 0.25 sec (after Bouchon and Aki, 1977).

BEST COPY AVAILABLE

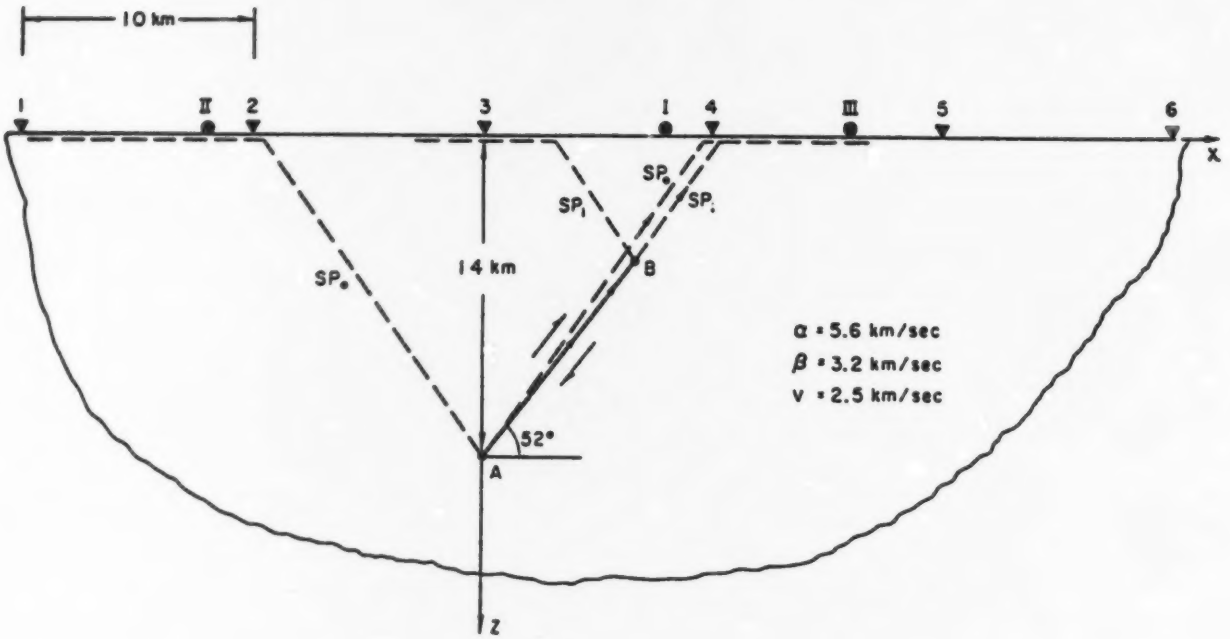

Fig. 3.4.7 Two-dimensional thrust fault model in a uniform half-space. The rupture starts at the lower point (A), propagates upward at velocity of 2.5 km/sec and stops at point B. The rupture length is 11 km. The rays associated with the arrivals of the *SP* starting and stopping phases are shown with segmented lines.

BEST COPY AVAILABLE

plane. The rupture stops after it has ruptured a length of 11 km. The stopping point is at a depth of 5.33 km. The projection of the fault on the free surface extends between $x = 0$ and $x = 6.77$ km and the extension of the fault breaks the free surface at $x = 10.94$ km. The medium corresponding to a uniform half-space is characterized by P-wave velocity $\alpha = 5.6$ km/sec and S-wave velocity $\beta = 3.2$ km/sec. The motion was calculated at the points numbered 1 through 6 which correspond to x = -20, -10, 0, 10, 20 and 30 km, respectively. The calculated horizontal (left column) and vertical (right column) displacement for a step dislocation as calculated by Bouchon (1978a) are shown in Fig. 3.4.8. The horizontal displacement is positive to the left while the vertical displacement is positive upwards. The arrival times of the P, SP and S starting (subscript 0) and stopping (subscript 1) phases are marked in Fig. 3.4.8. Each trace was normalized separately and consequently information as to the relative amplitudes at the various stations has been lost. The total duration of each trace is 10 seconds. The direction of the P and S first motions are consistent with the radiation patterns for the starting phases discussed in section 3.2. At locations where the SP wave arrives, the SP phase is the most pronounced feature of the horizontal motion time history. As expected, the vertical displacement is less affected by the SP phase. The regions were two, one or zero SP phases arrive are illustrated in Fig. 3.4.7. For $x < -9.75$ km and $x > 10.48$ both SP_0 and SP_1 arrive, for $-9.75 < x < 3.06$ km only SP_1 arrives, for $3.06 < x < 9.75$ km no SP phase arrives, and for $9.75 < x < 10.48$ only SP_0 arrives.

The velocity waveform at station 5 as calculated by Bouchon is shown in Fig. 3.4.9. The horizontal (left) and vertical (right) velocities have been normalized independently and include frequencies up to 10 Hz. The duration of the traces are 5 sec long. The velocities shown in Fig. 3.4 reveal the strong effect of the SP_0 and SP_1 phases on the horizontal motion at that station and the corresponding small effect on the vertical component.

Additional numerical results for the geometry described in Fig. 3.4.7 have been obtained by Madariaga (1980). The displacement time histories at $x = -12$ (point II in Fig. 3.4.7) and $x = 16$ km (point III in Fig. 3.4) normalized by the slip on the fault D, as calculated by

BEST COPY AVAILABLE

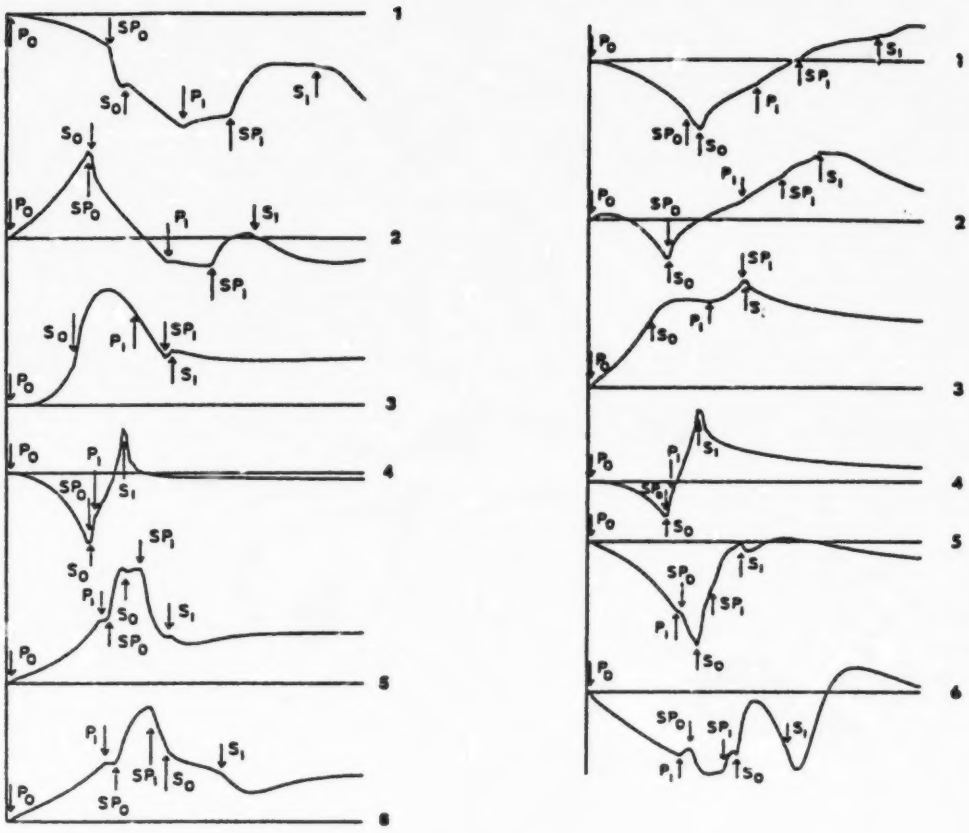

Fig. 3.4.8 Horizontal (left column) and vertical (right column) displacements at locations 1 through 6 for a step dislocation on the fault model shown in Fig. 3.4. Horizontal displacements are positive to the left (negative x), vertical displacements are positive upwards. The duration of the traces is 10 sec and each component is normalized independently (after Bouchon, 1978a).

BEST COPY AVAILABLE

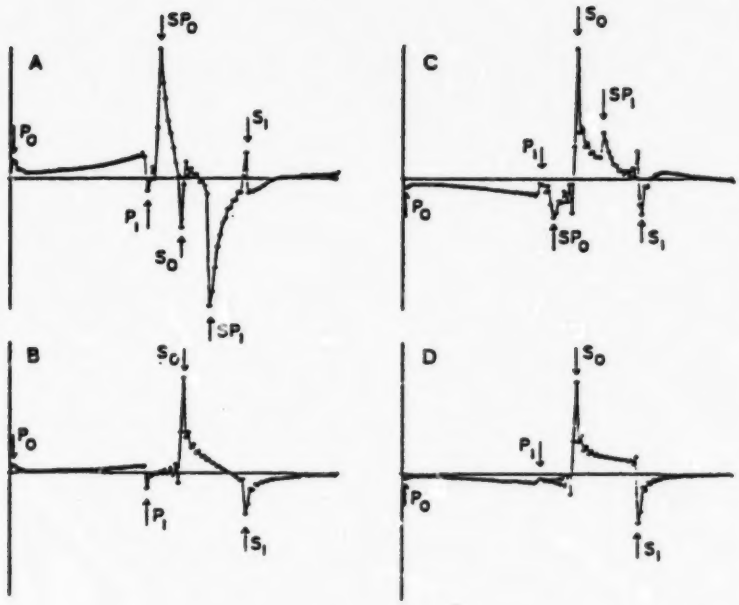

Fig. 3.4.9 Horizontal (A) and vertical (C) velocities at station 5 for a step dislocation on the fault model shown in Fig. 3.4.7. The traces are 5 sec long, have been normalized independently and the cutoff frequency is 10 Hz. The corresponding horizontal (B) and vertical (D) velocities in an infinite medium are also shown in the lower two frames (after Bouchon, 1978a).

BEST COPY AVAILABLE

Madariaga (1980), are shown in Fig. 3.4.10. The horizontal displacement is positive to the right and the vertical displacement is positive upwards. The results shown reveal strong S_e and SP_1 phases. The displacement field at several locations in the region from $x = -10$ km to $x = 20$ km, as obtained by Madariaga (1980), is shown in Fig. 3.4.11. The effects of directivity corresponding to larger amplitudes and shorter durations in the direction of the rupture (positive x) can be clearly seen. In addition, the decay of amplitudes away from the vicinity of the fault can also be seen.

The effects of the free surface of the half-space have been described on the basis of the results obtained by Niazy (1975) and Bouchon and Aki (1977). Additional comparisons presented by Bouchon (1978a) for the displacement and velocities for the configuration in Fig. 3.4.7 are shown in Fig. 3.4.9 and 3.4.12. The results are for station 5 and show that doubling the amplitude of the infinite medium displacements yields a reasonably good approximation to the half-space solution. The waveform of the vertical displacement is only slightly affected by the presence of the free surface. The horizontal displacement is more strongly affected. The two wave forms have some common characteristics, but they are shifted in time. The SP wave plays the role which was ascribed to the direct shear wave in the infinite medium solution.

BEST COPY AVAILABLE

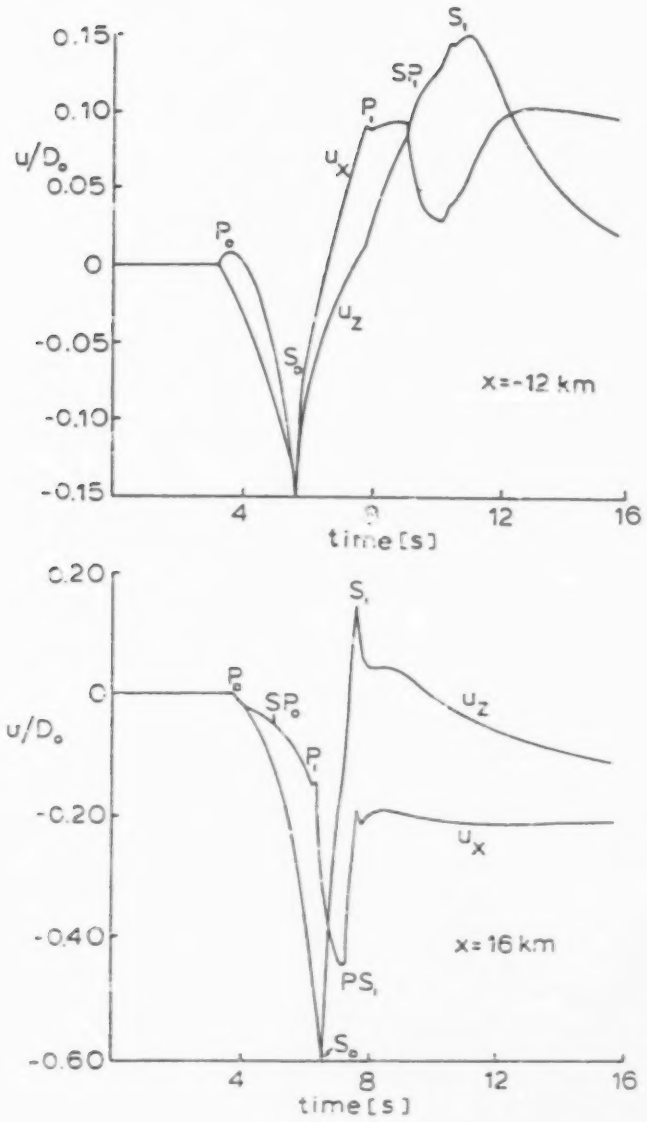

Fig. 3.4.10 Normalized displacements at $x = -12$ km (point II) and $x = 16$ (point III) for a step dislocation on the fault model shown in Fig. 3.4.7. The displacements are normalized by the slip D_0 on the fault (after Madariaga, 1980).

BEST COPY AVAILABLE

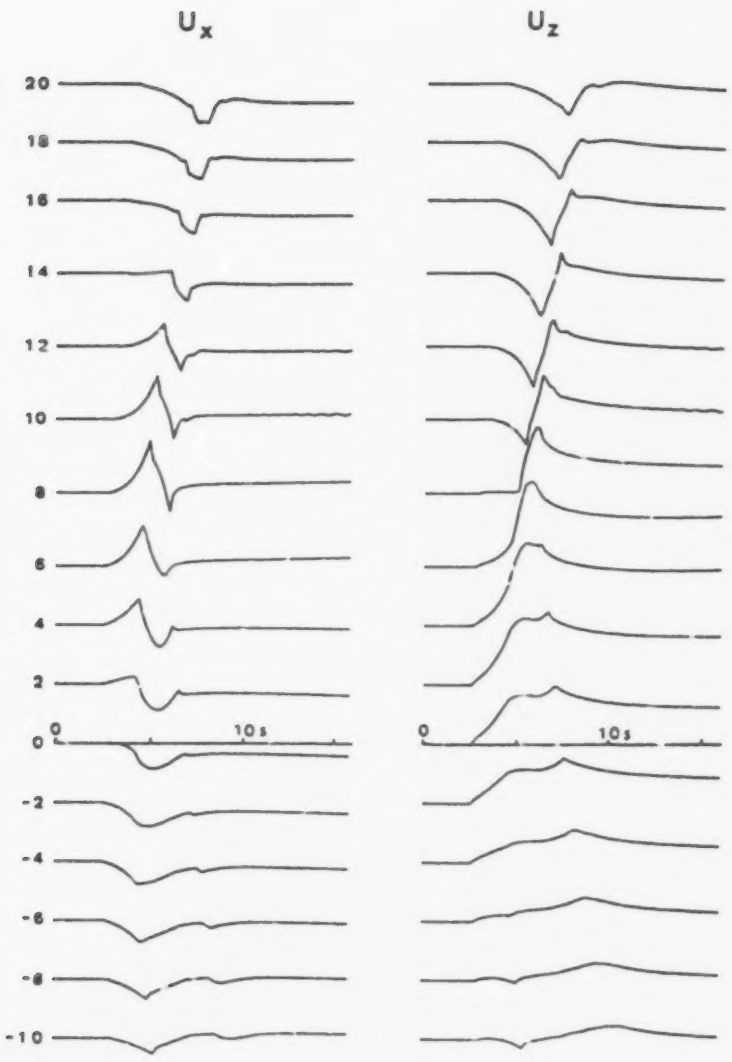

Fig. 3.4.11 Horizontal and vertical displacements at stations in the range from $x = -10$ km to $x = 20$ km for the fault model shown in Fig. 3.4.7. (after Madariaga, 1980).

BEST COPY AVAILABLE

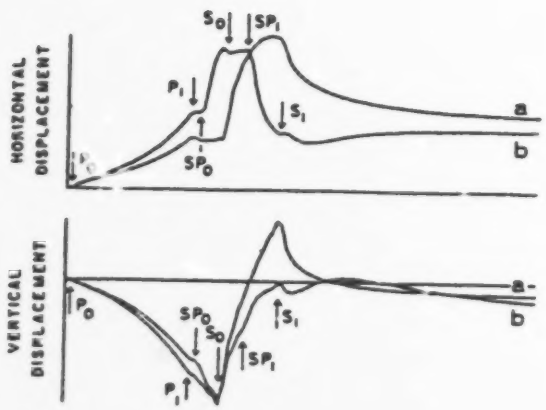

Fig. 3.4.12 Comparison of the horizontal (upper part) and vertical (lower part) displacements obtained for an infinite medium (a) and for a half space (b). The amplitude of the infinite medium has been doubled. The results are for station 5 in the configuration shown in Fig. 3.4.7 (after Bouchon, 1978a).

BEST COPY AVAILABLE

3.5 Comparison of Two- and Three-Dimensional Models

Comparisons of two-dimensional and three-dimensional models have been presented by Boore and Zoback (1974a) and Gelier (1976). Boore and Zoback (1974a) compared the three-dimensional solution of Haskell (1969) for a vertical strike-slip fault with a solution for a two-dimensional gliding dislocation model of finite length and concluded that the effect of a finite fault width influences the amplitude but not the shape of the wave forms for stations reasonably close to the fault. Geller (1974) conducted similar comparisons and found exact agreement until the arrival of P-waves from the finite width of the three-dimensional model. Further comments on the relationship between 2-D and 3-D solutions are given in Chapter 5.

BEST COPY AVAILABLE

3.6 Conclusions

The characteristics of the near-source ground motion as calculated by use of two-dimensional plane-strain dislocation models can be summarized as follows:

1(i) The motion in the vicinity of a starting plane-strain dislocation model in a full-space can be decomposed into starting phases emanating from the starting point of the fault and a rupture passage phase which is observed within the wedge $\theta <$ arc $\cos(v/\beta)$.

1(ii) For a step dislocation the velocity starting phases have singularities of the type $(t - r/\alpha)^{-1/2}$ and $(t - r/\beta)^{-1/2}$ at the time of arrival of P- and S-waves from the starting point. The radial and tangential component of the starting phases are characterized by radiation patterns $\sin 2\theta$ and $\cos 2\theta$, respectively, and are affected by directivity factors of the type $[1 - (v/\alpha)\cos\theta]^{-1}$ and $[1 - (v/\beta)\cos\theta]^{-1}$. The amplitudes of the starting phases are strongly affected by the character of the source-time function; the introduction of a non-zero rise time, for example, eliminates the singularity of the starting velocities obtained for a step dislocation.

1(iii) Close to the fault and away from the starting point, the rupture passage phase is very pronounced and can be calculated from a steady-state dislocation model. For a step dislocation the peak velocity and peak acceleration of the rupture passage phase (in the subsonic case) decay with distance to the fault as y^{-1} and y^{-2}, respectively. For a finite ramp dislocation with non-zero rise-time the decay of peak velocity with distance to the fault is also of the type y^{-1} for $y >> v\tau$ but is less pronounced for $y << v\tau$. In the subsonic case, the rupture passage phase can be written in terms of a nonhomogeneous plane wave and, consequently, the spectra of the velocity components for a step dislocation decay exponentially with frequency.

2(i) In the vicinity of a two-dimensional dipping dislocation fault model in an elastic half-space, the total ground motion includes: (a) starting and stopping body waves emanating

BEST COPY AVAILABLE

from the beginning and end of the fault, (b) critically reflected SP-waves originating from the beginning and end of the fault, (c) Rayleigh waves and (d) a rupture passage phase.

2(ii) The starting and stopping phases are dominated by the direct S-waves from the beginning and end of the fault.

2(iii) At high frequencies, the Rayleigh waves felt are generated at the upper end of the fault. Rayleigh waves generated at depth are attenuated and, at high frequencies, contribute little to the surface ground motion.

2(iv) The rupture passage phase can be observed on the region above the fault and is more pronounced close to the upper end of the fault.

2(v) In regions of the free-surface where critically reflected SP waves from the beginning and end of the fault are received, these waves contribute significantly, particularly, to the horizontal ground motion.

2(vi) Break points of the fault surface also generate P, S and SP waves.

3(i) Comparison of the solutions for a half-space with those for a full-space indicate that doubling the amplitudes of the results for the full-space leads to a reasonable approximation to the results for the half-space. The major deviations result from the appearance of SP and Rayleigh waves in the half-space solution.

BEST COPY AVAILABLE

8.7 References.

Aki, K. and P. G. Richards (19800). *Quantitative seismology: Theory and methods*, Vol. II, W. H. Freeman and Co., San Francisco.

Ang, D. D. and M. L. Williams (1959). The dynamic stress field due to an extensional dislocation, Midwestern Conference on Solid Mechanics, 4th, University of Texas, Austin, TX.

Boore, D. M., K. Aki and T. Todd (1971). A two-dimensional moving dislocation model for a strike slip fault, *Bull. Seism. Soc. Am.* 61, 133-138.

Boore, D. M. and M. D. Zoback (1974a). Near-field motions from kinematic models of propagating faults, *Bull. Seism. Soc. Am.* 64, 321-342.

Boore, D. M. and M. D. Zoback (1974b). Two-dimensional fault modeling of the Pacoima Dam strong-motion recordings of February 9, 1971, San Fernando earthquake, *Bull. Seism. Soc. Am.* 64, 555-570.

Bouchon, M. and K. Aki (1977). Discrete wave-number representation of seismic-source wave fields, *Bull. Seism. Soc. Am.* 67, 259-277.

Bouchon, M. (1978a). The importance of the surface or interface P wave in near-earthquake studies, *Bull. Seism. Soc. Am.* 68, 1293-1311.

Bouchon, M. (1978b). A dynamic crack model for the San Fernando earthquake, *Bull. Seism. Soc. Am.* 68, 1555-1576.

Eshelby, J. D. (1949). Uniformly moving dislocations, *Proc. Phys. Soc.* (London) A62, 307-314.

Geller, R. J. (1974). Representation theorems for an infinite shear fault, *Geophys. J. R. astr. Soc.* 39, 123-131.

Kiusalaas, J. and T. Mura (1964). On the elastic field around an edge dislocation with applications to dislocation vibration, *Phil Mag.* 97, 1-8.

Luco, J. E. and D. A. Sotiropoulos (1985). On a decomposition of near-source earthquake motion *Soil Dynamics and Earthquake Engineering, 4*, 210-220.

BEST COPY AVAILABLE

Litehiser, J. J. (1976). Near-field seismograms from a two-dimensional propagating dislocation, *Ph.D. Thesis*, University of California, Berkeley, CA.

Lund, F. (1985). A note on the synthesis of near field ground motion (submitted for publication).

Madariaga, R. (1980). A finite two-dimensional kinematic fault in a half-space, *Publ. Inst. Geophys. Pol. Acad. Sci.*, A-10(42), 33-47.

Mal, A. K. (1972). Rayleigh waves from a moving thrust fault, *Bull. Seism. Soc. Am.* 62, 751-762.

Niazy, A. (1973). Elastic displacements caused by propagating crack in an infinite medium: an exact solution, *Bull. Seism. Soc. Am.* 63, 357-379.

Niazy, A. (1975). An exact solution for a finite, two-dimensional moving dislocation in an elastic half-space with application to the San Fernando earthquake of 1971, *Bull. Seism. Soc. Am.* 65, 1797-1826.

Schafer, J. (1973). Strong ground motion from dip-slip faulting, *M.S. Thesis*, Dept. of Mechanics and Structures, University of California, Los Angeles, CA.

Sotiropoulos, D. A. (1983). On synthesis of ground motions from earthquakes, *Ph.D. Thesis*, University of California, San Diego, La Jolla, CA.

BEST COPY AVAILABLE

4. THREE-DIMENSIONAL MODELS

4.0 Introduction.

The near-source ground motion resulting from dislocation models in a uniform, elastic, full-space, and, in uniform and layered half-spaces has been the subject of numerous investigations. These models attempt to give more realistic representations than the two-dimensional anti-plane and plane-strain models described in Chapters 2 and 3. The most complex models of this type include a fault surface consisting of one or more planes and involve variable distributions of slip and rupture velocity over the fault and a propagation medium represented as a multilayered elastic or viscoelastic half-space. These complex models are required to obtain realistic quantitative estimates of ground motion and to solve the inverse problem giving the rupture process consistent with a set recorded ground motions. Much can be gained, however, by examination of simpler dislocation models in a three dimensional medium.

Some of the models considered are illustrated in Fig. 4.0.1. The simplest model corresponds to a steady-state dislocation of finite width in an unbounded elastic medium (Fig. 4.0.1a). The other models, in order of increasing complexity, correspond to strike-slip (Fig. 4.0.1b), dip-slip (Fig. 4.0.1c) and opening dislocation models on a finite fault in a uniform full space. Models in a half-space include steady-state dislocation models (Fig. 4.0.1d) and finite fault models with rectilinear (Fig. 4.0.1e) and curvilinear (Fig. 4.0.1f) rupture fronts as well as faults in multi-layered media (Fig. 4.0.1.g). The characteristic of the near-source ground motion for these various models are described in the rest of this chapter.

BEST COPY AVAILABLE

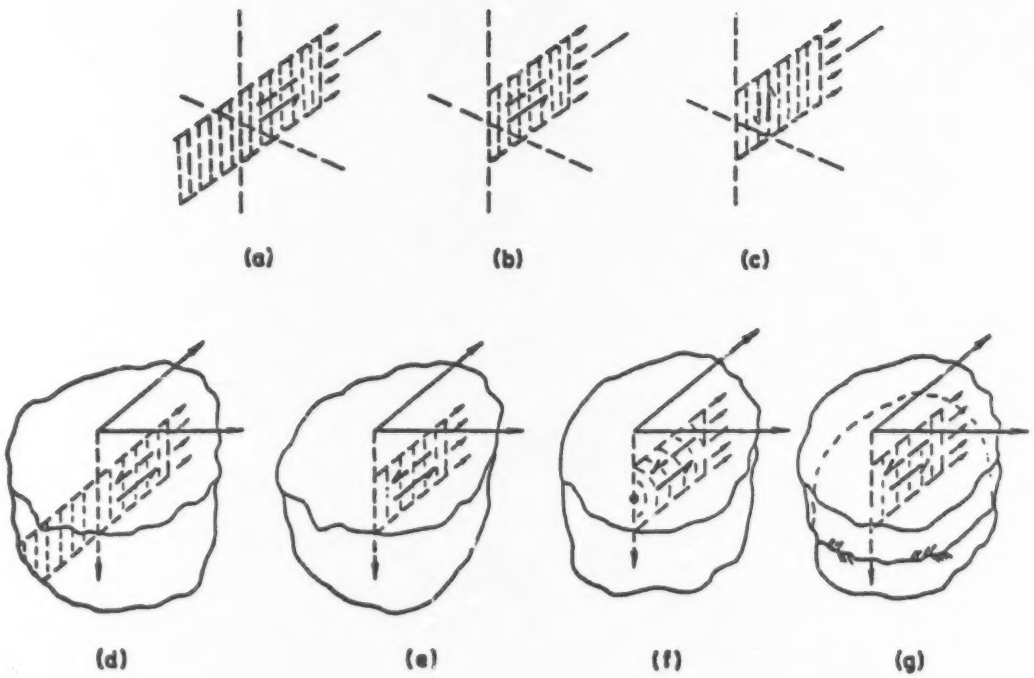

Fig. 4.0.1 Dislocation models in three-dimensional media.

BEST COPY AVAILABLE

4.1 Steady-State Dislocation Model in a Full-Space

The simplest three-dimensional dislocation model in a uniform unbounded elastic medium corresponds to a uniform steady-state dislocation contained in the half- plane $z = 0$, $y < 0$ (Fig. 4.1.1) and described by

$$\begin{aligned} u_x(x,y,0^+,t) - u_x(x,y,0^-,t) &= \Delta\bar{u}_x H(-y) H(t - \frac{x}{v}) \\ u_y(x,y,0^+,t) - u_y(x,y,0^-,t) &= \Delta\bar{u}_y H(-y) H(t - \frac{x}{v}) \\ u_z(x,y,0^+,t) - u_z(x,y,0^-,t) &= \Delta\bar{u}_z H(-y) H(t - \frac{x}{v}) \end{aligned} \tag{4.1.1}$$

in which $(\Delta\bar{u}_x, \Delta\bar{u}_y)$ is the slip in the fault plane, $\Delta\bar{u}_z$ is the opening in the z-direction and v is the rupture velocity. The rupture front corresponding to the semi-infinite line $x = vt$, $y < 0, z = 0$ starts from $x = -\infty$ at $t = -\infty$ and moves with constant rupture velocity v so that at time t it is at the position $x = vt$. The uniform dislocation is assumed to have a step time dependence.

The response at any point in the unbounded elastic medium to this steady-state dislocation can be obtained by a variation of the Cagniard-deHoop technique. In particular, for a subsonic $(v < \beta < \alpha)$ strike-slip dislocation $\Delta\bar{u}_y = \Delta\bar{u}_z = 0$, the particle velocity vector $\{\dot{U}\}$ can be written in the form (Luco and Georgevich, 1986)

$$\{\dot{U}\} = \{\dot{U}_I\} H(-y) + \{\dot{U}_{II}\} \tag{4.1.2}$$

in which $\{\dot{U}_I\}$ and $\{\dot{U}_{II}\}$ are functions of $(t - \frac{x}{v})$. The term $\{\dot{U}_I\}$ for $x = 0$ is given by

$$\begin{Bmatrix} \dot{U}_{xI}(0,y,z,t) \\ \dot{U}_{yI}(0,y,z,t) \\ \dot{U}_{zI}(0,y,z,t) \end{Bmatrix} = -\frac{\Delta\bar{u}_x}{\pi} \left(\frac{\beta}{v}\right)^2 \begin{Bmatrix} \left[-\dfrac{(z\gamma_\alpha/v)}{t^2 + (z\gamma_\alpha/v)^2} + \dfrac{(1+\gamma_\beta^2)(z\gamma_\beta/v)}{2[t^2 + (z\gamma_\beta/v)^2]} \right] \\ O \\ \left[-\dfrac{\gamma_\alpha t}{t^2 + (\gamma_\alpha z/v)^2} + \dfrac{(1+\gamma_\beta^2)t}{2\gamma_\beta[t^2 + (z\gamma_\beta/v)^2]} \right] \end{Bmatrix} \tag{4.1.3}$$

where

BEST COPY AVAILABLE

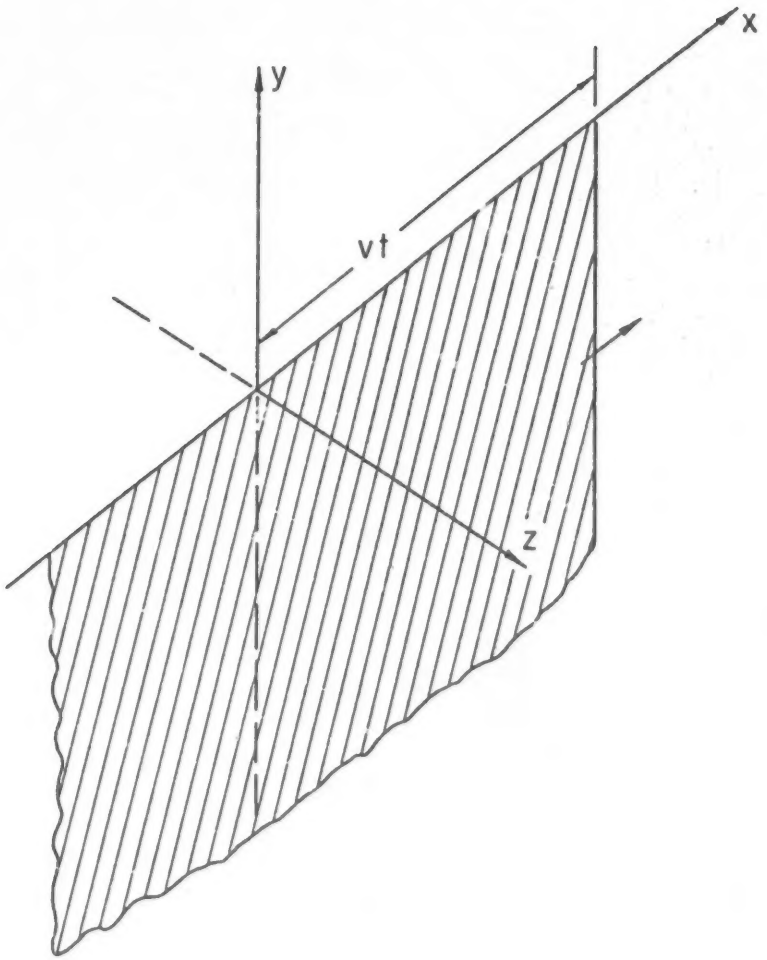

Fig. 4.1.1 Steady-state dislocation model in an unbounded elastic medium.

BEST COPY AVAILABLE

$$\gamma_\alpha = \sqrt{1 - (v/\alpha)^2} \ , \ \gamma_\beta = \sqrt{1 - (v/\beta)^2} \ . \tag{4.1.4}$$

The term $\{\dot{U}_I\}$ depends only on z and t and corresponds exactly to the two-dimensional response when the rupture front extends from $y = +\infty$ to $y = -\infty$. As indicated by Eq. (4.1.2), the term $\{\dot{U}_I\}$ appears only in the half-space in front of the fault ($y < 0$).

The term $\{\dot{U}_{II}(0,y,z,t)\}$ is given by

$$\{\dot{U}_{II}\} = \{\dot{U}_o\} + \frac{1}{2}\, sgn\,(y)\{\dot{U}_I\} \tag{4.1.5}$$

in which

$$\dot{U}_{zo} = -\frac{\Delta\bar{U}_z}{2\pi}\left(\frac{\beta}{v}\right)^2\left(\frac{v}{r}\right)\left[\frac{\gamma_\alpha^2}{\sqrt{\tau^2+\gamma_\alpha^2}\,(\tau^2+\gamma_\alpha^2\sin^2\theta)} - \frac{(1+\gamma_\beta^2)\gamma_\beta^2}{2\sqrt{\tau^2+\gamma_\beta^2}\,(\tau^2+\gamma_\beta^2\sin^2\theta)}\right]\sin\theta\cos\theta$$

$$\dot{U}_{yo} = -\frac{\Delta\bar{U}_z}{2\pi}\left(\frac{\beta}{v}\right)^2\left(\frac{v}{r}\right)\left[-\frac{1}{\sqrt{\tau^2+\gamma_\alpha^2}} + \frac{1}{\sqrt{\tau^2+\gamma_\beta^2}}\right]\tau\sin\theta \tag{4.1.6}$$

$$\dot{U}_{zo} = -\frac{\Delta\bar{U}_z}{2\pi}\left(\frac{\beta}{v}\right)^2\left(\frac{v}{r}\right)\left[\frac{\tau^2+\gamma_\alpha^2(1+\sin^2\theta)}{\sqrt{\tau^2+\gamma_\alpha^2}\,(\tau^2+\gamma_\alpha^2\sin^2\theta)} - \frac{\tau^2+(1+\sin^2\theta)\,\gamma_\beta^2+\frac{1}{2}(1-\gamma_\beta^2)}{\sqrt{\tau^2+\gamma_\beta^2}(\tau^2+\gamma_\beta^2\sin^2\theta)}\right]\tau\cos\theta$$

In Eq. (4.1.6), $\tau = (vt/r)$, $\sin\theta = z/r$, $\cos\theta = y/r$ and $r = \sqrt{y^2+z^2}$. The term $\{\dot{U}_{II}\}$ depends on r, θ and, $(t - \frac{x}{v})$, and corresponds to waves radiated by the edge of the fault (x-axis). These waves decay as r^{-1}. Some of the components of the particle velocity field $\{\dot{U}_{II}\}$ are discontinuous on the plane $y = 0(\theta = \frac{\pi}{2})$; the total field given by Eq. (4.1.2), however, is continuous across that plane.

The type of velocity pulses obtained in the vicinity of the fault plane are shown in Fig. 4.1.2 which illustrates the three components of particle velocity as a function of time for observers at $x = 0$, $y = \pm$ 2 km, $z = 2$ km. The results shown correspond to the case of a step strike-slip dislocation with $\Delta\bar{U}_z = 100$ cm and $v = 2.5$ km/sec in a medium characterized by $\alpha = 6.0$ km/sec and $\beta = 3.464$ km/sec. The results in Fig. 4.1.2 show that the longitudinal

BEST COPY AVAILABLE

(x and transverse (z components of velocity at $x = 0$, $y = -2$ km, $z = 2$ km, i.e. in front of the faulted area, are significantly stronger than the corresponding components at $x = 0$, $y = 2$ km, $z = 2$ km. These components have the same pulse shapes as obtained in two-dimensional plane-strain models. The y-component of velocity at $y = 2$ km is equal to the corresponding component at $y = -2$ km.

Contours of equal peak amplitude for the x, y, and z components of velocity on a plane transverse to the fault (yz-plane) are shown in Fig. 4.1.3 for the same parameters listed above. These results also show that larger amplitudes are obtained in the region in front of the fault ($y < 0$).

In the case of a subsonic ($v < \beta < \alpha$) dip-slip dislocation ($\Delta\bar{U}_x = \Delta\bar{U}_z = 0$), the total particle velocity vector at $x = 0$ is also given by Eqs. (4.1.2) and (4.1.5). In this case,

$$\begin{Bmatrix} \dot{U}_{xI}(0, y, z, t) \\ \dot{U}_{yI}(0, y, z, t) \\ \dot{U}_{zI}(0, y, z, t) \end{Bmatrix} = \frac{\Delta\bar{U}_y}{2\pi} \begin{Bmatrix} 0 \\ 1 \\ 0 \end{Bmatrix} \frac{(z\gamma_\beta/v)}{t^2 + (z\gamma_\beta/v)^2} \tag{4.1.7}$$

and

$$\dot{U}_{xo} = -\frac{\Delta\bar{U}_y}{2\pi}\left(\frac{\beta}{v}\right)^2\left(\frac{v}{r}\right)\left[-\frac{1}{\sqrt{\tau^2+\gamma_\alpha^2}} + \frac{1}{\sqrt{\tau^2+\gamma_\beta^2}}\right]\tau\sin\theta$$

$$\dot{U}_{yo} = -\frac{\Delta\bar{U}_y}{2\pi}\left(\frac{\beta}{v}\right)^2\left(\frac{v}{r}\right)\left[-\frac{2\tau^2+\gamma_\alpha^2}{\sqrt{\tau^2+\gamma_\alpha^2}} + \frac{2\tau^2+\gamma_\beta^2}{\sqrt{\tau^2+\gamma_\beta^2}} + \frac{\gamma_\beta^2(1-\gamma_\beta^2)}{2\sqrt{\tau^2+\gamma_\beta^2}\,(\tau^2+\gamma_\beta^2\sin^2\theta)}\right]\sin\theta\cos\theta$$

$$\dot{U}_{zo} = -\frac{\Delta\bar{U}_y}{2\pi}\left(\frac{\beta}{v}\right)^2\left(\frac{v}{r}\right)\left[\frac{\tau^2\cos2\theta + \gamma_\alpha^2\cos^2\theta}{\sqrt{\tau^2+\gamma_\alpha^2}} - \frac{1+(2\tau^2+\gamma_\beta^2)\cos2\theta}{2\sqrt{\tau^2+\gamma_\beta^2}}\right] \tag{4.1.8}$$

The term $\{\dot{U}_I\}$ corresponds exactly to the solution of the two-dimensional anti-plane dislocation model in which the rupture front extends from $y = -\infty$ to $y = +\infty$. The term $\{\dot{U}_{II}\}$ represents, again, the effect of the edge (x-axis) of the semi-infinite fault.

BEST COPY AVAILABLE

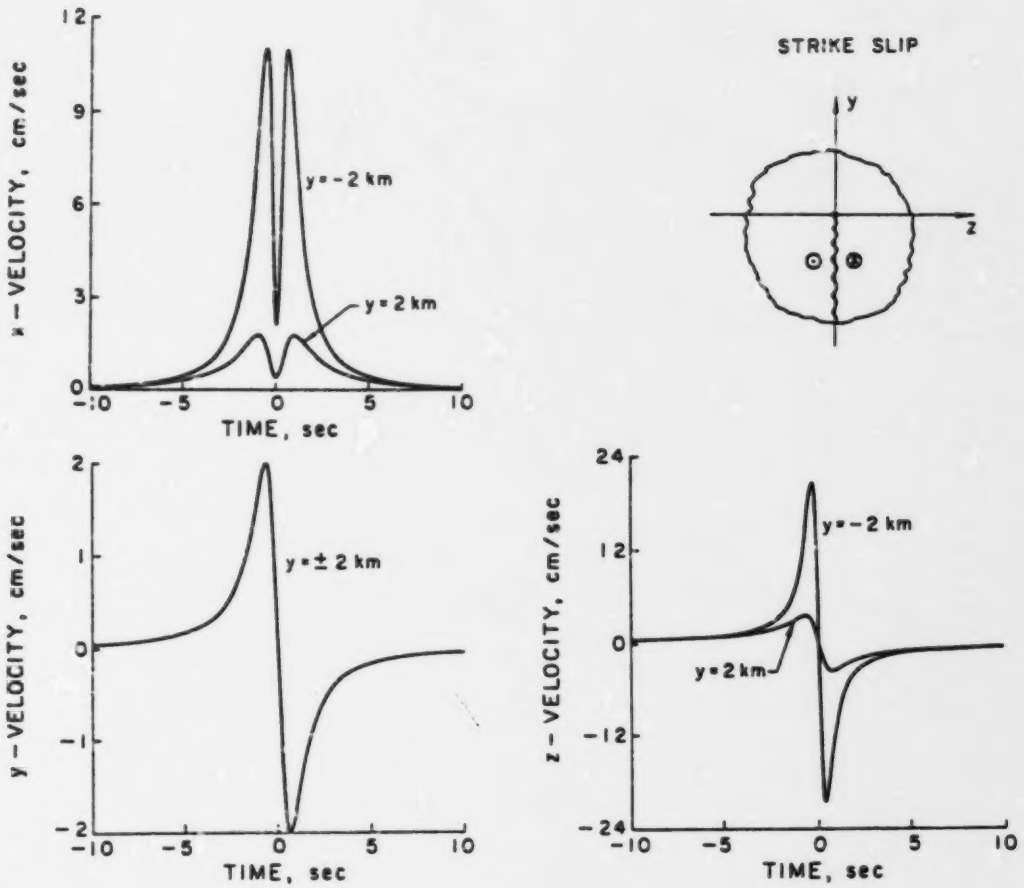

Fig. 4.1.2 Velocity pulses at $x = 0$, $y \pm 2$ km, $z = 2$ km for a steady-state strike-slip dislocation model in a full-space ($\Delta U_o = 100$cm, $v = 2.5$ km/sec, $\alpha = 6.0$ km/sec., $\beta = 3.464$ km/sec) (Luco and Georgevich, 1986).

BEST COPY AVAILABLE

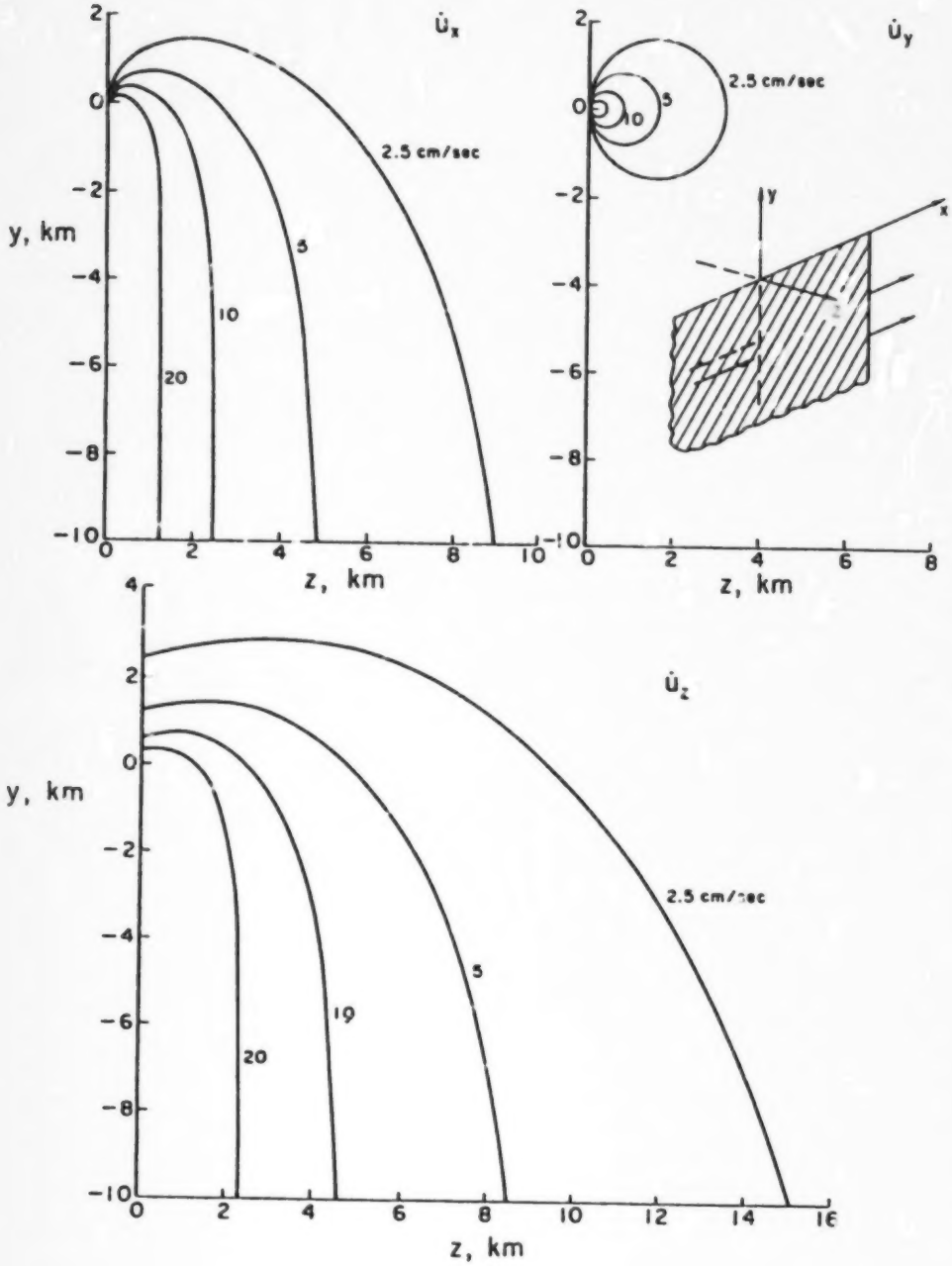

Fig. 4.1.3 Contours of equal peak velocity in a plane transverse to the fault (strike-slip dislocation, $\Delta\bar{U}_z$ = 100 cm, v = 2.5 km/sec, α = 6.0 km/sec, β = 3.464 km/sec (Luco and Georgevich, 1986).

BEST COPY AVAILABLE

Typical velocity pulse shapes in the vicinity of the fault are shown in Fig. (4.1.4). Contours of equal peak velocities are shown in Fig. (4.1.5). The results presented show that the y-component of velocity is much stronger in front of the rupture area ($y < 0$) than above it ($y > 0$).

The previous discussion refers to a fault of semi-infinite width. The solution for a steady-state fault of finite width W can be obtained by superposition. If $\{\dot{U}(x,y,z,t)\}$ represents the solution for semi-infinite width given above and $\{\dot{U}_W(x,y,z,t,)\}$ represents the solution for a fault of finite width, then

$$\{\dot{U}_W(x,y,z,t)\} = \{\dot{U}(x,y,z,t)\} - \{\dot{U}(x,y+W,z,t)\} \tag{4.1.9}$$

which after substitution from Eqs. (4.1.2) and (4.1.5) leads to

$$\left\{\dot{U}_W(x,y,z,t)\right\} = \begin{cases} \{\dot{U}_{II}(x,y,z,t)\} - \{\dot{U}_{II}(x,y+W,z,t)\} & y > 0 \\ \{\dot{U}_I(x,y,z,t)\} + \{\dot{U}_{II}(x,y,z,t)\} - \{\dot{U}_{II}(x,y+W,z,t)\} & -W < y < 0 \\ \{\dot{U}_{II}(x,y,z,t)\} - \{\dot{U}_{II}(x,y+W,z,t)\} & y < -W \end{cases} \tag{4.1.10}$$

in which $\{\dot{U}_I\}$ and $\{\dot{U}_{II}\}$ are given by Eqs. (4.13), (4.15) and (4.16) for strike-slip faults and by Eqs. (4.17), (4.15) and (4.18) for dip slip faults. We note again that all of these velocities do not depend on x and t independently but on the combination $(x-vt)$.

BEST COPY AVAILABLE

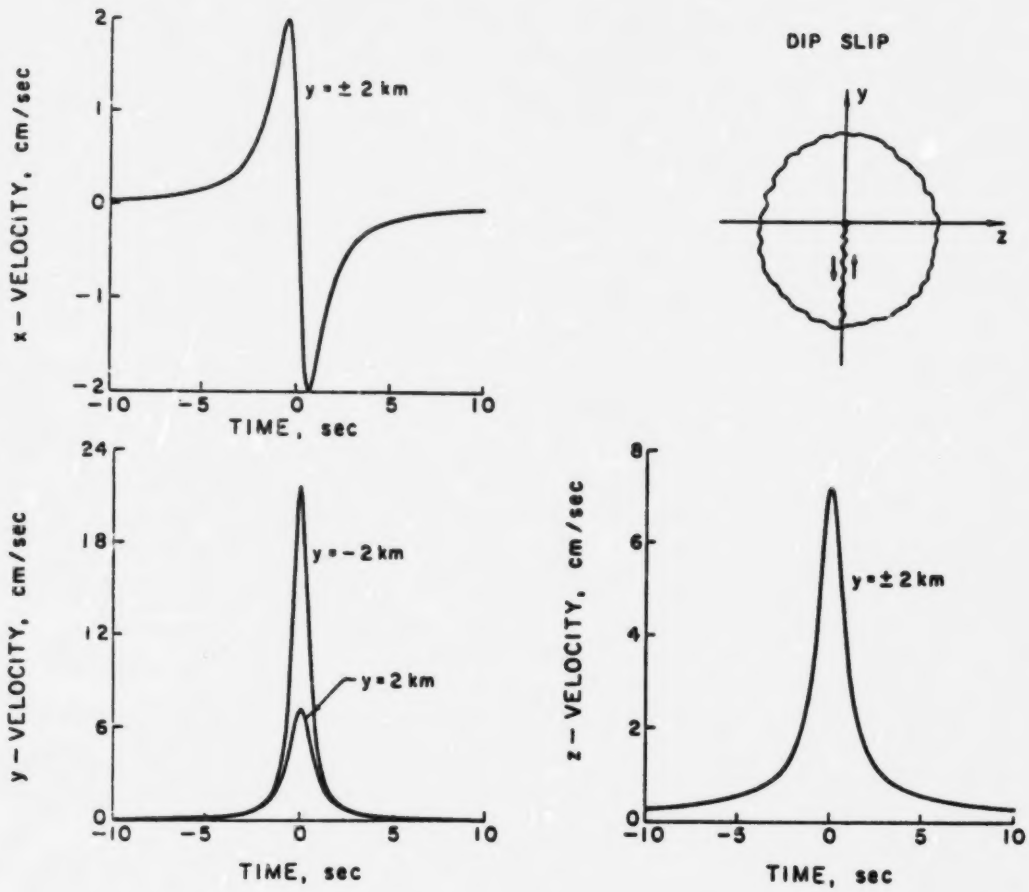

Fig. 4.1.4 Velocity pulses at $x = 0$, $y = \pm 2$ km, $z = 2$ km for a steady-state dip-slip dislocation model in a full-space. ($\Delta \bar{U}_y$ = 150cm, v = 2.5 km/sec, α = 6.0 km/sec, β = 3.464 km/sec) (Luco and Georgevich, 1986).

BEST COPY AVAILABLE

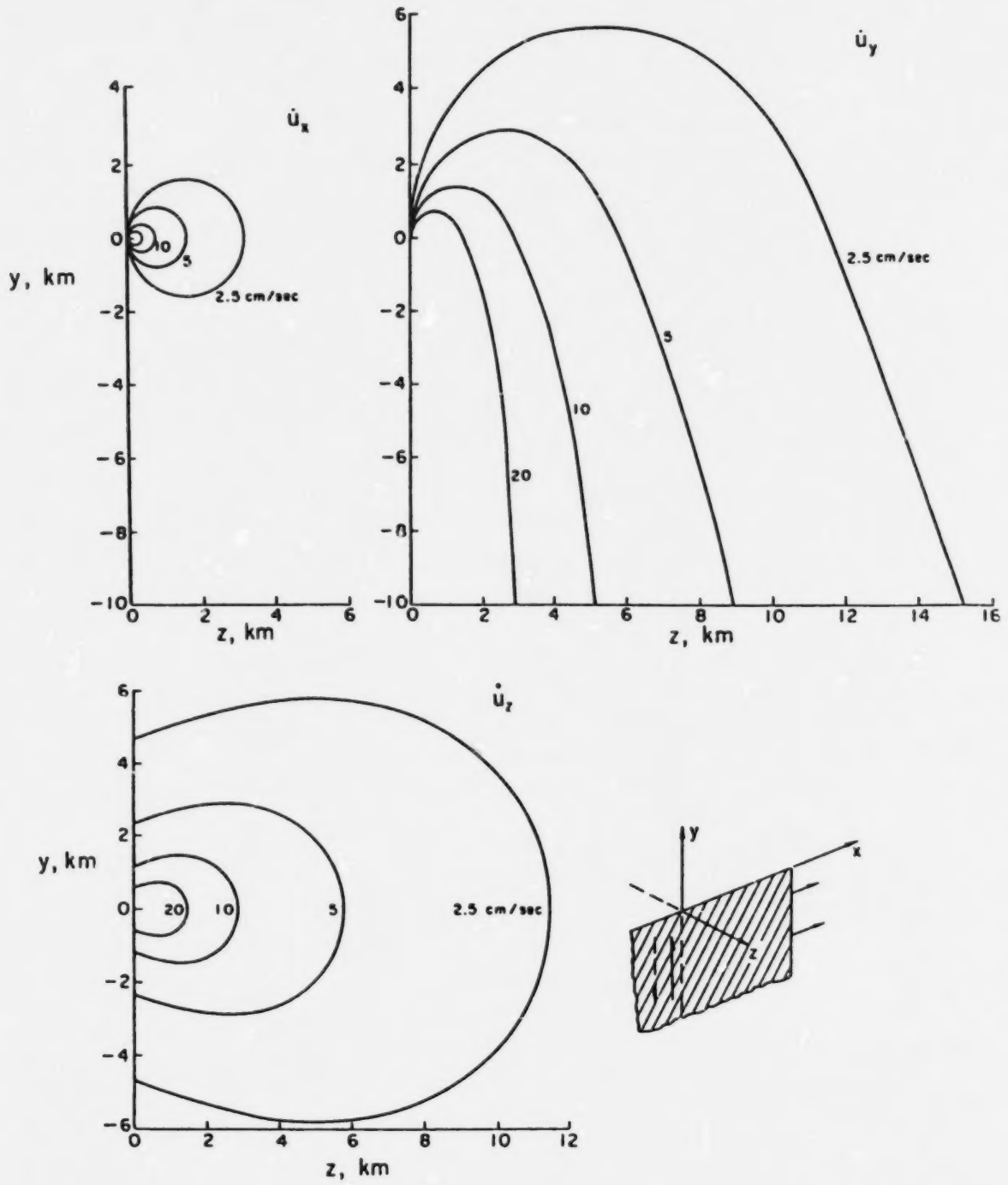

Fig. 4.1.5. Contours of equal peak velocity in a plane transverse to the fault (dip-slip dislocation, ΔU_y = 100cm/sec, v = 2.5 km/sec, α = 6.0 km/sec, β = 3.464 km/sec) (Luco and Georgevich, 1986).

BEST COPY AVAILABLE

4.2 Three-Dimensional Dislocation Models in a Full Space (Haskell's Fault Model).

The most commonly used three-dimensional dislocation model in an unbounded medium corresponds to a uniform dislocation moving with constant rupture velocity over a rectangular fault. A model of this type was utilized by Aki (1968) to synthesize near-field ground motion for a shear dislocation with slip normal to the rupture front. In Aki's study, the response in the frequency domain for the extended fault was obtained by superposition of the contributions of a number of fault elements calculated using the approximation derived by Ben-Menahem (1961). The response in the time domain for a step function dislocation was then obtained by Fourier synthesis. The same model for a finite ramp dislocation was studied by Haskell (1969) by use of the representation theorem in which the response in the time domain is obtained as an integral over the fault plane of time convolutions of the slip function with the Green's functions for a full-space. For simple dislocation time functions, the time convolutions can be obtained analytically, the integrations over the fault plane are conducted by numerical methods. The method of Haskell has been extensively used by a number of researchers, among which we can mention Kanamori (1971, 1972), Thomson and Haskell (1972), Haskell and Thomson (1972), Mikumo (1973), Abe (1974a,b), Anderson (1974), Trifunac (1974), Trifunac and Udwadia (1974), Anderson and Richards (1975), and Anderson and Fletcher (1976). Some variations of the standard Haskell's model have been introduced. In particular, Thomson and Haskell (1972) considered a shear dislocation with slip parallel to the rupture front while Haskell and Thomson (1972) considered a tensile dislocation. Trifunac (1974) and Trifunac and Udwadia (1974) considered nonuniform slip amplitudes while Anderson and Richards (1975) studied the effects of various fault and rupture front shapes. An alternative approach to the evaluation of integrals over the fault plane has been presented by Boatwright and Boore (1975) and Sato (1975). In this approach, the analytical solution for a moving dislocation of zero width (Knopoff and Gilbert, 1959; Savage, 1965) is integrated numerically over the fault width to obtain the response for an extended fault. Finally, an entirely different approach has been taken by Madariaga (1978) who utilized the Cagniard-de Hoop technique to obtain a closed-form solution for a uniform

BEST COPY AVAILABLE

dislocation over a rectangular fault. The case of a nonuniform dislocation has been considered by List (1982).

Aki (1968), in his study of the motion in the vicinity of a unilaterally-propagating, vertical strike-slip fault in a homogeneous medium, found that: (i) for sufficiently short distances to the fault and sufficiently high frequencies, the width of the fault was not important, (ii) for a station close to the fault and at some distance from either end, the length of the fault was not important and the motion was controlled only by the slip on the fault and by the rupture velocity, and, (iii) the synthetic motion included a marked pulse-like displacement in the component perpendicular to the fault which was associated with the time at which the dislocation front passes the nearest point from the station.

Haskell (1969) as part of his now classic study on the motion in the near-field of a propagating fault calculated and plotted displacement, velocity and acceleration time histories for the motion in the vicinity of a vertical strike-slip fault. Haskell also presented contours of maximum range (variation from greatest positive value to greatest negative value) in the vicinity of the fault for the parallel and normal components of displacement, velocity and acceleration. Based on these results he concluded that for stations close to the plane of the fault and beyond the ends of the fault, correlatable features of the calculated waveforms propagate at either the P or S wave velocities. Within the ends of the fault, he found that correlative peaks and troughs of velocity or acceleration travel at the rupture velocity and that within this region the motion has the character of a "bound wave" forced to travel at the rupture velocity by the assumed boundary conditions.

Some typical results obtained by Haskell (1969) for a vertical strike-slip fault of length $L = 10$ units of length and width $W = 2.5$ units of length ($0 < x_1 < L$, $0 < x_2 < W$, $x_3 = 0$) are presented in Fig. 4.2.1. The unit of length is vT in which v is the rupture velocity in the x_1-direction ($\alpha/v = 2.25$, $\beta/v = 1.30$) and T is the rise time of the uniform ramp dislocation. The results correspond to contours of maximum range for the parallel (u_1) and perpendicular (u_3) components of the calculated displacement, velocity and acceleration pulses in the

BEST COPY AVAILABLE

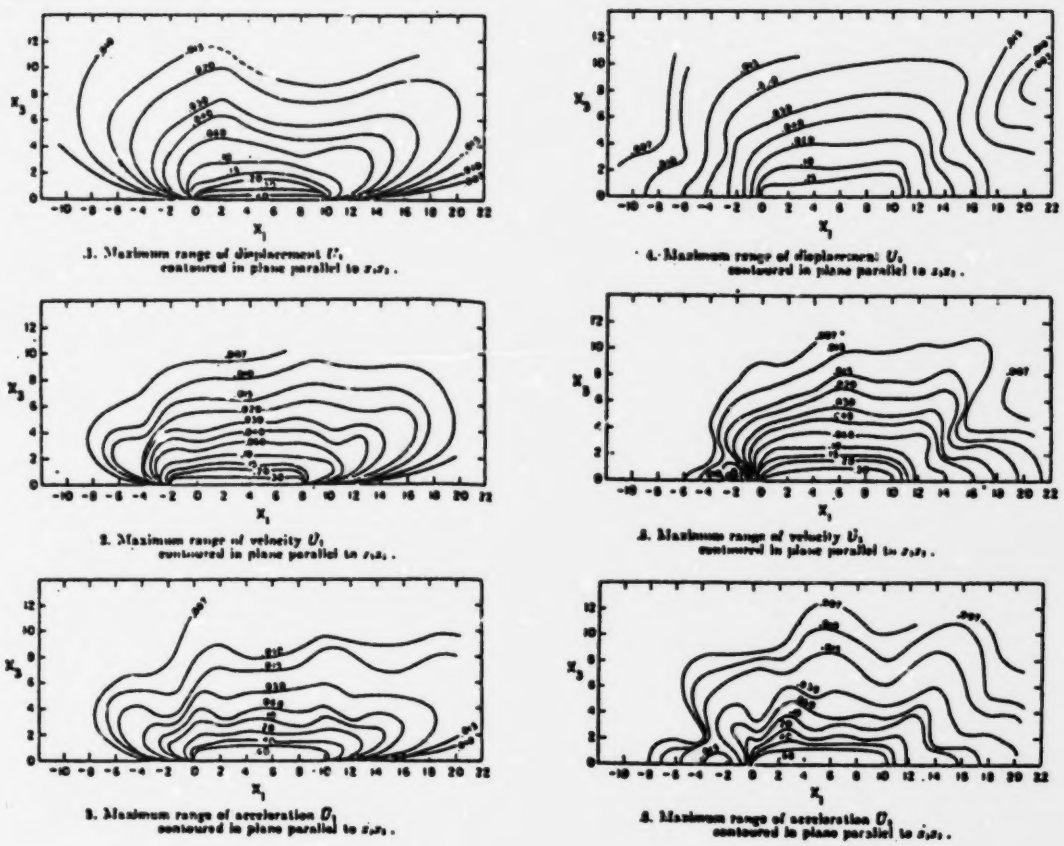

Fig. 4.2.1 Contours of maximum range of displacement, velocity and acceleration for the parallel (u_1) and perpendicular (u_3) components in the vicinity of a vertical strike slip fault (Haskell, 1969).

BEST COPY AVAILABLE

mid-plane of the fault ($x_2 = W/2 = 1.25vT$). Displacements, velocities and accelerations are normalized by $\Delta U_1(1, T^{-1}, T^{-2})$, respectively, in which ΔU_1 is the final slip. These contours, and, particularly those corresponding to acceleration, show at the beginning and end of the fault ($x_1 = 0$ and $x_1 = 10$) areas in which the radiation patterns of the starting and stopping phases are clearly visible. Within the ends of the fault ($0 < x_1 < 10$) and close to the fault ($x_3 < 4$) the contours are relatively independent of the coordinate x_1. In this region, the 'bound wave' or 'rupture passage' phase, using the designation introduced in Chapter 2, is predominant (some of Haskell's numerical results are believed to be erroneous, e.g. Boore and Zoback, 1974; however, it is not expected that the patterns shown in Fig. 4.2.1 would be significantly affected).

Time histories for the three components of velocity obtained by Haskell (1969) for a rectangular strike-slip fault $0 < x_1 < L = 60$, are shown in Fig. 4.2.2. In this case the observers are located on the line $x_1 = 55$, $x_2 = 0$ and x_3 variable ranging from 1 unit (top of each panel) to 30 units (bottom of each panel). The particle velocities are normalized so that the range is equal for all stations, consequently, only comparative wave form information is available. Time is normalized by T, the rise time of the dislocation of final slip ΔU_1. The results in Fig. 4.2.2 show a marked pulse occurring in the vicinity of 55T corresponding to the time of passage of the rupture front, this pulse is most pronounced for stations within a distance of 6 from the fault. The starting P and S waves from the corner $x_1 = x_2 = x_3 = 0$ are noticeable only for observers at distances beyond 6 from the fault. The arrival time of the starting P waves ranges from 24.45T for $x_3 = 1$ to 27.84T for $x_3 = 30$. The corresponding arrival time of starting S waves ranges from 42.31T for $x_3 = 1$ to 48.19T for $x_3 = 30$. The stopping P and S waves from the corner $x_1 = L, x_2 = 0, x_3 = 0$ are clearly visible, particularly, at larger distances to the fault. The stopping P-phases arrive at times ranging from 62.27T for $x_3 = 1$ to 73.52T for $x_3 = 30$. The stopping S-waves arrive at times ranging from 63.92T for $x_3 = 1$ to 83.40T for $x_3 = 30$. The results in Fig. 4.2.2 emphasize the importance of the rupture passage phase relative to the starting and stopping pulses for observers close to the fault plane but away from the ends of the fault.

BEST COPY AVAILABLE

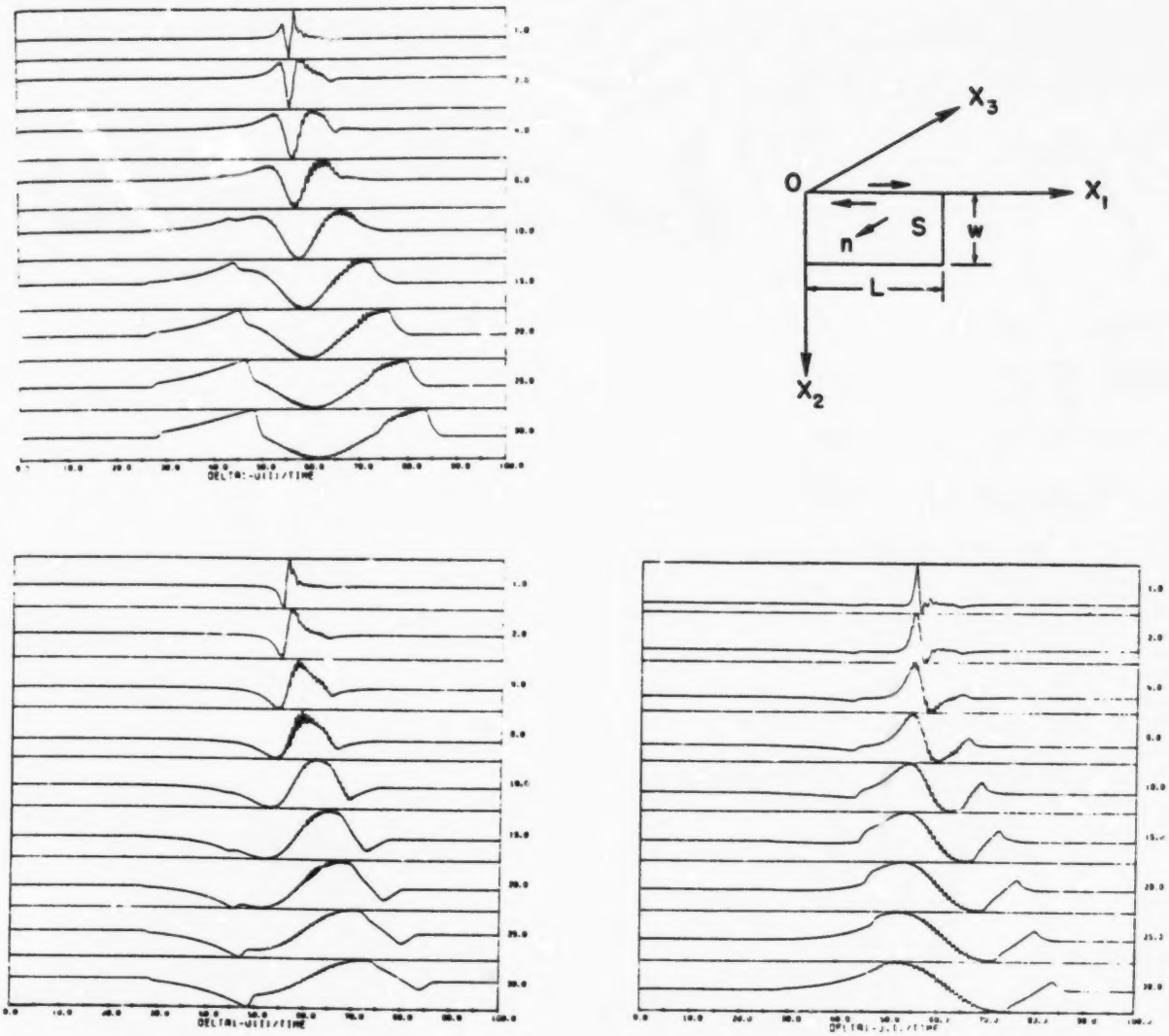

Fig. 4.2.2. $\dot{U}_1$ (upper left), $\dot{U}_2$ (lower left) and $\dot{U}_3$ (lower right) components of velocity versus time for $L = 60$, $W = 15$, $x_2 = 0$, $x_1 = 55$ and variable x_3 ranging from 2 (top) to 30 (bottom). Peak--to-peak amplitudes are normalized to be equal at all distances. The time of passage of the rupture front in front of the observers is $t = 55$ (Haskell, 1969).

BEST COPY AVAILABLE

The picture which emerges from the results of Aki (1968) and Haskell (1969) for idealized fault models with uniform slip and constant rupture velocity is that the motion in the vicinity of the fault consists of starting and stopping phases, emanating from the geometrical beginning and end of the fault, and of a phase which is associated with the passage of the rupture front.

The solution of Madariaga (1978) for the particle velocities in a Haskell's rectangular fault model offers additional insight into the characteristics of the near-source ground motion. Madariaga found that for a rectangular fault ($0 < x < L$, $-W < y < 0$) there are two distinct regions of radiation. In the region $-W < y < 0$, the field is dominated by waves which correspond exactly to the two-dimensional problem in which $W \to \infty$, i.e. to the solution given by Eqs. (3.2.2) and (3.2.3) for a strike-slip (longitudinal) dislocation and by Eq. (2.2.2) for a dip-slip (transverse) dislocation. As shown by the results presented in Chapters 2 and 3 for two-dimensional models, these waves which Madariaga designates as "cylindrical" include starting and stopping phases as well as a rupture passage phase for observers close to the plane of the fault. For a step strike-slip dislocation, the P and S starting velocity pulses are given by

$$\dot{U}_I^P = \frac{\Delta \bar{U}_x}{2\pi} \left(\frac{\beta}{\alpha}\right)^3 \left(\frac{v}{\beta}\right) \cdot \frac{\sin 2\psi}{1 - \left(\frac{v}{\alpha}\right)\cos\psi} \frac{H(t - \rho/\alpha)}{\sqrt{t^2 - (\rho/\alpha)^2}}, \quad t \to \rho/\alpha \tag{4.2.1}$$

$$\dot{U}_I^S = \frac{\Delta \bar{U}_x}{2\pi} \cdot \left(\frac{v}{\beta}\right) \cdot \frac{\cos 2\psi}{1 - \left(\frac{v}{\beta}\right)\cos\psi} \frac{H(t - \rho/\beta)}{\sqrt{t^2 - (\rho/\beta)^2}}, \quad t \to \rho/\beta \tag{4.2.2}$$

in which $\rho = (x^2 + z^2)^{1/2}$, $\cos\psi = x/\rho$ and $\sin\psi = z/\rho$. For a dip-slip (transverse) dislocation, the starting velocity pulse is a shear wave given by

$$\dot{U}_I^S = \frac{\Delta \bar{U}_y}{2\pi} \left(\frac{v}{\beta}\right) \frac{\sin\psi}{1 - \left(\frac{v}{\beta}\right)\cos\psi} \frac{H(t - \rho/\beta)}{\sqrt{t^2 - (\rho/\beta)^2}}, \quad t \to \rho/\beta \tag{4.2.3}$$

All of these starting pulses are cylindrical waves radiating from the starting edge $x = 0$, $z = 0$, $-W < y < 0$. Eqs. (4.2.1), (4.2.2) and (4.2.3) indicate that the particle velocities associated with the 'cylindrical' waves have square-root singularities of the type $(t - r/\alpha)^{-1/2}$ and

BEST COPY AVAILABLE

$(t - r/\beta)^{-1/2}$ for a step dislocation on the fault. The high-frequency components of the velocity spectra for these waves show a $\omega^{-1/2}$ decay with frequency.

Madariaga (1978) also found that in the regions above ($y > 0$) and below ($y < -W$) the fault, the field is associated with waves which radiate from the upper ($z = 0$, $y = 0$, $0 < x < L$) and lower ($z = 0$, $y = -W$, $0 < x < L$) edges of the fault. Madariaga designates these waves as 'spherical' waves. The first motion approximations for these waves correspond indeed to spherical waves radiating from the four corners of the rectangular fault. For a step strike-slip (longitudinal) dislocation, the spherical P and S waves radiated from the corner $x = y = z = 0$ are given by

$$\dot{U}_{II}^{P} = \frac{\Delta \bar{U}_x}{2\pi} \left(\frac{\beta}{\alpha}\right)^2 \left(\frac{v}{R}\right) \frac{\nu_x \nu_z / \nu_y}{\left[1 - (v/\alpha)\nu_x\right]} H\left(t - \frac{R}{\alpha}\right), \quad t \to \frac{R}{\alpha} \tag{4.2.4}$$

$$\dot{U}_{II}^{S} = \frac{\Delta \bar{U}_x}{4\pi} \left(\frac{v}{R}\right) \frac{(\nu_x^2 - 4\nu_x^2\nu_z^2 + \nu_z^2)^{1/2}/\nu_y}{\left[1 - (v/\beta)\nu_x\right]} H\left(t - \frac{R}{\beta}\right), \quad t \to \frac{R}{\beta} \tag{4.2.5}$$

in which $R = (x^2 + y^2 + z^2)^{1/2}$ and $(\nu_x, \nu_y, \nu_z) = (x, y, z)/R$. For a dip-slip (transverse) dislocation the corresponding starting phases are

$$\dot{U}_{II}^{P} = \frac{\Delta \bar{U}_y}{2\pi} \left(\frac{\beta}{\alpha}\right)^2 \left(\frac{v}{R}\right) \frac{\nu_z}{1 - (v/\alpha)\nu_x} H\left(t - \frac{R}{\alpha}\right), \quad t \to \frac{R}{\alpha} \tag{4.2.6}$$

$$\dot{U}_{II}^{S} = \frac{\Delta \bar{U}_y}{4\pi} \left(\frac{v}{R}\right) \frac{(\nu_z^2 - 4\nu_y^2\nu_z^2 + \nu_y^2)^{1/2}/\nu_y}{1 - (v/\beta)\nu_x} H\left(t - \frac{R}{\beta}\right), \quad t \to \frac{R}{\beta} \tag{4.2.7}$$

The first motions show a step discontinuity in particle velocity for a step dislocation on the fault. The high-frequency components of the particle velocities associated with the spherical waves decay with frequency as ω^{-1}. It must be noted that the first motion approximations to the 'spherical' waves given by Eqs. (4.2.4), (4.2.5) and (4.2.7) fail on the plane $y = 0$ on which $\nu_y = 0$. In the vicinity of the fault, the waves radiated by the upper and lower boundaries of the fault also include a passage of the rupture front pulse given by the steady-state solution $\{\dot{U}_{II}\}$ discussed in the previous section.

BEST COPY AVAILABLE

The results of Madariaga (1978) as well as those shown in Figs. (4.1.3) and (4.1.5) suggest that for a dipping fault, the high-frequency components of motion on the upper block could be significantly higher than those for a vertical strike-slip fault which does not intercept the free-surface. In the case of the dipping fault, a portion of the upper block would receive the stronger 'cylindrical' waves while for the vertical strike-slip fault observers on the ground surface would receive only the weaker 'spherical' waves. The results of Madariaga also clarify the regions for which the two-dimensional approximations may be valid.

Finally, from the point of view of inverting near-source data to determine the characteristics of the rupture process it is important to note that Anderson and Richards (1975) found that models with fault motions and rupture geometries quite different from Haskell's propagating ramp model can often have near-field displacements similar to those from a ramp model.

BEST COPY AVAILABLE

4.3 Three-Dimensional Steady-State Dislocation Models in a Uniform Half-Space.

The simplest three-dimensional dislocation model in an elastic half-space corresponds to a uniform dislocation moving with constant rupture velocity over an infinitely long fault of finite width (Fig. 4.3.1). The dislocation is assumed to have a rectilinear rupture front characterized by finite rupture velocities in the direction of both the strike and dip of the fault. A solution for this steady-state dislocation model has been obtained by Luco and Anderson (1983) for the subsonic case. Extensive parametric studies of the solution have been presented by Anderson and Luco (1983a,b).

Some typical results for a vertical strike slip fault extending from a depth of 2 to 10 km are shown in Fig. 4.3.2. The acceleration, velocity and displacement pulses shown in Fig. 4.3.2 correspond to a step dislocation propagating along the infinite length of the fault with a rupture velocity of 3.184 km/sec. The rupture front is assumed to be vertical and the x and y components correspond to horizontal directions parallel and perpendicular to the fault respectively. The variation of the particle velocity pulse with distance to the fault for a vertical strike-slip fault is illustrated in Fig. 4.3.3. The results show among other characteristics that the peak longitudinal and vertical responses are obtained at a distance from the plane of the fault approximately equal to the depth of the top of the fault (2 km). The results also show a very marked velocity pulse in the component perpendicular to the fault.

The distributions of peak acceleration, velocity, and displacement versus distance to the fault are shown in Fig. 4.3.4 for three fault models. The upper (solid) curves correspond to a vertical, strike-slip fault of width W = 8 km located between the depths z_u = 1 km and z_d = 9 km. The intermediate (dash) curves correspond to a fault of width W = 8 km located between the depths z_u = 2 km and z_d = 10 km. Both of these models are characterized by a slip Δ_o = 100 cm. The lower (dash-dot) curves are for a fault of width W = 16 km located between the depths z_u = 2 km and z_d = 18 km with a slip of amplitude Δ_o = 50 cm. All three models are characterized by the same seismic moment per unit length of fault and by rupture velocities c_1 = 3.0 km/sec (c_1 = 0.94 c_R) and $c_2 = \infty$.

BEST COPY AVAILABLE

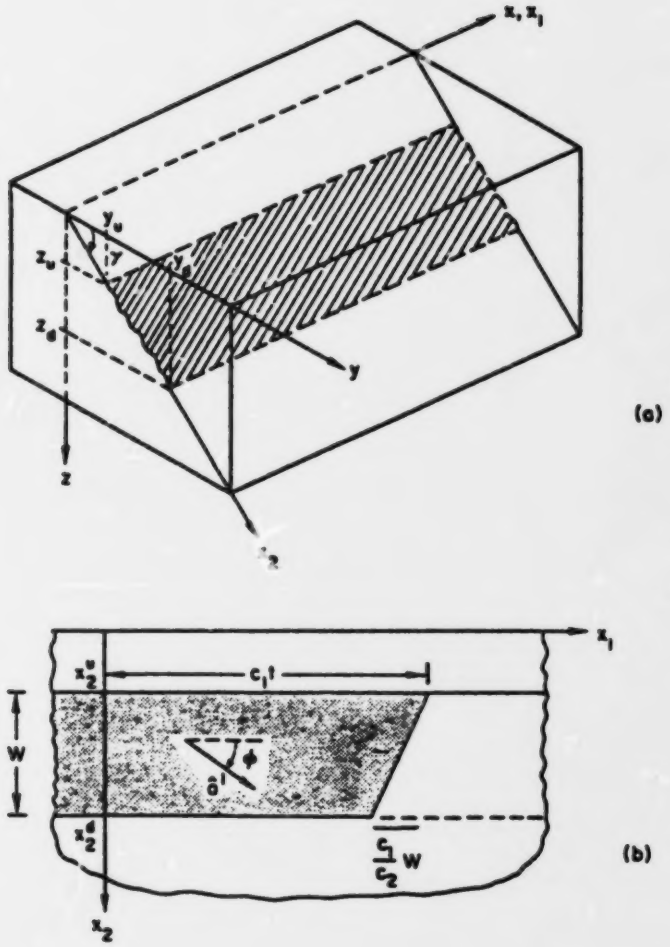

Fig. 4.3.1 Description of the fault model and coordinate systems. (a) Three-dimensional view. The plane $z = 0$ corresponds to the free surface. The shaded plane area represents the dipping fault; rupture occurs only between depths z_u and z_d, but extends to $\pm \infty$ in the x direction. (b) Plan view of the plane which contains the fault. The shaded portion represents the area which has ruptured at time t. Slip on the fault is independent of location within the shaded area; material above the plane of the figure moves in an arbitrary direction $\hat{d}'$ relative to material below the plane of the figure (Luco and Anderson, 1983).

BEST COPY AVAILABLE

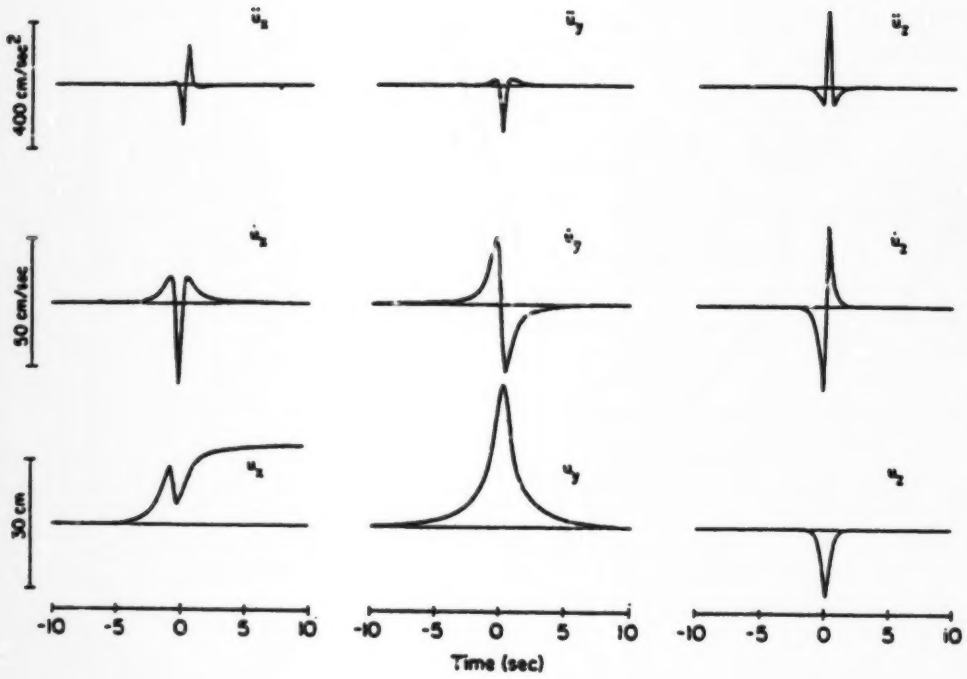

Fig. 4.3.2. Synthetic acceleration, velocity and displacement at a distance y = 2 km from a vertical strike-slip fault of infinite length characterized by z_s = 2 km, z_d = 10 km, c_1 = 3.184 km/sec, and $c_2 = \infty$ in a medium with $\alpha = \sqrt{3}\,\beta$ = 6.0 km/sec. The results are for a step dislocation of amplitude Δ_o = 100 cm (Luco and Anderson, 1983).

BEST COPY AVAILABLE

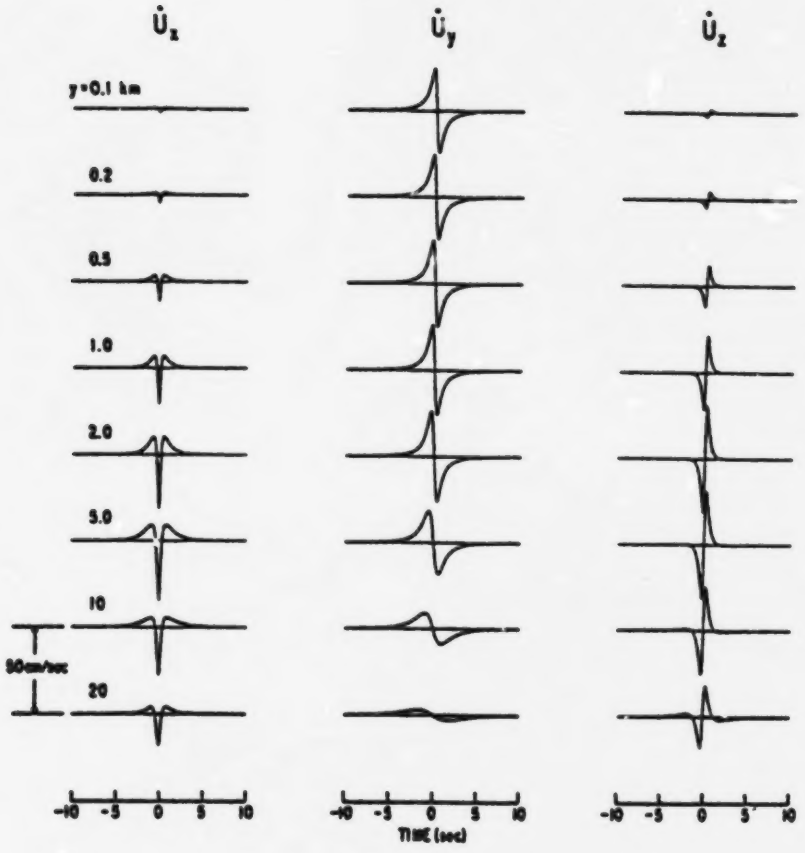

Fig. 4.3.3 Synthetic velocity pulses at various distances from a vertical strike slip fault characterized bay z_s = 2 km, z_d = 10 km. The slip on the fault corresponds to a step dislocation of amplitude Δ_o = 100 cm propagating with velocity c_1 = 3.184 km/sec and $c_2 = \infty$ in a medium with $\alpha = \sqrt{3}\,\beta$ = 6.0 km/sec (Anderson and Luco, 1983a).

BEST COPY AVAILABLE

Inspection of Fig. 4.3.4 reveals that the largest peak amplitudes occur at a distance comparable to the depth of the top of the fault, z_s. Furthermore, as z_s increases, the peak amplitudes decrease. For $y < z_s$, the peak values of $\ddot{u}_y$ are approximately proportional to z_s^{-2}, while the peak values of $\dot{u}_y$ are approximately proportional to z_s^{-1}. The additional factor of z_s^{-1} in $\ddot{u}_y$ arises because the velocity pulse width decreases as z_s. For $y < z_s$, the location of the bottom of the fault has little effect on peak amplitudes as evidenced by the uniform factor of 2 difference between the results for z_s = 2 km, z_d = 10 km, Δ_e = 100 cm, and z_s = 2 km, z_d = 18 km, and Δ_e = 50 cm. For larger values of y ($y >$ 10 km), all three fault models lead to similar peak amplitudes.

In Fig. 4.3.5, profiles of peak values of acceleration, velocity, and displacement along the free surface for a thrust fault with a dip of 30° and c_2 infinite are presented. The upper edge of the fault lies beneath y = 3.46 km. Peak values in the x and z components of motion occur in the vicinity of this point (y = 3.46 km), while the peaks of the y components are shifted slightly toward smaller values of y. Fig. 4.3.5 shows considerable asymmetry in y, with a less rapid decrease in peak values at $y > 0$, above the fault plane. Fig. 4.3.5 also illustrates the extreme dependence of peak amplitude on position.

BEST COPY AVAILABLE

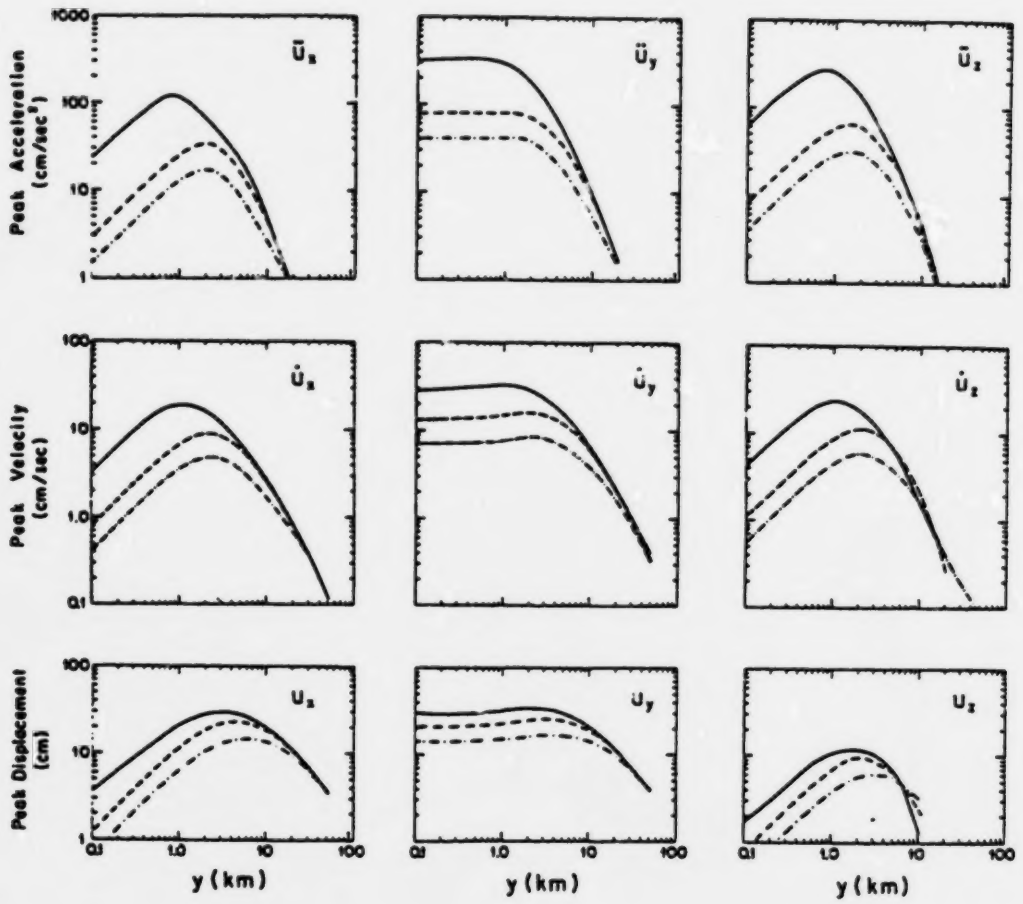

Fig. 4.3.4 Peak values of synthetic acceleration, velocity, and displacement as a function of distance y for three vertical, strike-slip faulting models. All three models have the same moment per unit length. All three models have c_1 = 3.0 km/sec and $c_2 = \infty$. The solid line corresponds to a model with z_s = 1 km, z_d = 9 km, and Δ_s = 100 cm. The dash line corresponds to a fault with z_s = 2 km, z_d = 10 km, and Δ_s = 100 cm. The dash-dot line corresponds to a fault with z_s = 2 km, z_d = 18 km, and Δ_s = 50 cm (Anderson and Luco, 1983a).

BEST COPY AVAILABLE

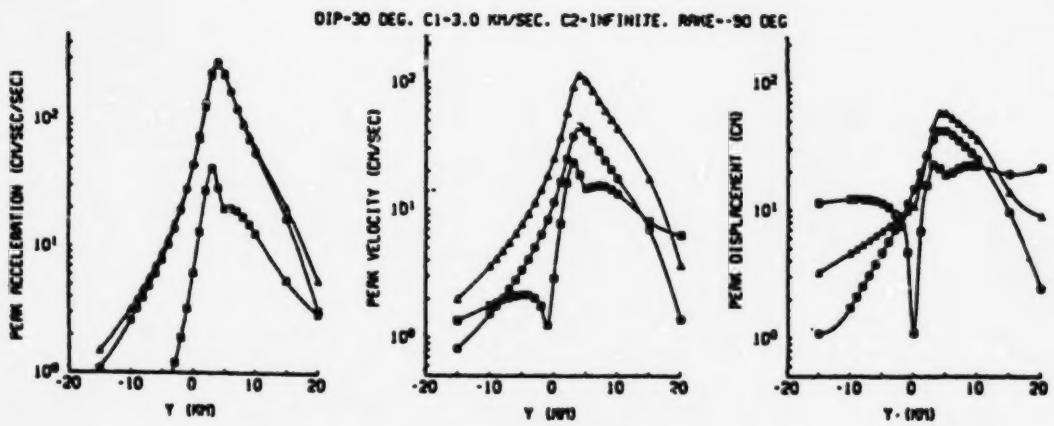

Fig. 4.3.5 Peaks in acceleration, velocity, and displacement along a profile of sites perpendicular to a thrust fault with dip 30°. The upper edge of the fault occurs at y_u = 3.464 km. Model parameters are dip 30°, c_1 = 3.0 km/sec, c_2 = ∞, Δ_σ = 100 cm, z_u = 2.0 km, and z_d = 10.0 km. Symbols are: circle, u_z; square, u_y; triangle, u_x (Anderson and Luco, 1983b).

BEST COPY AVAILABLE

4.4 Finite Three-Dimensional Dislocation Models in a Uniform Half-Space.

Several techniques have been proposed for the study of finite three-dimensional kinematic dislocation models in a uniform elastic half-space. Kawasaki (1975), Anderson (1976), and Hartzell *et al.* (1978) have evaluated near-field motion for rectangular faults embedded in a uniform elastic half-space. Archuleta and Hartzell (1981) have considered a circular fault buried in an elastic half-space. In these studies, the response in the time domain has been obtained by numerical integration of space and time convolutions of Green's functions for an elastic half-space (Johnson, 1974) with a prescribed slip function. An alternative approach has been taken by Levy and Mal (1976) who calculated first the response in the frequency domain by numerical integration of Green's functions over the fault surface and then evaluated the response in time by a Fourier synthesis. A third approach has been utilized by Israel and Kovach (1977) who obtained analytical expression for a suddenly appearing vertical line dislocation and represented an extended vertical fault by numerical superposition of a number of vertical line sources. Finally, Tanimoto (1982) used the Cagniard-de Hoop technique to obtain a solution for a vertical fault in an elastic half-space.

In the earlier studies, the effects of the free-surface were approximated by doubling the amplitudes resulting from the response of a full space. Anderson (1976) found that this approximation was valid for the horizontal components of displacement resulting from a strike-slip dislocation if the angle of incidence at the station was less than 80° with respect to the vertical. For angles of incidence of less than 60° the same approximation can be used for the vertical component. For dip-slip faults the approximation would be valid only for angles of incidence at the station of less than 30°.

As already discussed for the case of two-dimensional plane-strain models (section 3.4), the presence of the free-surface introduces a number of effects including amplification of waves and generation of Rayleigh and *SP*-waves. In the general case, the need to include these effects dictates the use of models including a free surface.

BEST COPY AVAILABLE

4.5 Three-Dimensional Dislocation Models in a Layered Half-Space.

In the last few years three-dimensional dislocation models of extended faults in a layered half-space have been utilized in the study of recorded near-source ground motion from a number of earthquakes including the Parkfield (Bouchon 1979b), Coyote Lake (Bouchon, 1982) and the 1979 Imperial Valley (Olson and Apsel, 1982; Archuleta, 1982,1984; Hartzell and Helmberger, 1982; Hartzell and Heaton, 1983) earthquakes. One of the methods to synthesize ground motion is based on writing the response, in the frequency domain, as a double integral over two horizontal wavenumbers. This approach is particularly attractive for simple dislocation models for which the Fourier transforms of the slip with respect to time and space (along the fault) can be obtained analytically. This approach has been utilized effectively by Bouchon (1979a,b) who in addition has discretized the integration over wavenumbers by considering a periodic arrangement of sources. A second approach is based on the use of the representation theorem in which the response of the medium is expressed in terms of spatial and temporal convolutions of Green's functions with the slip function. This approach is best suited for models in which the slip function and the rupture velocities may be strong functions of position. The use of this synthesis approach has been made possible by the recent development of effective methods to evaluate Green's functions for layered media (Apsel, 1979; Luco and Apsel, 1983; Apsel and Luco, 1983; Bouchon, 1981; Yao and Harkrider, 1983; Olson, 1982; Olson *et al.* 1984). The required discretization of the spatial convolution involving the Green's functions and the slip on the fault limits the application of this synthesis approach to low frequencies. Some of the numerical difficulties encountered in attempts at extending the calculations to moderate and high frequencies have been discussed by Sotiropoulos (1983).

One of the most interesting effects of layering on the amplitude of near-source ground motion has been described by Bouchon (1979b). For a model of the Parkfield 1966 earthquake (Fig. 4.5.1), Bouchon found that the calculated transverse displacement for a model consisting of a soft layer over an elastic half-space was eight times larger than that calculated for a uniform half-space model (Fig. 4.5.2). The vertical and parallel displacement components were amplified

BEST COPY AVAILABLE

by factors of the order of 2. In the layered model the top of the fault coincided with the interface between the layer and the half-space (depth of 1.5 km) and the shear-wave velocity in the layer was lower than the rupture velocity. The amplification is attributed by Bouchon (1979b) to the generation of a shock wave in the soft layer. Further parametric studies involving variation of the position of the top of the fault from 4 km to 100 m depth revealed that when the dislocation is buried under the sediments, the displacement is small, but a drastic change occurs when the top of the fault reaches the base of the layer (Fig. 4.5.3). At that point, the high-frequency content and the amplitude of the signal increase suddenly. Further penetration of the fault in the sediment leads to a less drastic but steady increase in amplitude. These important results are fully consistent with those for the simplified two-dimensional anti-plane shear model described in section 2.6 and illustrate the need to include the effects of layering.

BEST COPY AVAILABLE

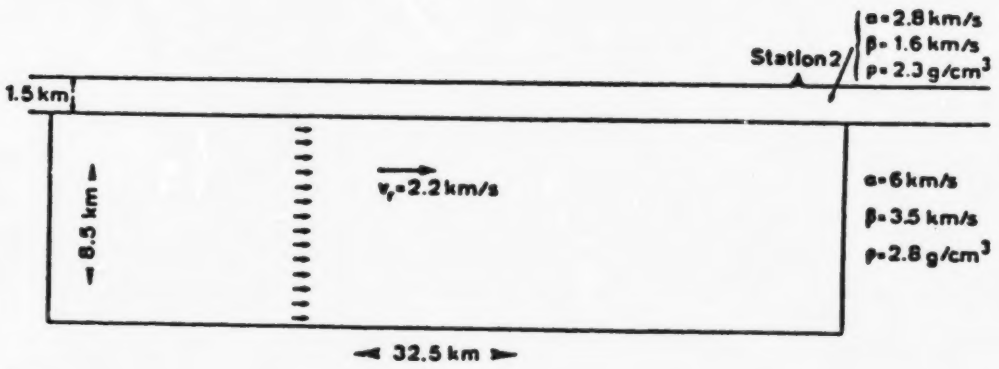

Fig. 4.5.1 Source-medium-station configuration used by Bouchon (1979b). The station is 80 m away from the plane of the fault. For the calculations shown in Figs. 4.5.2 and 4.5.3, the length of the fault was reduced to the 8.5 km closer to the station.

BEST COPY AVAILABLE

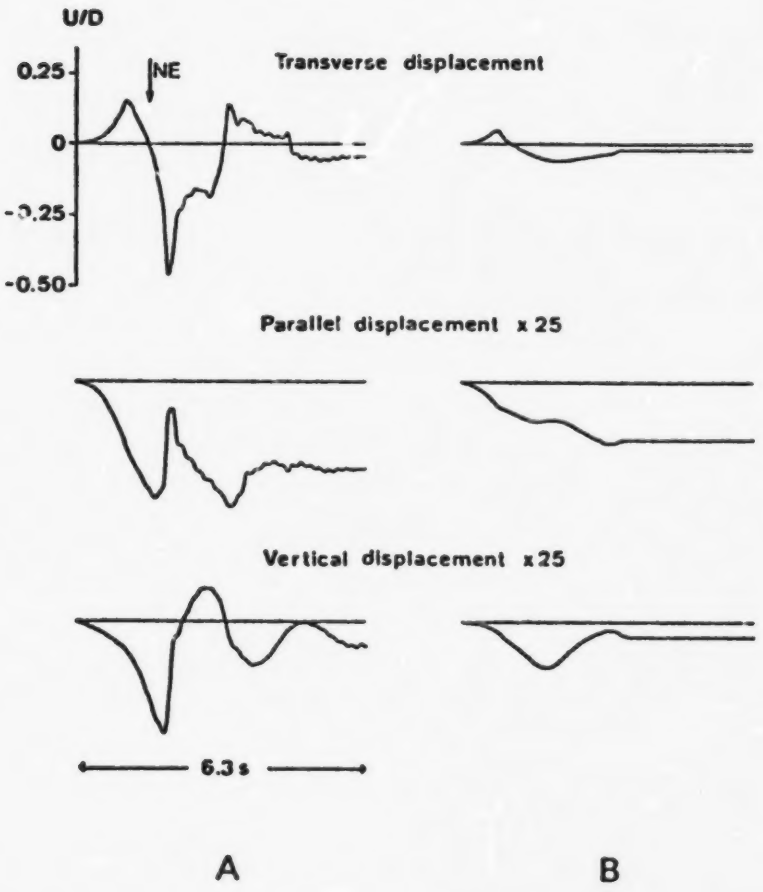

Fig. 4.5.2 (A) Calculated ground displacement at station 2. The parallel and vertical components have been amplified 25 times. The signals start with the arrival of the *P* wave from the hypocentral region. The amplitudes are normalized to the value of the slip *D* on the fault. B) Calculated ground displacement which would have been obtained in the absence of sediments (Bouchon, 1979b).

BEST COPY AVAILABLE

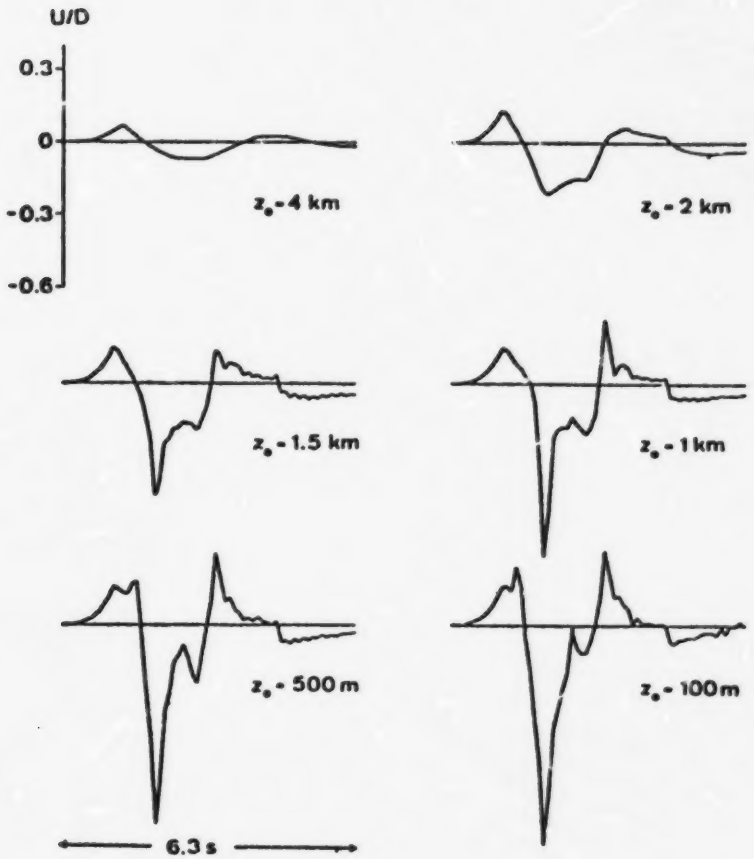

Fig. 4.5.3 Effect of the depth of burial of the fault (z_o) on the transverse displacement pulse (Bouchon, 1979b).

BEST COPY AVAILABLE

4.6 Conclusions.

The study of dislocation fault models in a three-dimensional medium leads to the following conclusions:

1(i). The ground motion in the vicinity of faults can be considered to consist of starting, rupture passage and stopping phases

1(ii). The starting and stopping phases dominate the motion in the vicinity of the beginning and end of the fault. Close to the fault and away from the ends, the rupture passage pulses are dominant.

2(i). In the case of rectangular dislocations, the starting and stopping phases include spherical waves radiating from the corners of the fault and cylindrical waves radiating from the starting and stopping edges of the fault.

2(ii). The first motion of the velocity pulses corresponding to the spherical starting phases is a step for a step dislocation on the fault. These pulses attenuate as r^{-1} where r is distance to the corner and show a directivity effect of the type $[1 - (v/\beta)\nu_x]^{-1}$ or $[1 - (v/\alpha)\nu_x]^{-1}$.

2(iii). The starting cylindrical pulses can only be felt within a slab-like region in front of the fault and correspond exactly to the starting pulses in the corresponding two-dimensional problem. The first motion of the velocity pulses for the cylindrical waves show a square-root singularity (for a step dislocation) and decay with ρ^{-1} in which ρ is distance to the starting or stopping edge. In general, the starting cylindrical waves are stronger than the corresponding spherical pulses.

3(i). In the case of rectangular dislocations, two types of rupture passage phases can be distinguished.

BEST COPY AVAILABLE

3(ii). The first type arises from the presence of the upper and lower edges of the fault. The corresponding velocity pulses for a step dislocation on the fault decay as ρ_*^{-1} where ρ_* is distance to the upper or lower edge.

3(iii). The second type of rupture passage pulse can only be felt within a slab-like region in front of the fault and corresponds exactly to the rupture passage pulse for the corresponding two-dimensional problem. This velocity pulse decays as $1/z$ where z is distance to the plane of the fault and is stronger than the rupture passage pulse due to the upper and lower edges of the fault.

4(i). The free-surface of the earth introduces effects which, in general, cannot be approximated by doubling the amplitudes of the motion for a dislocation in a full-space. This approximation may be better for strike-slip than for dip-slip fault models.

4(ii). Layering has very important effects particularly when the rupture velocity is larger than the shear wave velocity in the softer sediments. In this case, the amplitudes of motion on the ground surface can be several times larger than those calculated for a uniform half-space with the properties of the lower medium.

4(iii). Finally, it is important to note that models with very different fault motions and rupture geometries can produce very similar near-field displacements. In these cases, it may be necessary to resort to higher frequencies or to the use of several stations to determine the rupture characteristics.

BEST COPY AVAILABLE

4.7 References.

Abe, K. (1974a). Seismic displacement and ground motion near a fault: the Saitana earthquake of September 21, 1931, *J. Geophys. Res.*, 79, 4393-4399.

Abe, K. (1974b). Fault parameters determined by near-and far-field data: the Wakara Bay earthquake of March 26, 1963, *Bull. Seism. Soc. Am.* 64, 1369-1382.

Aki, K. (1968). Seismic displacements near a fault, *J. Geophys. Res.* 73, 5359-5376.

Aki, K. and P. G. Richards (1980). *Quantitative seismology: Theory and methods*, Vol. II, W. H. Freeman and Co., San Francisco.

Anderson, J. G. (1974). A dislocation model for the Parkfield earthquake, *Bull. Seism. Soc. Am.* 64, 671-686.

Anderson, J. G. and P. G. Richards (1975). Comparison of strong ground motion from several dislocation models, *Geophys. J. R. astr. Soc.* 42, 347-373.

Anderson, J. G. (1976). Motions near a shallow rupturing fault: evaluation of the effects due to the free surface, *J. Geophys. Res.* 16, 575-593.

Anderson, J. G. and J. B. Fletcher (1976). Source properties of a Blue Mt. Lake earthquake, *Bull. Seism. Soc. Am.* 66, 677-683.

Anderson, J. G. and J. E. Luco (1983a). Parametric study of near-field ground motion for a strike-slip dislocation model, *Bull. Seism. Soc. Am.* 73, 23-43.

Anderson, J. G. and J. E. Luco (1983b). Parametric study of near-field ground motions for oblique-slip and dip-slip dislocation models, *Bull.. Seism. Soc. Am.* 73, 45-57.

Apsel, R. J. (1979). Dynamic Green's functions for layered media and applications to boundary-value problems, *Ph D. Thesis*, University of California, San Diego, La Jolla, CA.

Apsel, R. J. and J. E. Luco (1983). On the Green's functions for a layered half-space: Part II, *Bull. Seism. Soc. Am.* 73, 931-951.

BEST COPY AVAILABLE

Archuleta, R. J. and S. H. Hartzell (1981). Effects of fault finiteness on near-source ground motion, *Bull. Seism. Soc. Am.* 71, 939-957.

Archuleta, R. J. (1982). Analysis of near-source static and dynamic measurements from the 1979 Imperial Valley earthquake, *Bull. Seism. Soc. Am.* 72, 1927-1956.

Archuleta, R. J. (1984). A faulting model for the 1979 Imperial Valley earthquake, *J. Geophys. Res.* 89, 4559-4585.

Ben-Menahem, A. (1961). Radiation of seismic surface waves from finite moving sources, *Bull. Seism. Soc. Am.* 51, 401-435.

Bernard, P. and R. Madariaga (1984). A new asymptotic method for the modeling of near-field accelerograms, *Bull. Seism. Soc. Am.* 74, 534-557.

Bernard, P. and R. Madariaga (1984). High frequency seismic radiation from a buried circular crack, *Geophys. J. R. astr. Soc.* 78, 1-17.

Boatwright, J. and D. M. Boore (1975). A simplification in the calculation of motions near a propagating dislocation, *Bull. Seism. Soc. Am.* 65, 133-138.

Boore, D. M. and M. D. Zoback (1974). Near-field motions from kinematic models of propagating faults, *Bull. Seism. Soc. Am.* 64, 321-342.

Bouchon, M. (1979a). Discrete wave number representation of elastic wave fields in three-space dimensions, *J. Geophys. Res.* 84, 3609-3614.

Bouchon, M. (1979b). Predictability of ground displacement and velocity near an earthquake fault: an example: the Parkfield earthquake of 1966, *J. Geophys. Res.* 84, 6149-6156.

Bouchon, M. (1981). A simple method to calculate Green's functions for elastic layered media, *Bull. Seism. Soc. Am.* 71, 939-941.

Bouchon, M. (1982). The rupture mechanism of the Coyote Lake earthquake of 6 August 1979 inferred from near-field data, *Bull. Seism. Soc. Am.* 72, 745-758.

Campillo, M. (1983). Numerical evaluation of the near-field, high-frequency radiation from quasi-dynamic circular faults, *Bull. Seism. Soc. Am.* 73, 723-734.

BEST COPY AVAILABLE

Hartzell, S. B., G. A. Frazier, and J. N. Brune (1978). Earthquake modeling in a homogeneous half-space, *Bull. Seism. Soc. Am.* 68, 301-316.

Hartzell, S. H. and D. V. Helmberger (1982). Strong-motion modeling of the Imperial Valley earthquake of 1979, *Bull. Seism. Soc. Am.* 72, 571-596.

Hartzell, S. H. and T. H. Heaton (1983). Inversion of strong ground motion and teleseismic waveform data for the fault rupture history of the 1979 Imperial Valley, California, earthquake, *Bull. Seism. Soc. Am.* 73, 1553-1583.

Haskell, N. A. (1969). Elastic displacements in the near field of a propagating fault, *Bull. Seism. Soc. Am.* 59, 865-908.

Haskell, N. A., and K. C. Thomson (1972). Elastodynamic near-field of a finite propagating tensile fault, *Bull. Seism. Soc. Am.* 62, 657-697.

Israel, M. and R. L. Kovach (1977). Near-field motions from a propagating strike-slip fault in an elastic half-space, *Bull. Seism. Soc. Am.* 67, 977-994.

Johnson, L. R. (1974). Green's function for Lamb's problem, *Geophys. J. astr. Soc.* 37, 99-131.

Kanamori, H. (1971). Seismological evidence for a lithospheric normal faulting-Sanriku earthquake of 1983, *Phys. Earth Planet. Interiors* 4, 289-300.

Kanamori, H. (1972). Determination of effective tectonic stress associated with earthquake faulting, the Tottori earthquake of 1943, *Phys. Earth Planet. Interiors* 5, 426-434.

Kawasaki, I. (1975). On the dynamical process of the Parkfield earthquake of June 28, 1966, *J. Phys. Earth* 23, 127-144.

Knopoff, L. and F. Gilbert (1959). Radiation from a strike slip fault, *Bull. Seism. Soc. Am.* 49, 163-178.

Levy, N. A. and A. K. Mal (1976). Calculation of ground motion in a three-dimensional model of the 1966 Parkfield earthquake, *Bull. Seism. Soc. Am.* 66, 405-423.

List, R. D. (1982). The solution of the dynamic field of the Haskell model reconsidered, *Bull. Seism. Soc. Am.* 72, 1069-1083.

BEST COPY AVAILABLE

Luco, J. E. and J. G. Anderson (1983). Steady-state response of an elastic half-space to a moving dislocation of finite width, *Bull. Seism. Soc. Am.* 73, 1-22.

Luco, J. E. and R. J. Apsel (1983). On the Green's functions for a layered half-space: Part I, *Bull. Seism. Soc. Am.* 73, 909-929.

Luco, J. E. and J. G. Anderson (1985). Near source earthquake ground motion from kinematic fault models. *Strong Ground Motion Simulation and Earthquake Engineering Applications*, R. E. Scholl and J. L. King (Eds.), Publication No.85-02, EERI, 18-1/18-20.

Luco, J. E. and M. Georgevich (1986). A note on the steady-state response of an elastic medium to a moving dislocation of finite width (in preparation).

Madariaga, R. (1976). Dynamics of an expanding circular fault, *Bull. Seism. Soc. Am.* 66, 639-666.

Madariaga, R. (1977). High frequency radiation from crack (stress drop) models of earthquake faulting, *Geophys. J. R. Astron. Soc.* 51, 625-651.

Madariaga, R. (1978). The dynamic field of Haskell's rectangular dislocation fault model, *Bull. Seism. Soc. Am.* 68, 869-887.

Mikumo, T. (1973). Faulting process of the San Fernando earthquake of February 9, 1979 inferred from static and dynamic near-field displacements, *Bull. Seism. Soc. Am.* 63, 249-269.

Olson, A. H. (1982). Forward simulation and linear inversion of earthquake ground motions, *Ph.D. Thesis*, University of California, San Diego, La Jolla, CA.

Olson, A. H. and R. J. Apsel (1982). Finite faults and inverse theory with applications to the 1979 Imperial Valley earthquake, *Bull. Seism. Soc. Am.* 72, 1969-2001.

Olson, A. H., J. A. Orcutt and G. A. Frazier (1984). The discrete wavenumber finite element method of synthetic seismograms, *Geophys. J. R. Astr. Soc.*. 77, 421-460.

Richards, R. (1976). Dynamic motions near an earthquake fault: a three-dimensional solution, *Bull. Seism. Soc. Am.*, 66, 1-32.

BEST COPY AVAILABLE

Sato, R. (1975). Fast computation of theoretical seismograms for an infinite medium, Part I. Rectangular fault, *J. Geophys. Earth.* 23, 323-331.

Savage, J. C. (1965). The effect of rupture velocity upon seismic first motions, *Bull. Seism. Soc. Am.* 55, 263-275.

Sotiropoulos, D. A. (1983). On synthesis of ground motions from earthquakes, *Ph.D. Thesis*, University of California, San Diego, La Jolla, CA.

Tanimoto, T. (1982). Cagniard-de Hoop method for a Haskell type vertical fault, *Geophys. J. R. astr. Soc.*, 70, 639-646.

Thomson, K. C. and N. A. Haskell (1972). Elasto-dynamic near-field of a finite transverse shear fault, *J. Geophys. Res.* 77, 2574-2582.

Trifunac, M. D. (1974). A three-dimensional dislocation model for the San Fernando, California, earthquake of February 9, 1971, *Bull. Seism. Soc. Am.* 64, 149-172.

Trifunac, M. D. and F. E. Udwadia (1974). Parkfield, California earthquake of June 27, 1966: a three-dimensional moving dislocation, *Bull. Seism. Soc. Am.* 64, 511-533.

Yao, Z. X. and D. G. Harkrider (1983). A generalized reflection-transmission coefficient matrix and discrete wavenumber method for synthetic seismograms, *Bull. Seism. Soc. Am.* 73, 1685-1699.

BEST COPY AVAILABLE

5. SIMULATION OF NEAR-SOURCE RECORDS

5.0 Introduction.

In the previous chapters, the characteristics of the near-source ground motion resulting from simple two- and three-dimensional dislocation models have been examined. The application of these simple models as well as that of more complex representations to the simulation of recorded near-source ground motion is discussed here. Since the initial work of Aki in 1968 a large number of studies has been devoted to the modelling of near source records obtained during the Parkfield 1966, Borrego Mountain 1968, San Fernando 1971, Imperial Valley 1979, Coyote Lake 1979 and Morgan Hill 1984 earthquakes. In some cases, simple models of the rupture process are used and comparisons of the calculated and observed motions are utilized to determine some of the characteristics of the rupture model such as average slip on the fault, average rupture velocity or average rise time. In other cases, more complex fault models are involved and informal (trial-and-error) or formal inversion techniques are utilized to determine the spatial variation of slip, time of arrival of the rupture and duration of the rupture. These inversion studies have given a glimpse into the complexity of the rupture process and suggest the difficulty of obtaining estimates of the high-frequency components of near-source ground motion by use of deterministic models. At intermediate or low frequencies, on the other hand, near-source records obtained in several earthquakes show some very similar waveforms (Fig. 5.0.1) which can be synthesized by use of simple dislocation models.

Simulation studies for the Parkfield 1966 and Imperial Valley 1979 earthquakes are described in some detail in the following two sections. The studies for the Parkfield earthquake span the development of the forward simulation techniques; those for the Imperial Valley earthquakes illustrate the application of inversion techniques.

References to modelling studies for the 1968 Borrego Mountain [Heaton and Helmberger (1977), Ebel and Helmberger (1982)], 1971 San Fernando [Mikumo (1973), Niazy (1973), Trifunac (1974), Boore and Zoback (1974), Niazy (1975), Bouchon and Aki (1977), Bouchon

BEST COPY AVAILABLE

(1978), Heaton and Helmberger (1979), Heaton (1982)], 1979 Coyote Lake [Bouchon (1982), Liu and Helmberger (1983)] and 1984 Morgan Hill [Hartzell and Heaton (1983)] earthquakes are given at the end of the chapter.

BEST COPY AVAILABLE

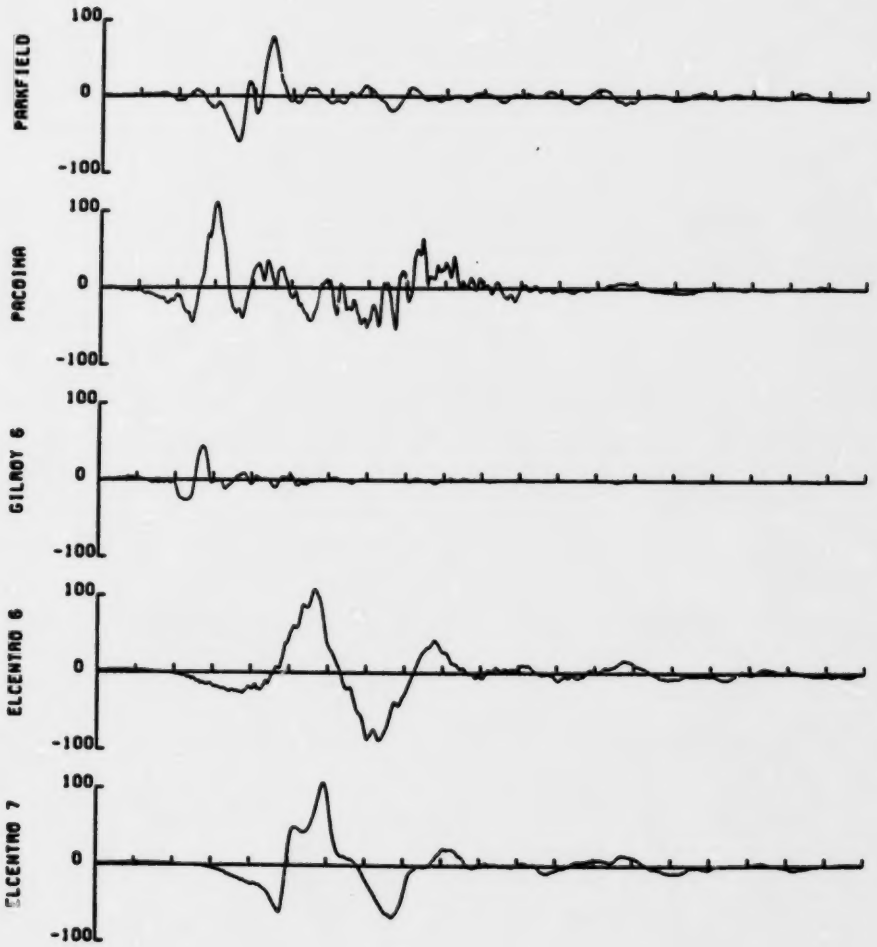

Fig. 5.0.1 Near-source horizontal particle velocity time-histories for California earthquakes (1966 Parkfield, 1971 San Fernando, 1979 Coyote Lake and 1979 Imperial Valley earthquakes). Amplitudes are in cm/sec and each tic mark represents 1 sec (Archuleta and Hartzell, 1981).

BEST COPY AVAILABLE

5.1 Parkfield 1966 Earthquake.

The Parkfield earthquake of June 27, 1966 (9:26 p.m. Pacific daylight time) was a moderate magnitude event (M_L = 5.5, m_b = 5.9, M_S = 6.5) with a fracture zone consisting of two segments separated by an echelon offset of 1 km (Fig. 5.1.1). The first segment with a total length of 25-30 km starts about 5 km to the northwest of the epicenter, extends to the southeast past Parkfield and ends about 5 km to the southeast of Gold Hill. The second segment with a total length of 8 - 10 km extends from 2-5 km to the southeast of Gold Hill to about 2 km past Cholame. The fault planes are characterized by a strike of N39° W and a dip of 86° SW. The focal depths of aftershocks range from 1 to 15 km with concentrations at depths between 2 and 4 km and also between 8 to 10 km.

The ground motion generated by the earthquake was recorded on 5 accelerographs located on an array across the fault near Cholame. Station 2 of the array was located only 80 m away from the fault trace. The record of the component of motion perpendicular to the fault (N65° E) at Station 2 exhibits a pronounced pulse with a duration of 1.5-2.0 sec, a peak acceleration of 0.5 g, a peak velocity of about 80 cm/sec and a peak displacement of about 30 cm (Fig. 5.1.2).

The record at Station 2 as well as those on the remaining four stations have had a very important role in the development of modeling techniques for near source ground motion and in the study of the rupture process on the basis of near source data. Since the pioneering work of Aki (1968) who used the near source field from a rectangular dislocation to model the record at Station 2, a large number of studies involving synthesis of ground motion and comparisons with the Parkfield data have been conducted [Aki (1968), Haskell (1969), Boore et al (1969), Tsai and Patton (1973), Niazy (1973), Boore and Zoback (1974), Trifunac and Udwadia (1974), Anderson (1974), Kawazaki (1975), Levy and Mal (1976), Hartzell et al (1978), Del Mar Tech. Assoc/Tera Corp. (1978), Bouchon (1979)]. Other studies dealing with interpretations of the rupture process include those of Murray (1973), Aki (1979) and Lindh and Boore (1981).

BEST COPY AVAILABLE

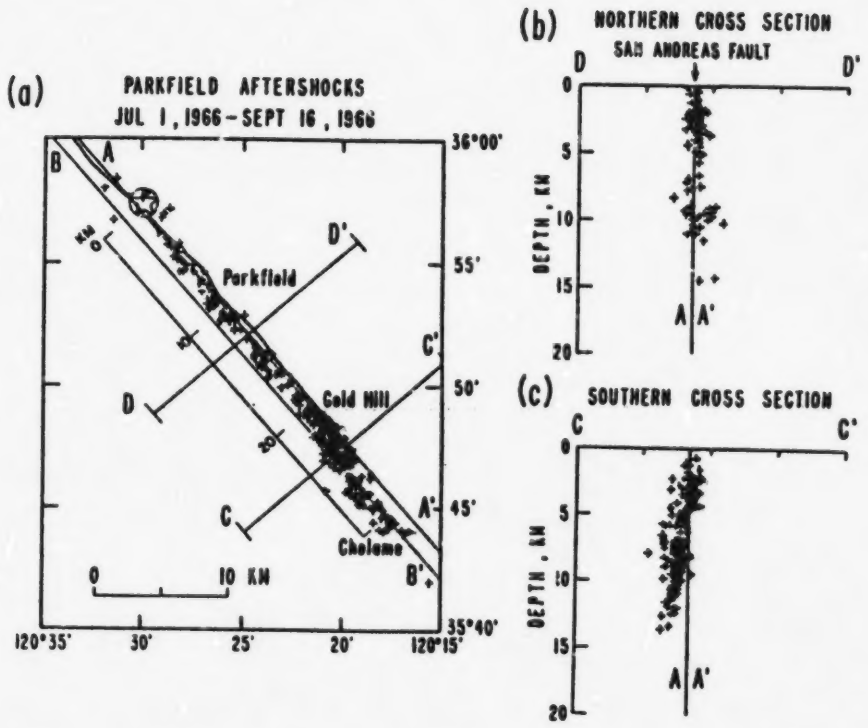

Fig. 5.1.1. (a) Map of Parkfield area showing well located aftershocks for the period 1 July to 15 September 1966 (Eaton *et al.*, 1970). (b) Transverse crossection of the northwestern half of the data in (a). (c) Same as (b), southeast half. (Lindh and Boore, 1981).

BEST COPY AVAILABLE

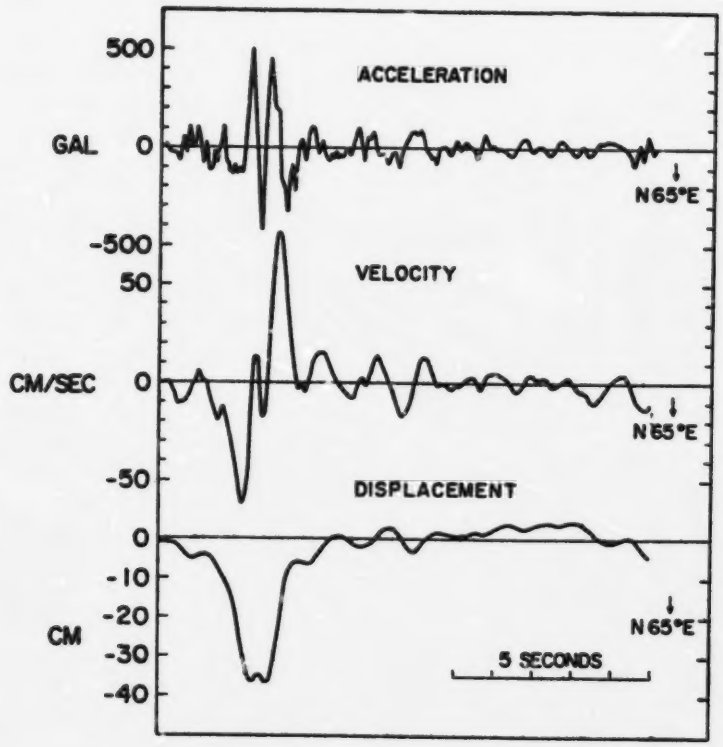

Fig. 5.1.2. Acceleration recorded at Station 2 (N65° E) and velocity and displacement obtained by Aki (1968) by integration. Similar velocities and displacements have been obtained by Housner and Trifunac (1967) [after Aki (1968)].

BEST COPY AVAILABLE

As noted by Lindh and Boore (1981), the simulation studies of the Parkfield earthquake can be grouped into three categories. The first category involves studies in which only the record at Station 2 is modelled [Aki (1968), Haskell (1969), Boore et al (1969), Niazy (1973), Boore and Zoback (1974)). Kawazaki (1975), Hartzell et al. (1978), Bouchon (1980), Luco and Anderson (1985)]. The second category involves studies which attempt to model the records at all five stations [Anderson (1974), Levy and Mal (1976), Del Mar Tech Assoc/ Tera Corp. (1978), Archuleta and Day (1980)]. The final category involves the work of Trifunac and Udwadia (1974) in which a least square inversion procedure was used to determine the slip characteristics on several segments of the fault which lead to the best fit with the displacements recorded at all five stations. The models, synthesis techniques and results obtained in the studies in each of these categories are examined next.

The first study in the first category corresponds to the work of Aki (1968) who synthesized the displacement at Station 2 by use of a dislocation model. In Aki's study, the response in the frequency domain for the extended fault was obtained by superposition of the contributions of a number of small fault elements calculated using the displacement for a point dislocation in a full space given by Maruyama (1963) and the approximate method of integration of Ben-Menaham (1961). The response in the time domain for a step-dislocation was then obtained by Fourier synthesis including frequencies up to 3 Hz. The effects of the free surface were approximated by doubling the displacements resulting from the full-space solution. In the calculations, the northern segment of the fault was taken to have a length of 30 km and the southern segment a length of 7 km. The station was located 2 km from the southern end of this segment and 80 m to the southwest of the fault. The fault planes were vertical and the rupture extended from the surface to a depth of 3 km. Sensitivity calculation showed that the location of the bottom of the fault had little effect on the calculated motion at Station 2 and that the rupture velocity was a significant but not a dominant factor. The amplitude of the slip was constant along the fault but varied elliptically with depth from an amplitude D_o on the surface to zero at the bottom of the fault. The calculations were made for a rupture velocity of 2.2 km/sec in a uniform medium

BEST COPY AVAILABLE

with P and S wave velocities of 6.0 and 3.5 km/sec respectively. The results obtained by Aki (1968) for the parallel and perpendicular displacements normalized by the total slip D_o on the surface are shown in Fig. 5.1.3. The displacement pulse obtained has the correct duration of about 1.5 sec and attains its peak value at the time of passage of the rupture front in front of the station (t_o). The major contribution to the perpendicular component results from the southern segment of the fault; for the parallel component most of the contributions come from a 2 km segment of the southern branch of the fault centered about the station. Comparison with the observed perpendicular pulse suggests a value of $D_o \approx 60$ cm which is more than 10 times larger than the surface offset observed immediately after the earthquake (~ 4 cm). A possible explanation offered by Aki is that a thin surface layer with a thickness of less than 100 m was mechanically decoupled from the underlying medium and thus masked the amplitude of the dislocation at depth.

Haskell (1969) modelled the record at Station 2 by use of a uniform finite-ramp (rise time = 0.9 sec) dislocation model on a vertical rectangular fault in an elastic full-space (α = 4.95 km/sec, β = 2.86 km/sec). The fault with a length of 20 km extended from the surface to a depth of 2.5 km. The station was located 4 km from the southern end of the fault and 2 km away from the fault trace. The rupture started at the northwestern end of the fault and propagated to the southeast with a constant rupture velocity of 2.2 km/sec. The effects of the free-surface were approximated by doubling the response calculated for a full space. The calculations are based on a representation of the displacement as an integral over the fault area and over time of the slip on the fault multiplied by appropriate Green's functions [de Hoop (1958)]. In the case of ramp dislocations, the integration over time can be performed analytically [Haskell (1964)] and the calculation of displacement reduces to a numerical integration over the fault plane. To match the amplitude of the perpendicular component of the displacement pulse at Station 2 the amplitude of the slip on the fault would have to be D_o = 93 cm.

BEST COPY AVAILABLE

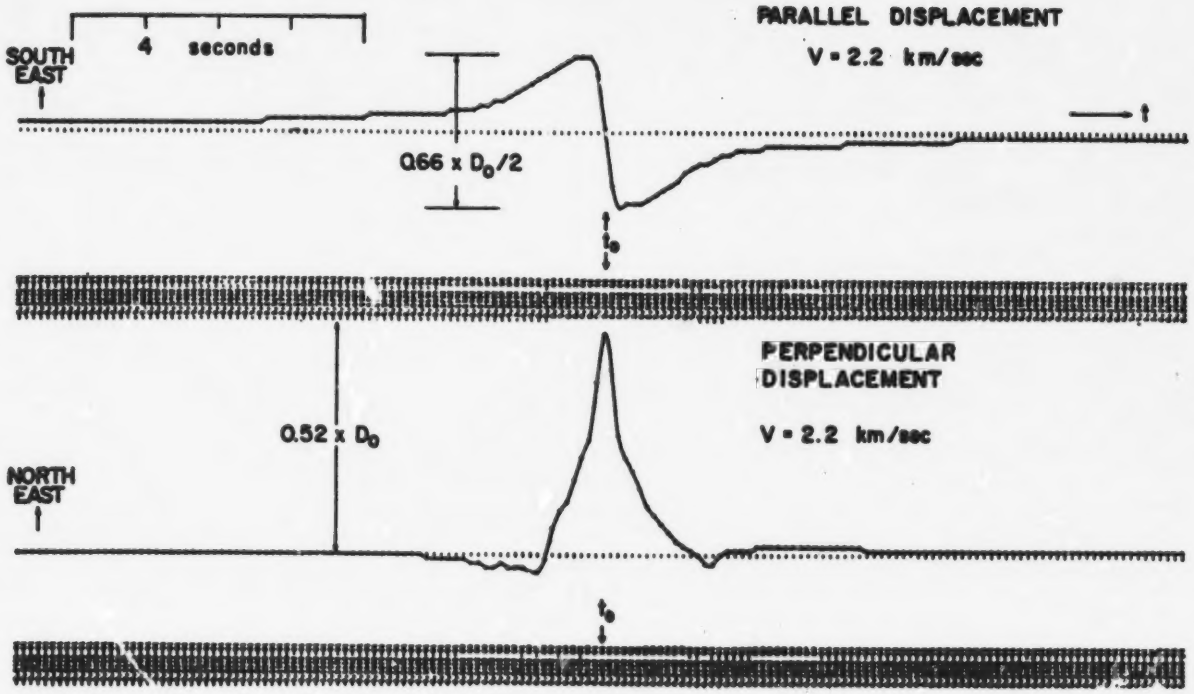

Fig. 5.1.3. Synthetic parallel and perpendicular displacement components at Station 2. Amplitudes are normalized by D_o, the maximum slip on the fault. The time of passage of the rupture front is marked at t_o (Aki, 1968).

BEST COPY AVAILABLE

Boore *et al.* (1971), Niazy (1973) and Boore and Zoback (1974), have used two-dimensional dislocation models to synthesise the motion at station 2. These models are based on the observation by Aki that, above certain frequency, the width of the fault has little effect on the calculated motion. Boore *et al.* (1971) considered a steady-state smeared-out-dislocation model (α = 6.0 km/sec, β = 3.5, km/sec v = 2.2 km/sec) and found results of the same order as those of Aki (1968) and Haskell (1969). Niazy (1973) using a two-dimensional dislocation of finite length also concluded that the slip on the fault would have to be several times larger than the amplitude of the perpendicular component of motion close to the fault. Boore and Zoback (1974) used a two dimensional dislocation model in which the rupture starts 8 km to the northwest of the station and ruptures at 2.2 km/sec to a point 2 km to the southeast of the station. The medium is characterized by α = 5.5 km/sec and β = 3.2 km/sec. A ramp and a rounded ramp dislocations with a rise time of 0.9 sec and a slip of 200 cm were used. A comparison of the perpendicular velocity component at Station 2 obtained by integration of the recorded acceleration and of that resulting from the model is shown in Fig. 5.1.4. The calculated results also agree with those of Tsai and Patton (1972) calculated by use of Haskell's synthesis technique for the corresponding three-dimensional rupture model.

Kawazaki (1975) modelled the displacement and acceleration at Station 2 and investigated the free surface effects. The rupture model used by Kawazaki (1975) is based on the work of Aki (1969) and consists of a fault of length 2 km centered about the station and extending from the free surface to a depth of 3 km. A ramp dislocation of variable amplitude with depth propagates horizontally with rupture velocity of 2.2 km/sec. The properties of the medium are α = 6.0 km/sec and β = 3.5 km/sec. Kawazaki found by comparison of a solution for a half-space with that for a full-space that the effects of the free surface on the calculated displacement could be accounted for by doubling the full-space results. Matching of the 'observed' displacement (pulse obtained by double integration of the recorded acceleration perpendicular to the fault) to the theoretical displacement pulse yields estimates of the average dislocation of 200 and 400 cm for rise times of 0.5 and 1.0 sec, respectively. On the other hand, Kawazaki found that

BEST COPY AVAILABLE

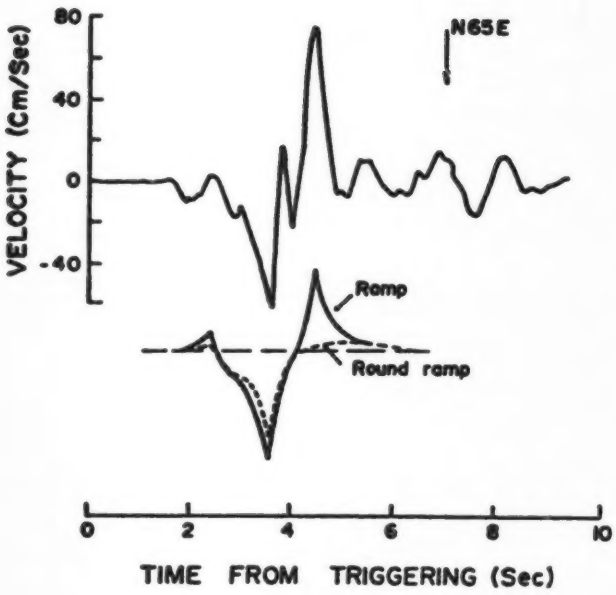

Fig. 5.1.4. Comparison of the velocity obtained by integration of the perpendicular acceleration recorded at Station 2 with the synthetic velocity wave form calculated by Boore and Zoback (1974) (after Boore and Zoback, 1974).

BEST COPY AVAILABLE

matching the theoretical acceleration to the recorded acceleration perpendicular to the fault yields estimates of the average slip of 50 and 70 cm for rise times of 0.5 and 0.7 sec, respectively. The recorded and calculated accelerations are shown in Fig. 5.1.5. The discrepancy between the displacement-based and acceleration-based estimates of the dislocation amplitude led Kawazaki to conclude that the displacement pulse calculated by double integration of the recorded acceleration is in error. A more probable explanation is that the theoretical accelerations calculated by Kawazaki are in error. The results obtained by Madariaga (1978) described in the previous chapter indicate that the starting "cylindrical" velocity pulse for a step dislocation is characterized by a singularity of the type $(t - \frac{r}{\alpha})^{-1/2}$ or $(t - \frac{r}{\beta})^{-1/2}$. For a ramp dislocation, the corresponding starting phase of the acceleration pulse would have the same singularity. An observer located at the depth of the top of the fault would feel the "cylindrical" waves and would observe infinite accelerations for a ramp dislocation on the fault. The finite acceleration amplitudes calculated by Kawazaki (1975) are probably an artifact of the discretization.

Hartzell et al. (1978) extended a method developed by Anderson (1976) to calculate the ground motion from a kinematic model of an extended rupture in a uniform elastic half-space and used it to synthesize the displacement and velocity at Station 2. The procedure is based on the representation of the displacement on the ground surface in terms of integrals over the fault surface and over time of the Green's functions for a half-space multiplied by the slip on the fault. The Green's functions for the uniform half-space are calculated by the method described by Johnson (1974). The procedure admits arbitrary spatial and temporal variation of the slip function. For the Parkfield calculations, the authors model the fault as a rectangular area with a length of 30 km extending from a depth of 3 km to a depth of 9 km. The final static slip varies elliptically over the length of the fault, being zero at the ends and having its maximum value at the center of the fault. The source-time function is constant over the fault and takes the form $\sqrt{1 - |(t' - \tau)/\tau|^2}$, $0 < t' < \tau$ in which τ is the rise time and t' is time after the arrival of the rupture. The rupture initiated at a depth of 6 km, 3.75 km from the northern end of the fault and grows outward, in a circular fashion, with a rupture velocity of

BEST COPY AVAILABLE

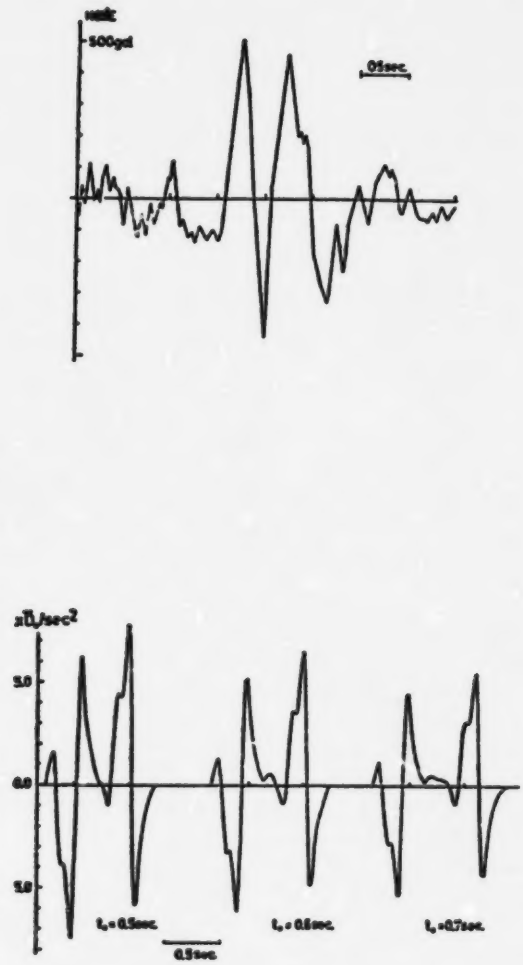

Fig. 5.1.5 Comparison of the recorded and calculated acceleration for rise times of 0.5, 0.6 and 0.7 sec (Kawazaki, 1975).

BEST COPY AVAILABLE

0.9β = 2.7 km/sec. The characteristics of the medium are α = 5.2 km/sec and β = 3.0 km/sec. Synthetics were calculated for models with various values for the maximum slip on the fault (100 and 150 cm), rise time (0.5 and 1.0 sec) and distance from the southern end of the fault to the station (0.5 and 4.5 km). It must be noted, that in this model, the fault stops before reaching Station 2 (Fig. 5.1.6). A comparison of the observed and synthetic displacements and velocities for various models is shown in Fig. 5.1.6. The preferred model is PARK 7 with a maximum slip of 100 cm, a rise time of 0.5 sec and a distance of 4.5 km from the end of the fault to Station 2.

Bouchon (1979) used the discrete wave number representation method to model the 1966 Parkfield earthquake as a Haskell-type dislocation source embedded in a layered medium. A fist model considered by Bouchon is shown in the upper part of Fig. 5.1.7. The displacement calculated at Station 2 for this model showed that the predominant motion was perpendicular to the fault. The wave form of the calculated perpendicular displacement, however, was quite different from the displacement obtained from the recorded acceleration. The calculated displacement showed marked Love waves which are not apparent on the record. To synthesize the motion at Station 2, Bouchon (1979) restricted his attention to the southern branch of the fault and modified the model by reducing the length to the 8.5 km closer to the station. In addition, he allowed the rupture to penetrate into the sediment to a depth z_o ranging from 100 m to 1.5 km. The calculated displacement and velocity time histories for the perpendicular component are compared with the 'observations' in the lower part of Fig. 5.1.7. The calculations for z_o = 0.1, 0.5, 1.0 and 1.5 km required fault slips of 35, 40, 50 and 65 cm, respectively, to match the observations. The calculations assumed a ramp dislocation with a rise time of 0.3 sec. According to Bouchon, the best fit is obtained for z_o = 100 m which leads to a slip of 35 cm and a slip velocity of 120 cm/sec. Based on these results Bouchon concluded that the northern branch of the fault must have been buried well below the sediments and that the southern branch was characterized by a much shallower rupture penetrating into the sediments. Bouchon also concludes that the rupture must propagate at least up to the station and that the sedimentary layer

BEST COPY AVAILABLE

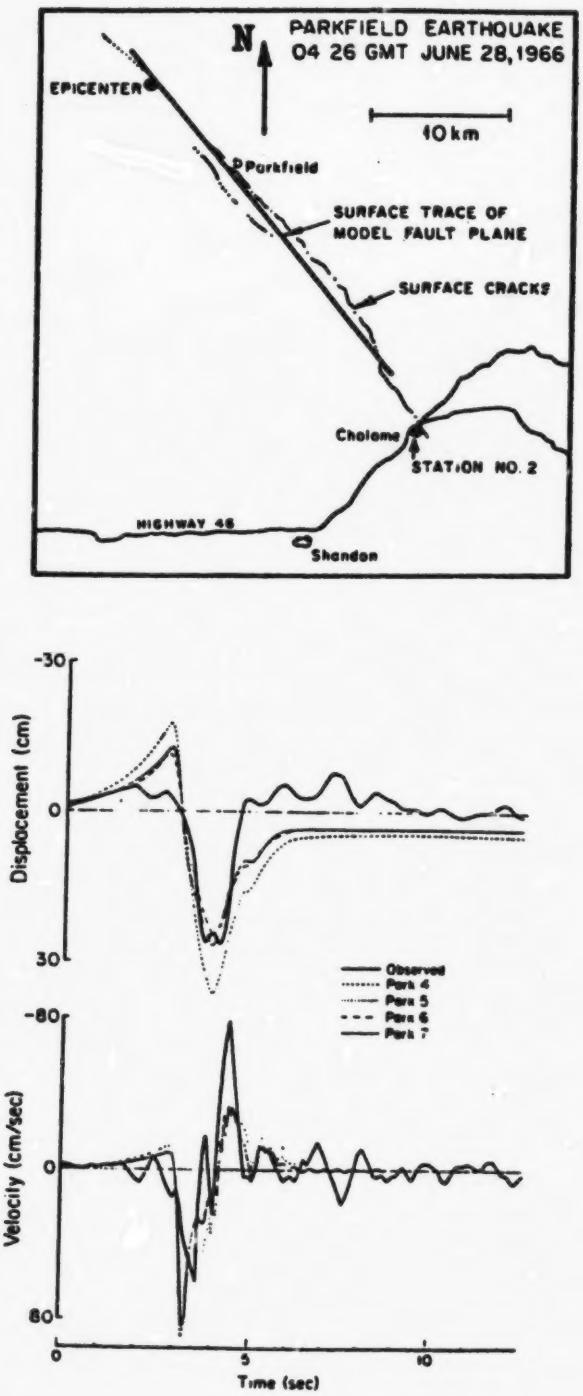

Fig. 5.1.6 **Fault model considered by Hartzell *et al.* (1978) and comparison of observed and synthetic displacements and velocities at Station 2 (Hartzell *et al.*, 1978).**

BEST COPY AVAILABLE

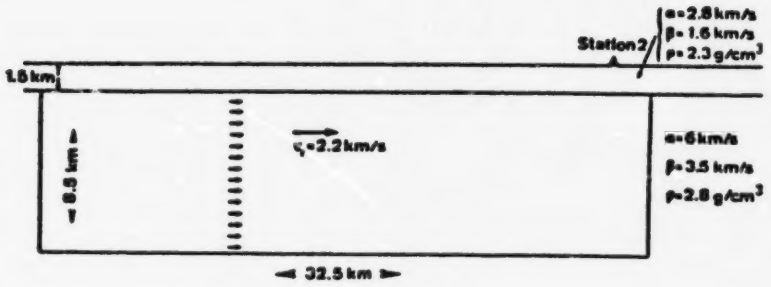

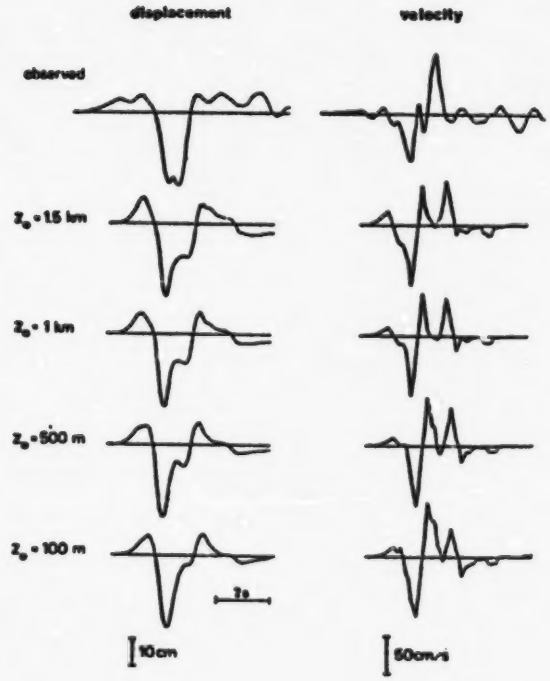

Fig. 5.1.7 Initial source-medium-station configuration used by Bouchon (1979) and comparison of observed and synthetic displacement and velocities for various positions of the top of the fault (Bouchon, 1979).

BEST COPY AVAILABLE

strongly amplified the motion recorded at Station 2.

Finally, Luco and Anderson (1985) have modelled the velocity pulse at Station 2 by use of a steady-state dislocation model in an elastic half-space. The half-space is characterized by α = 5.6 km/sec and β = 3.23 km/sec. The rupture plane dips 85° to the SW and the rupture area extends from a depth of 0.5 km to a depth of 9 km. The step dislocation of amplitude 50 cm moves along the infinite length of the fault with a rupture velocity of 2.5 km/sec. The station is at a distance of 500 m from the intersection of the plane of the fault and the free-surface. The calculated velocity pulses parallel and perpendicular (65°) to the fault are shown in Fig. 5.1.8. The velocity pulse calculated by integration of the recorded acceleration is also shown in the Figure. It is apparent that the steady-state dislocation model in a uniform half-space leads to the correct velocity pulse shape but underestimates the amplitude by a factor of the order of 5 (notice the difference of scale). As shown by the work of Bouchon (1979), the inclusion in the model of the softer shallow layers would increase the amplitude of the calculated pulses.

The second group of modelling studies attempts to synthesize the motion at all five accelerograph stations of the Cholame array. Anderson (1974) used the formulation of Haskell to calculate the displacement field for a uniform ramp dislocation propagating over a rectangular rupture surface in an unbounded elastic medium. The medium was characterized by α = 6.0 km/sec and β = 3.436 km.sec. The fault, of total length 38 km, extended 5 km to the northwest of the epicenter and also ruptured past station No. 2 to the southeast. The model of the rupture extends from a depth of 2 km to a depth of 10 km. The slip on the fault, calculated on the basis of a seismic moment of 1.9×10^{25} dyne-cm, was taken to be 25 cm. The remaining two parameters in the model corresponding to the rupture velocity and to the rise time were selected by comparison of the synthetic displacements with those obtained by double integration of the recorded accelerations. According to Anderson (1974) the best fit is obtained for rupture velocities in the range from 2.8 to 3.0 km/sec and for rise times less than 1.0 sec. The quality of the fit at stations 2 and 5 is shown in Fig. 5.1.9. Clearly, the model gives reasonable results for

BEST COPY AVAILABLE

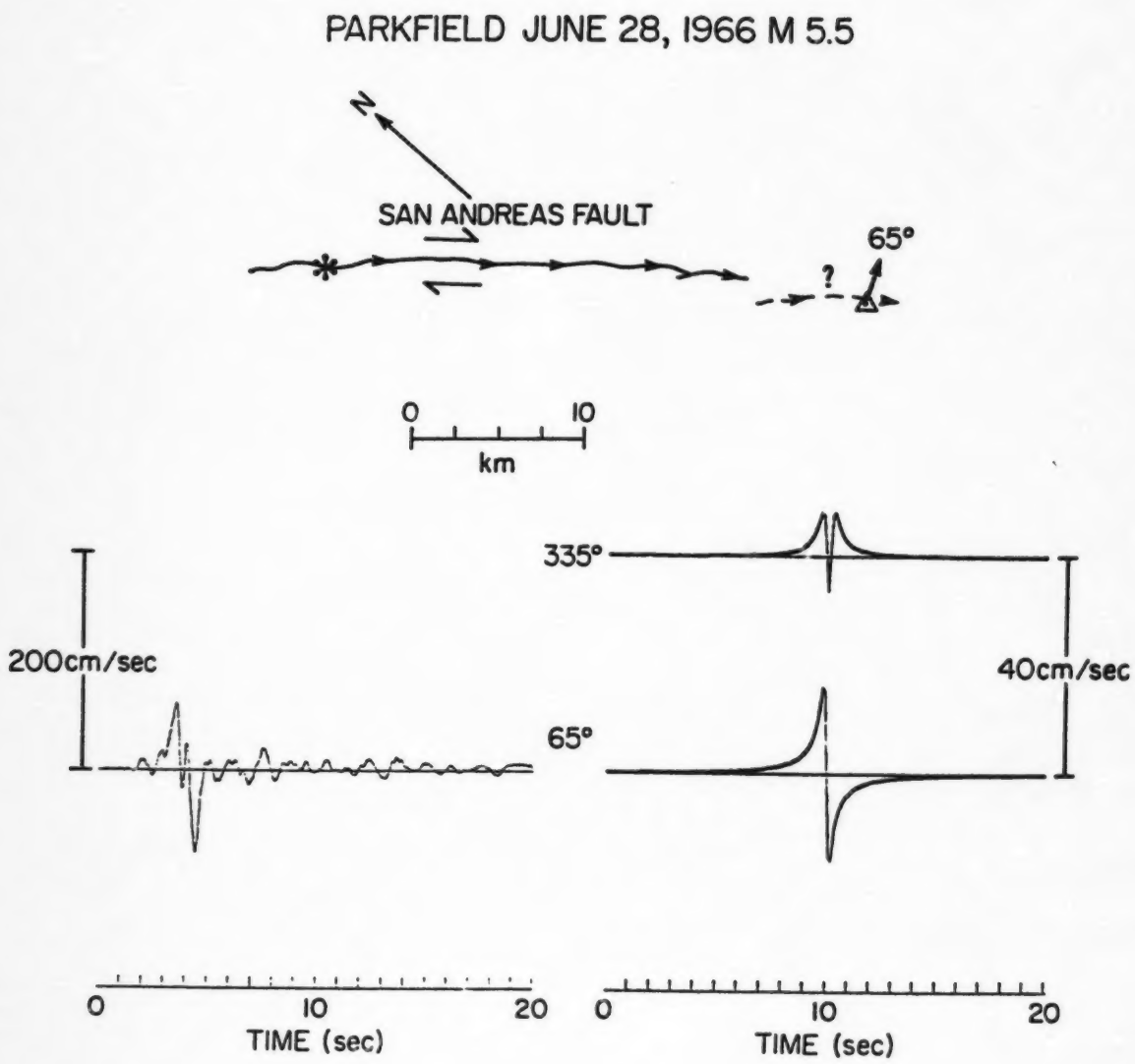

Fig. 5.1.8. Comparison of 'observed' (left) and synthetic (right) velocity pulses calculated by use of a steady-state dislocation model (notice scale differences) (Luco and Anderson, 1985).

BEST COPY AVAILABLE

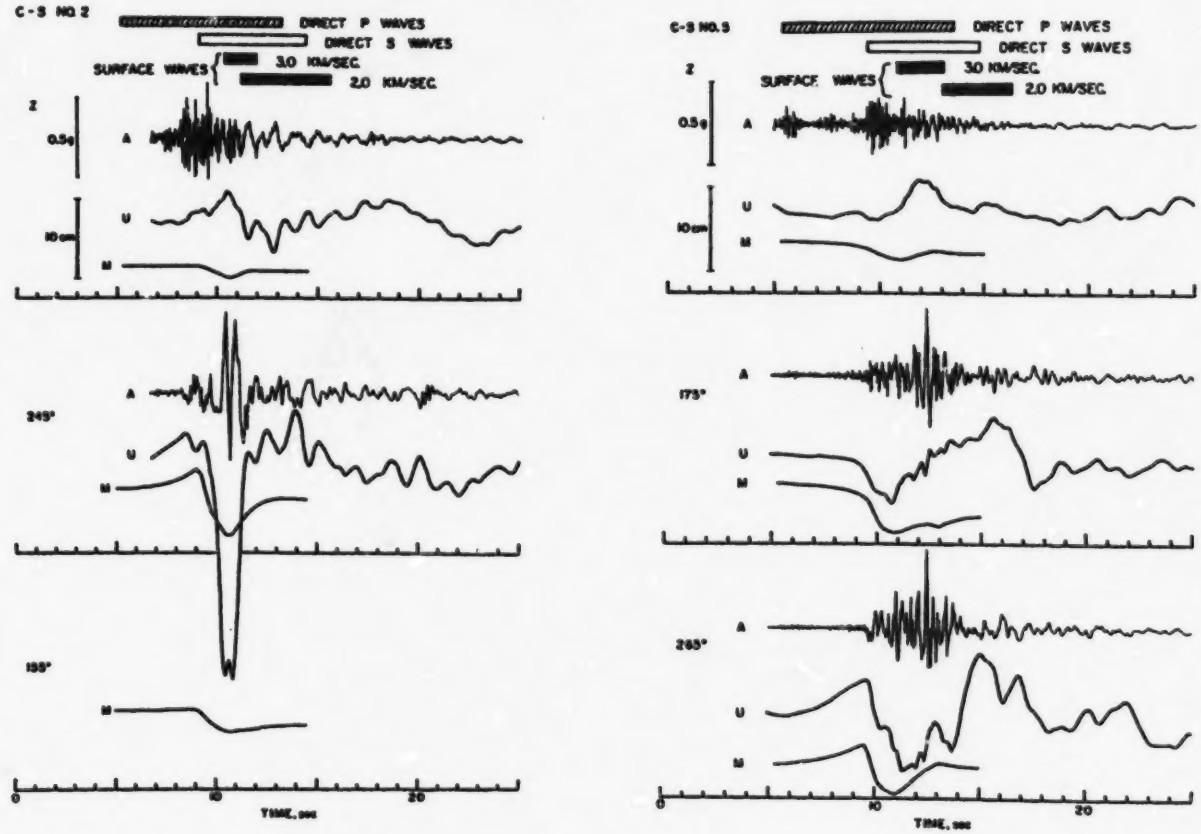

Fig. 5.1.9 Comparison of 'observed' (U) and synthetic (M) displacements at stations 2 and 5. The time histories designated by A correspond to the recorded accelerations. The bars at the top indicate the time windows for arrival of P, S and surface waves with velocities of 2.0 and 3.0 km/sec (Anderson, 1974).

BEST COPY AVAILABLE

the initial displacement at station 5 (also at stations 8 and 12) but a very poor fit to the displacement pulse at station 2.

Levy and Mal (1976) used the representation theorem in the frequency domain to obtain the Fourier Transform of the displacement for a rectangular fault in a uniform elastic half-space. Time domain results were obtained by Fast Fourier synthesis. The slip on the fault varies elliptically with respect to time and along the length of the fault. The model used for the Parkfield earthquake involved a rupture on a vertical plane over a length of 38 km extending from a depth of 3 km to a depth of 9 km. The medium was characterized by α = 5.6 km/sec and β = 3.23 km/sec. The dislocation had a maximum static value of 200 cm and the rupture velocity was 2.4 km/sec. Frequencies in the range from 0.05 to 3 Hz were included in the calculations. A comparison of the synthetic displacements with those obtained by integration of the recorded accelerations are shown in Fig. 5.1.10. Levy and Mal (1976) consider the agreement reasonable for the horizontal components but fair or poor for the vertical components.

Archuleta and Day (1980) calculated theoretical displacement-time-histories for the Parkfield earthquake as resulting from a propagating stress relaxation in a vertically heterogeneous medium. The two-step procedure starts with the calculation of the slip on the fault resulting from a propagating stress relaxation. The second step involves the calculation of the response of the layered medium by use of the representation theorem involving the slip on the fault and the Green's functions for the layered half-space. The stress relaxation and the calculation of the Green's function are performed by use of the finite element method. The Parkfield earthquake model used involved a fault of length 30km extending from the epicenter to 2 km past Station 2. The rupture was confined between depths of 3 and 9 km and the rupture velocity was 3.1 km/sec. A constant effective stress of 25 bars was used. The Parkfield structure was modelled by two elastic layers overlying an elastic half-space (H_1 = 2 km, α_1 = 3.0 km/sec, β_1 = 1.73 km/sec; H_2 = 2 km, α_2 = 5.0 km/sec, β_2 = 2.89 km/sec; H_3 = ∞, α_3 = 6.0 km/sec, β_3 = 3.46 km/sec). The average slip resulting from the stress relaxation is 43 cm. Comparisons of theoretical and 'observed' displacements at stations 2 and 5 are shown in Fig. 5.1.11.

BEST COPY AVAILABLE

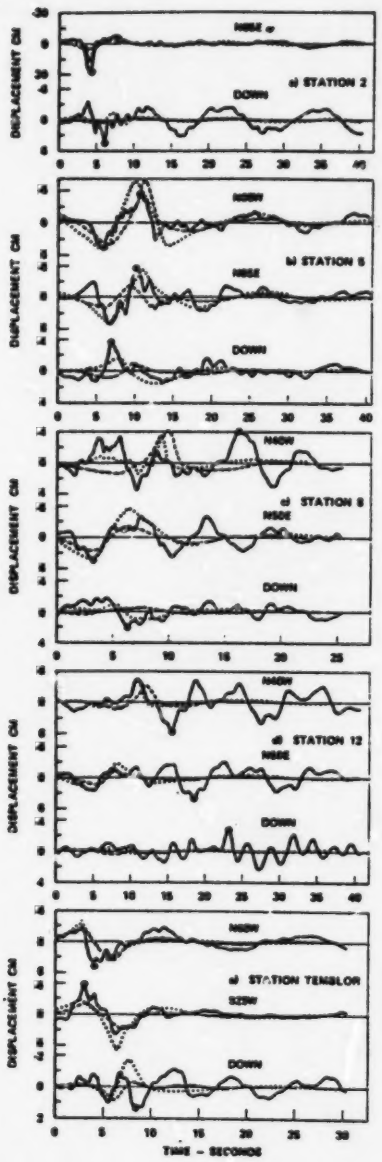

Fig. 5.1.10 Comparison of calculated and 'observed' displacements. The solid line corresponds to the 'observed' displacements, the dotted line to the calculated displacements for a half-space, and the segmented line to the calculated displacements for a full space (Levy and Mal, 1976).

BEST COPY AVAILABLE

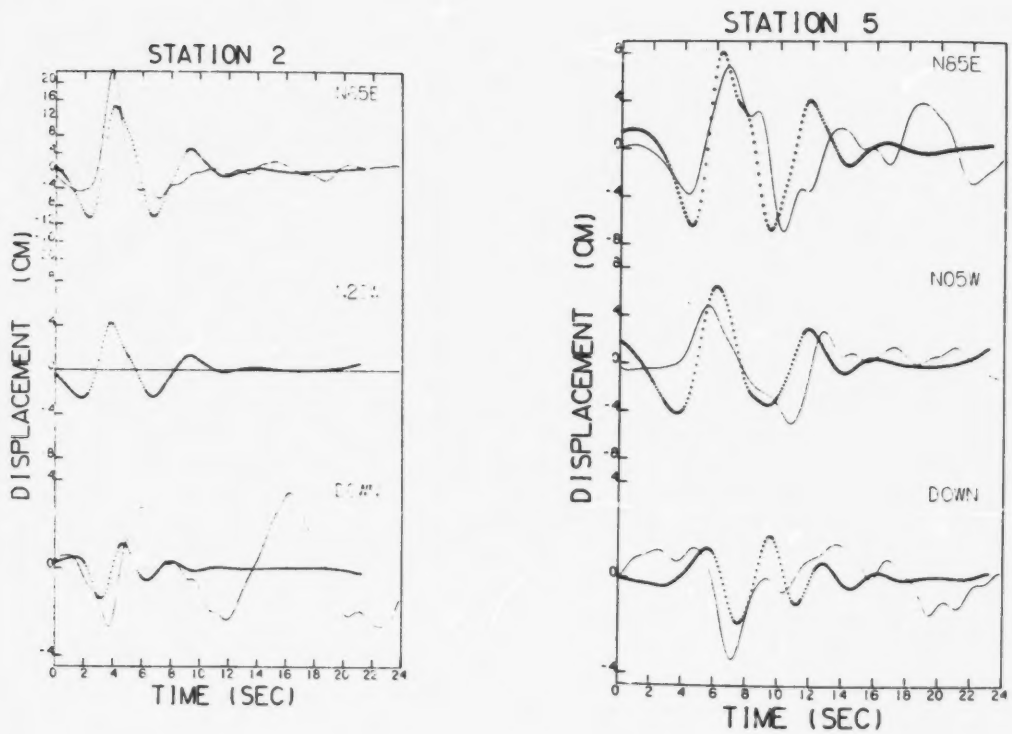

Fig. 5.1.11. 'Observed' (solid line) and synthetic (dotted line) displacements at Stations 2 and 5 (Archuleta and Day, 1980).

BEST COPY AVAILABLE

A simulation of the ground motion recorded at the five accelerograph stations of the Cholame array was presented in a report by Del Mar Technical Associates/Tera Corporation (1978). The fault with a total length of 32 km was modelled by three segments extending from a depth of 1.5 km to 10.5 km (Fig. 5.1.12). The structure was modelled by 6 elastic layers overlying an elastic half-space. The rupture initiated at the northwestern end of the fault at a depth of 10.5 km and propagated upward and to the southeast with a local rupture velocity equal to ninety percent of the local shear wave velocity. The average slip of the order of 50 cm corresponded to a seismic moment of 3.9×10^{25} dynes-cm. Comparison of the 2% velocity response spectra based on the observed and calculated accelerations at station 2, 5, 8 and 12 are shown in Fig. 5.1.12.

The final category of simulation studies involves the work of Trifunac and Udwadia (1974) who applied the method of Haskell (1969) to a fault area divided into seven segments. The slip in each segment was determined to give the best fit, in a least square sense, to the 'observed' displacements at the five accelerograph stations. The Parkfield earthquake model corresponded to a rupture extending from a depth of 3 km to a depth of 6 km. The northern portion of the fault was divided into 4 equal segments; the southern portion was divided into 3 equal segments. The length of each segment varied from 4.4 to 5.2 km depending on the rupture velocity. The northern and southern fault planes strike N43° W and N31° W, respectively. The dip angle of both planes was 85.5° SW. The rupture velocity and the rise time (0.7 sec) were considered to be equal for all segments; the slip was uniform within each segment and the free-surface effects were approximated by doubling the calculated amplitudes for a full space. The uniform elastic medium was characterized by α = 5.6 km/sec and β = 3.2 km/sec. The observed and calculated displacements were filtered to consider only frequencies in the band from 0.11 to 1 Hz. Trifunac and Udwadia (1974) on the basis of calculations for rupture velocities ranging from 2.2 to 2.6 km/sec conclude that the rupture velocity must have been between 2.3 and 2.5 km/sec. The resulting dislocation amplitudes are of the order of 120 cm for the northern fault plane and less than 20 cm for the southeastern section. Comparison of the

BEST COPY AVAILABLE

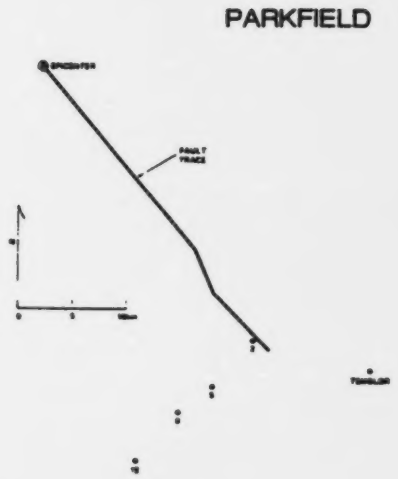

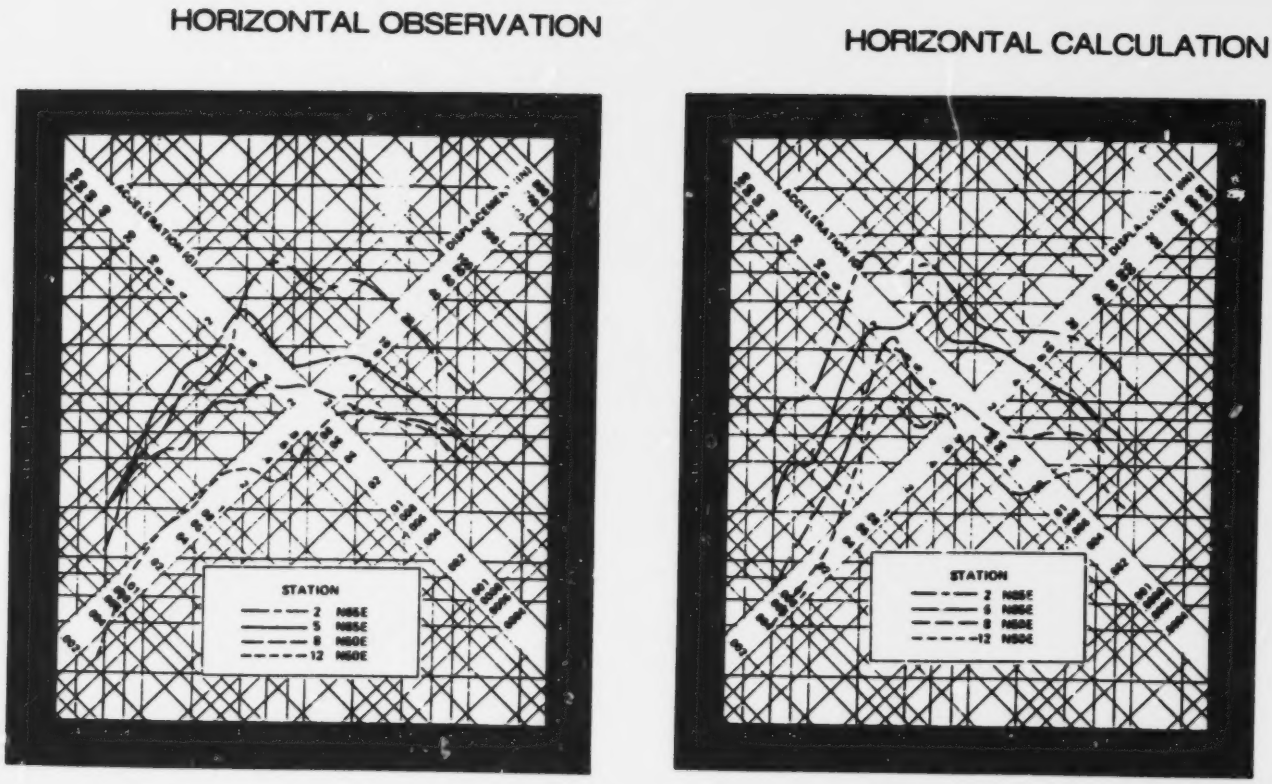

Fig. 5.1.12. Fault model used in the DELTA/TERA study and comparison of the 2% velocity response spectra based on the recorded (left) and calculated (right) accelerations at Stations 2, 5, 8 and 12 (Del Mar Technical Associates/Tera Corp., 1978).

BEST COPY AVAILABLE

synthetic and 'observed' displacements at stations 2 and 5 are shown in Fig. 5.1.13. The agreement between the calculated and 'observed' displacements is considered good except for Station 2 (component N65° S) and station Temblor (component S25° W) where the differences may be as high as a factor of two. The agreement in the vertical components is considered poor to fair. These statements refer to the beginning of the records prior to the arrival of surface waves.

The previous review of efforts to synthesize the near-source ground motion for the Parkfield earthquake illustrates the development of models and synthesis techniques which has taken place since 1968. The models have evolved from the uniform dislocation models in a uniform unbounded elastic medium which were used in the earlier studies to the current models involving variable slip and layered viscoelastic media. The review also indicates the importance of including layering. The studies which focused on the transverse motion recorded at Station 2 and which did not include layering yielded estimates for the slip on the fault ranging from 60 to 400 cm which are excessive. When the effects of layering are included, a reasonable agreement can be obtained for a slip of 35 cm. Studies involving a uniform or slowly varying slip and which consider all five stations require average fault slips in the range from 25 to 50 cm to obtain a reasonable overall agreement but usually underestimate the motion recorded at Station 2. These results, the conclusions of Trifunac and Udwadia (1974), as well as those of Bouchon (1979), indicate the need to consider a spatially variable rupture process to explain all of the characteristics of the ground motion recorded during the Parkfield earthquake.

BEST COPY AVAILABLE

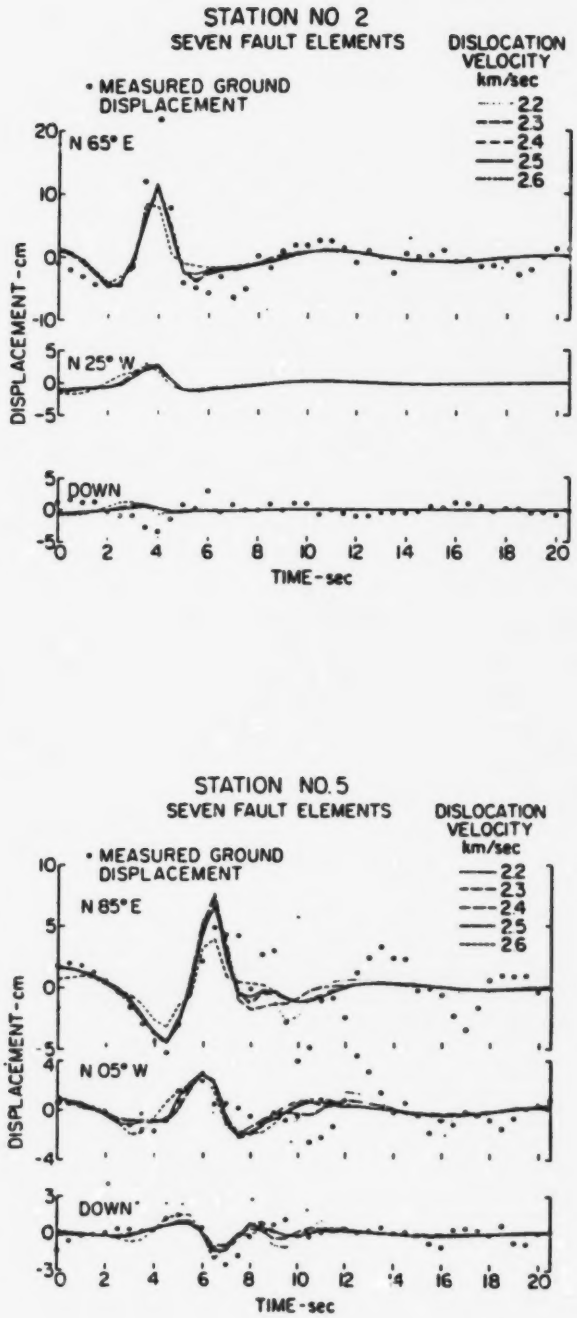

Fig. 5.1.13. Comparison of 'observed' (dots) and calculated displacements at Stations 2 and 5 (Trifunac and Udwadia, 1974).

EST COPY AVAILABLE

5.2 Imperial Valley 1979 Earthquake.

The near-source ground motion generated by the October 15, 1979 Imperial Valley earthquake (M_L = 6.6) was recorded on over 30 accelerographs operating in the United States and Mexico. The fault geometry and the location of some of the stations are shown in Fig. 5.2.1. The rupture area extends some 35-40 km to the NW of the epicenter and some 5 to 10 km to the SE. The rupture extends to a depth of 12-13 km. During the 1979 earthquake, ground breakage occurred on both the Imperial and Brawley faults. Surface faulting on the Imperial fault is primarily right lateral with maximum offsets of 60 to 70 cm on the section of the fault extending 5 to 10 km north of the border. The magnitudes of the surface offset decreases as one moves further north. There are no surface offsets in the epicentral region or within 5 km of the international border. The offsets on the Brawley fault are secondary in amplitude to those on the Imperial fault. The seismic moment for the event is $M_o \sim 7.0 \times 10^{25}$ dyne-cm.

The large number of records obtained and the comparatively simple geologic setting, consisting of a deep sedimentary basin with relatively horizontal layering, created an opportunity to construct detailed models of the rupture process. Hartzell and Helmberger (1982), Olson and Apsel (1982), Hartzell and Heaton (1983) and Archuleta (1984) have proposed fairly detailed faulting models in a layered half-space. Some of the characteristics of the models are listed in Table 5.2.1. Hartzell and Helmberger (1982) proposed a rupture model with uniform rupture velocity (2.5 km/sec) and rise time (1.0 sec) and considered several spatial distributions of slip in an attempt at matching the displacements calculated by integration of recorded accelerations. The preferred model, 9WM, is shown in Fig. 5.2.2. The preferred model is such that the majority of the slip would occur at depths larger than 5 km. In addition, two zones in which the slip reaches 2.5 km are located 8 and 20 km north of he epicenter. A comparison of calculated and 'observed' displacements is shown in Fig. 5.2.3.

Olson and Apsel (1982) used a formal inversion technique to determine the distribution of slip on the fault as well as the time of rupture initiation. The Brawley fault was included in the model and the basis of comparison was accelerations filtered between 0.0 and 0.33 Hz. Olson

BEST COPY AVAILABLE

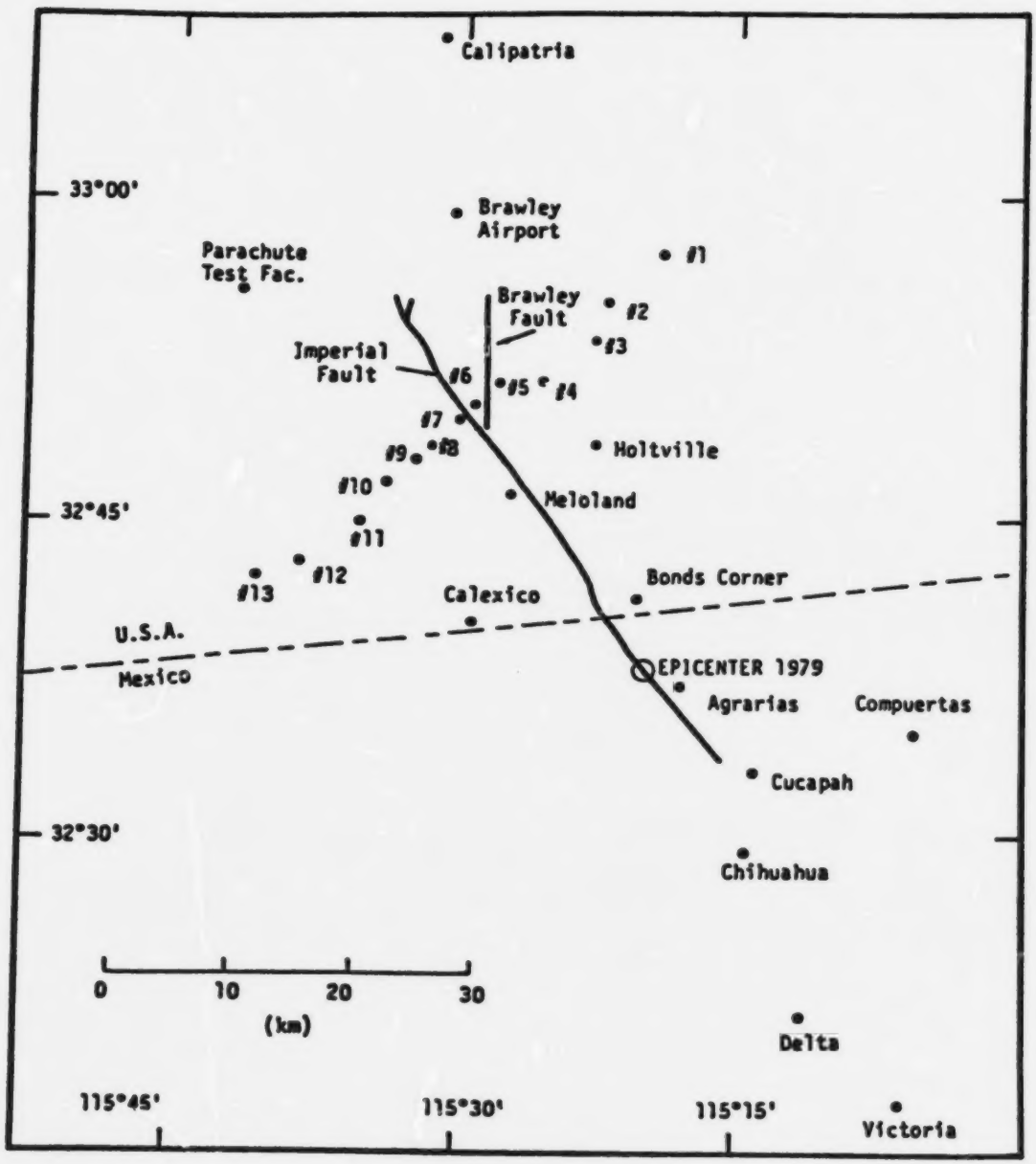

Fig. 5.2.1. Fault geometry and strong-motion instrument locations for the October 15, 1979 Imperial Valley earthquake.

BEST COPY AVAILABLE

TABLE 5.2.1

Characteristics of Models for the Imperial Valley 1979 Earthquake

	Hartzell and Helmberger (1982)	Olson and Apsel (1982)	Hartzell and Heaton (1983)	Archuleta (1984)
Length	36 (36 + 0) km	50 (40 + 10) km	42 (36 + 6) km	35 (35 + 0) km
Depth	10.5 km	10 km	10 km	13 km
Dip	90°	90°	90°	80° NE
Strike	323° (corrugated)	323°	323°	323°
Brawley fault	No	Yes	No	Yes
Type of slip	strike	strike & dip	strike & dip	strike & dip
Rise time	1 sec	0.75-3.0 sec	0.7-1.7 sec	0-1.9 sec
Rupture velocity	2.5 km/sec	variable (ave. 0.9β)	variable (ave. 0.85β)	variable
Max. slip	2.5 m	1.6 m	1.8 m	1.8 m
Epicentral dist. of zone of max. slip	8 and 18 km	15-20 km	16-20 km	20 km
Seismic moment (dyne−cm)	5.0×10^{25}	9.1×10^{25}	4.9×10^{25}	6.7×10^{25}
Frequency range	0.-1.0 Hz	0.-0.33 Hz	0.1-1.0 Hz	0.-1.0 Hz
Basis of comparison	Displacements	Accelerations	Velocities	Velocities
Type of inversion	Trial-and-error	Formal	Formal	Trial-and-error

BEST COPY AVAILABLE

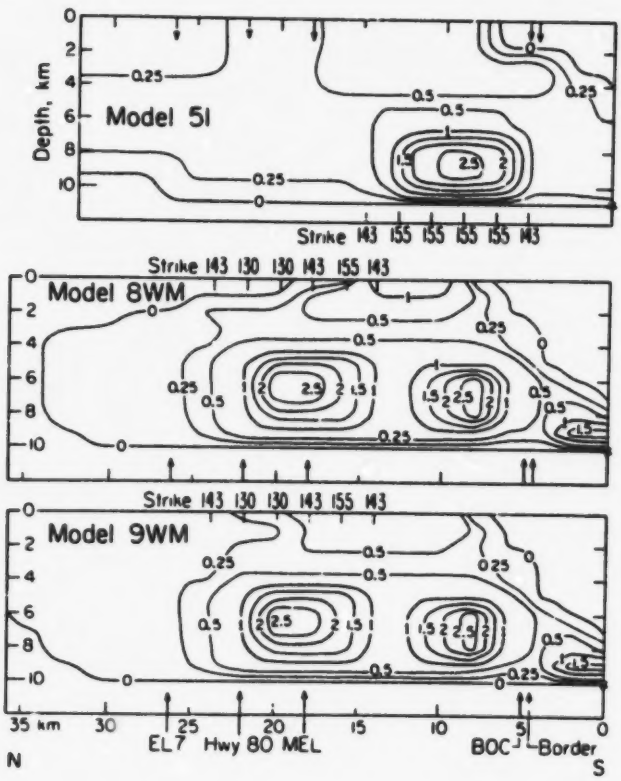

Fig. 5.2.2. Contoured dislocation in meters on the Imperial fault for the preferred fault model (Hartzell and Helmberger, 1982).

BEST COPY AVAILABLE

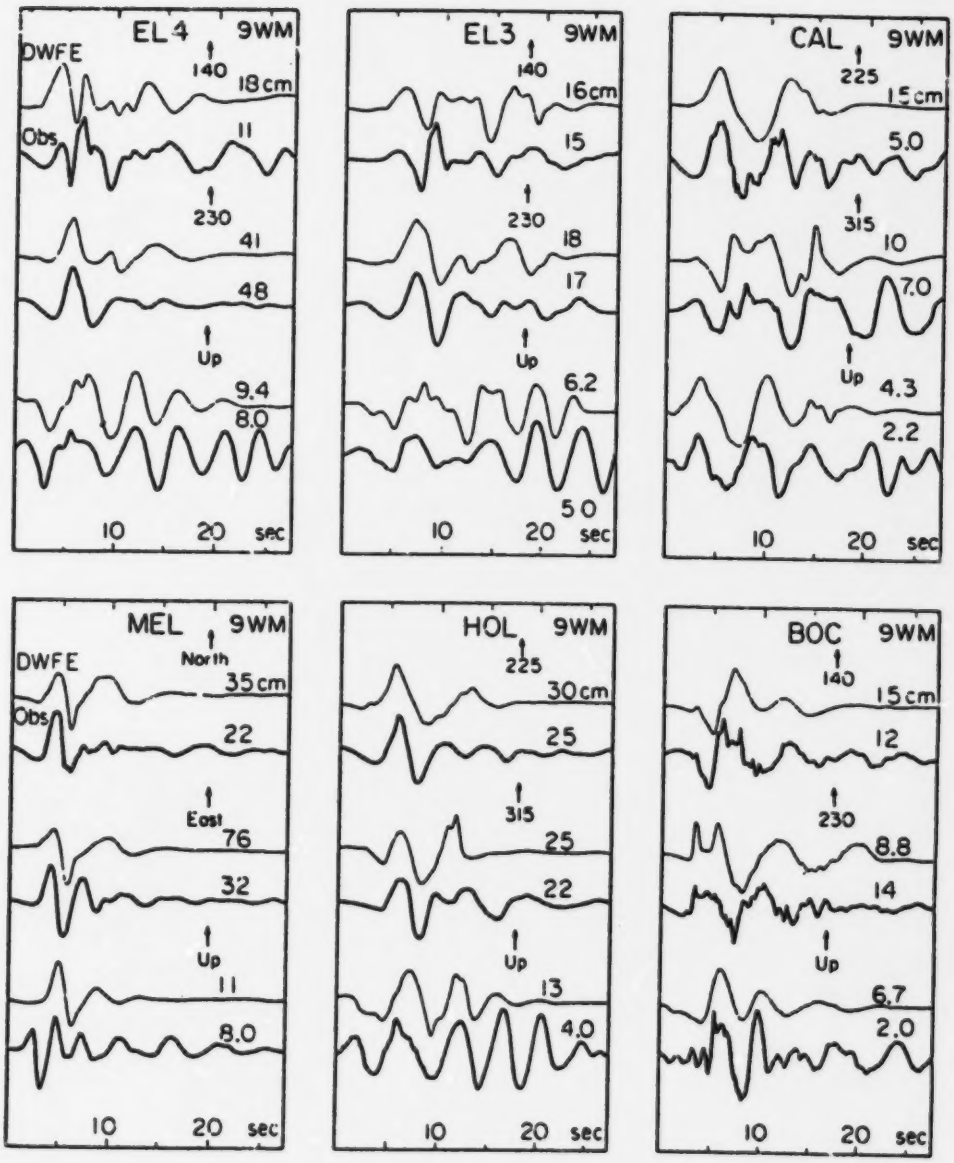

Fig. 5.2.3. Comparison of 'observed' and synthetic displacements for Stations 4, 3, Calexico, Meloland Overpass, Holtville and Bonds Corner. The synthetics are labelled DWFE (Hartzell and Helmberger, 1982).

BEST COPY AVAILABLE

and Hartzell (1982) found that the resulting slip was predominantly right-lateral and smoothly varying reaching a peak value of 1.65 m at a depth between 5 and 10 km and at a distance of 15 to 20 km north of the epicenter. The time behavior of slip could be explained by a rupture front propagating at an average velocity of 90 percent of the local shear wave speed; however, over a distance of 20 to 30 km on the Imperial Fault, the local horizontal rupture velocity approached the compressional wave speed. A comparison of 'observed' and calculated waveforms is shown in Fig. 5.2.4.

Hartzell and Eaton (1983) used a least-squares point-by-point inversion of strong ground motion and teleseismic body waves to infer the rupture history. The inversion yielded the spatial and temporal variation of the dislocation on the fault plane. The fault was divided into 56 subfaults arranged on four rows (at depth 0-2.5, 2.5-5.0, 5.0-7.5 and 7.5-10.5 km) of 14 subfaults (each of 3 km. length). Contours of the strike slip and dip slip components of the dislocation at times T_1, T_2 and T_3 for the preferred model are shown in Fig. 5.2.5. Times T_1, T_2 and T_3 correspond to 0.7, 1.2 and 1.7 sec after the passage of the rupture front which travels at 85 percent of the local shear wave velocity. The maximum horizontal slip of 1.8 m is reached at a depth of 6-8 km and at a distance of 16-20 km from the epicenter. The results suggest a variable rupture velocity, with the rupture front accelerating from about 0.8β near the hypocenter of 0.9β under Interstate 8.

Archuleta (1984) reviewed the comparisons of observed and calculated motions based on the models of Hartzell and Helmberger (1982), Olson and Apsel (1982) and Hartzell and Heaton (1983) and concluded that the synthetics misfit the largest near-source amplitudes by a factor of two or more and that the synthetic amplitudes show a much different dependence on distance from the fault than the data. By a trial-and-error procedure Archuleta constructed a rupture model involving distributions over the fault of the strike-slip rate, dip-slip rate, rupture arrival time and duration. Contours of the rupture parameters are shown in Fig. 5.2.6. The distribution of final offsets are shown in Fig. 5.2.7. A comparison of data and synthetics at stations 5, 6, 7 and 8 is shown in Fig. 5.2.8. The model obtained by Archuleta (1984) is characterized by a

BEST COPY AVAILABLE

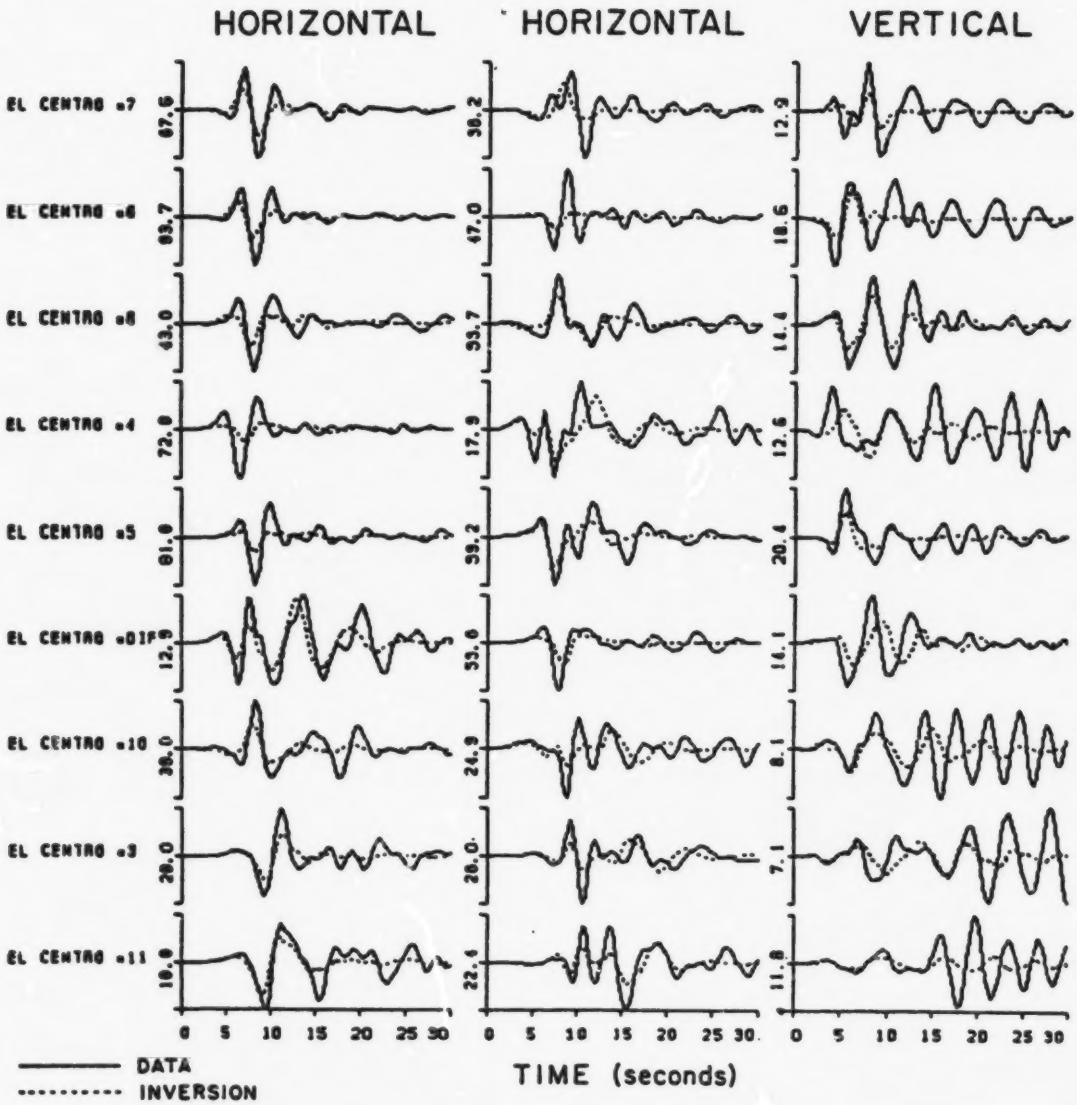

Fig. 5.2.4. Comparison of data (solid line) and synthetics (dashed line) at several stations. The information plotted corresponds to accelerations filtered to include frequencies in the range 0-0.33 Hz (Olson and Apsel, 1982).

BEST COPY AVAILABLE

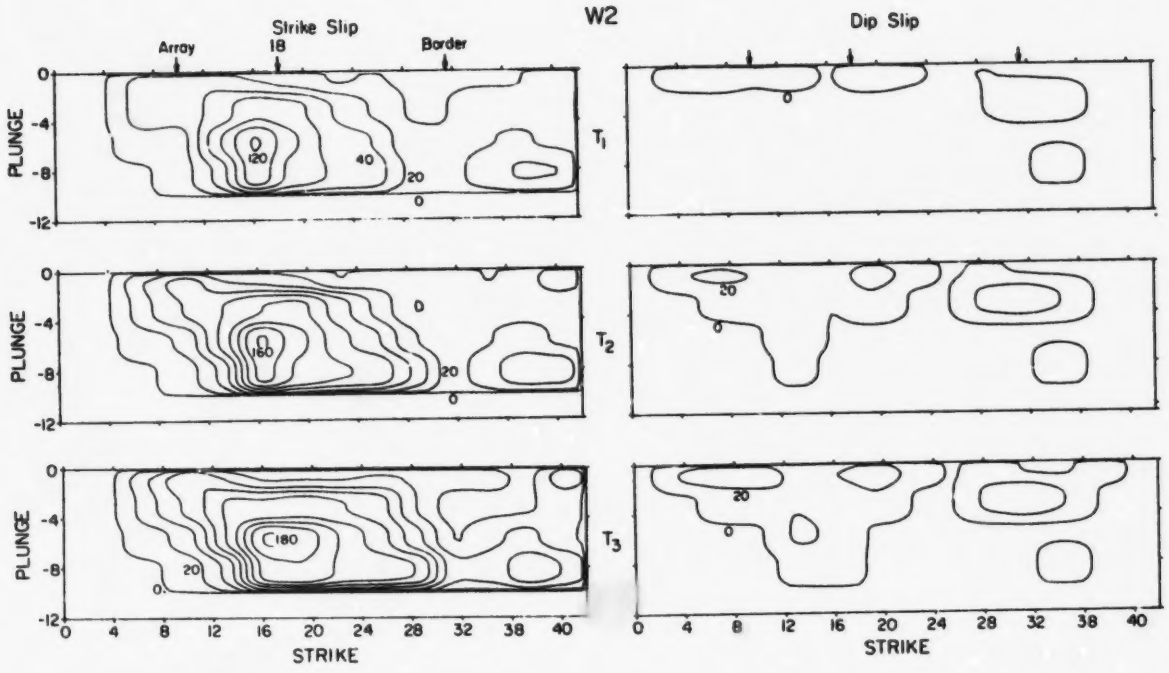

Fig. 5.2.5. Contours of dislocation in centimeters on the Imperial fault plane (Hartzell and Heaton, 1983).

BEST COPY AVAILABLE

very complex behavior of the rupture front. At a depth of 8 km, "the rupture starts slowly, accelerates to a supershear velocity, propagates at this supershear velocity for about 8 km, suddenly accelerates to a supercompressional velocity, suddenly decelerates to a subshear velocity, and again accelerates to a slightly higher velocity." On the average, however, the rupture velocity at depth is about 3.1 km/sec roughly 0.94 times the local shear wave velocity.

The faulting models for the Imperial Valley earthquake described above give an indication of the variability of the slip, rupture velocity and duration over the fault area. These studies also illustrate the advanced dislocation models currently available to synthesize near-source ground motion.

BEST COPY AVAILABLE

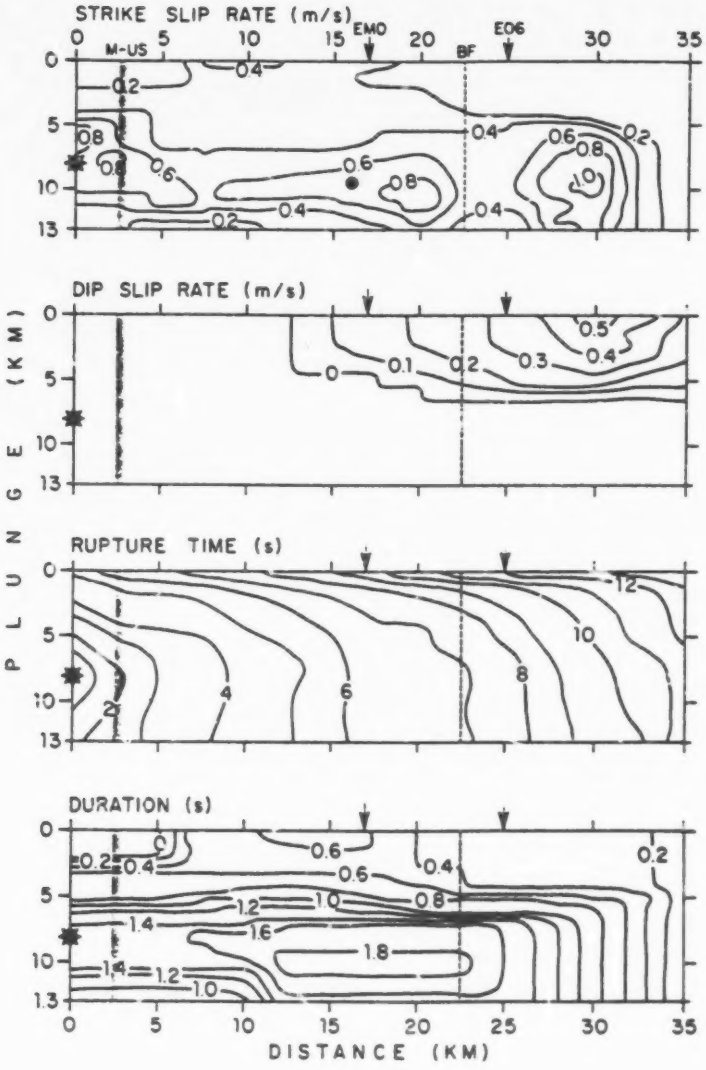

Fig. 5.2.6. Contours of slip rate parameters on the Imperial fault plane. The epicenter is on the left and the northwestern end of the fault is on the right (Archuleta, 1984).

BEST COPY AVAILABLE

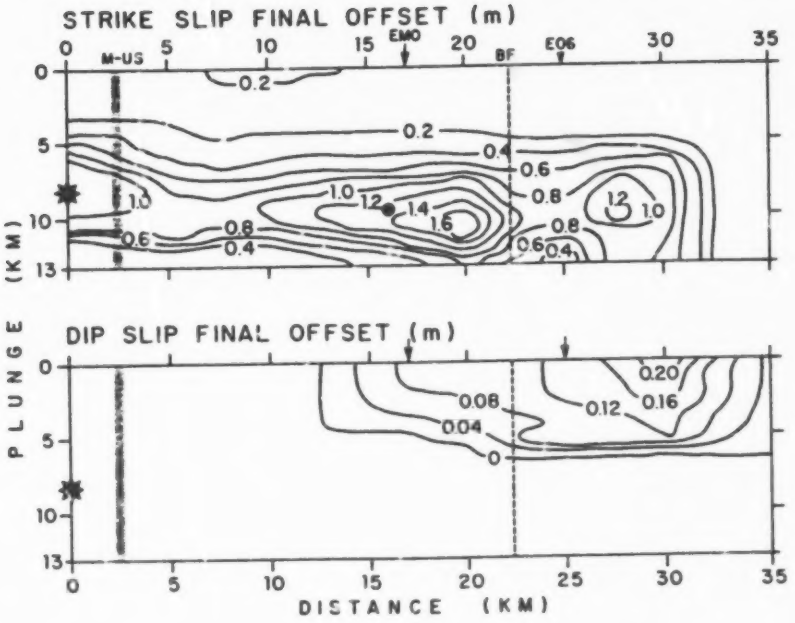

Fig. 5.2.7. Contours of final static offsets on the Imperial fault plane (Archuleta, 1984).

BEST COPY AVAILABLE

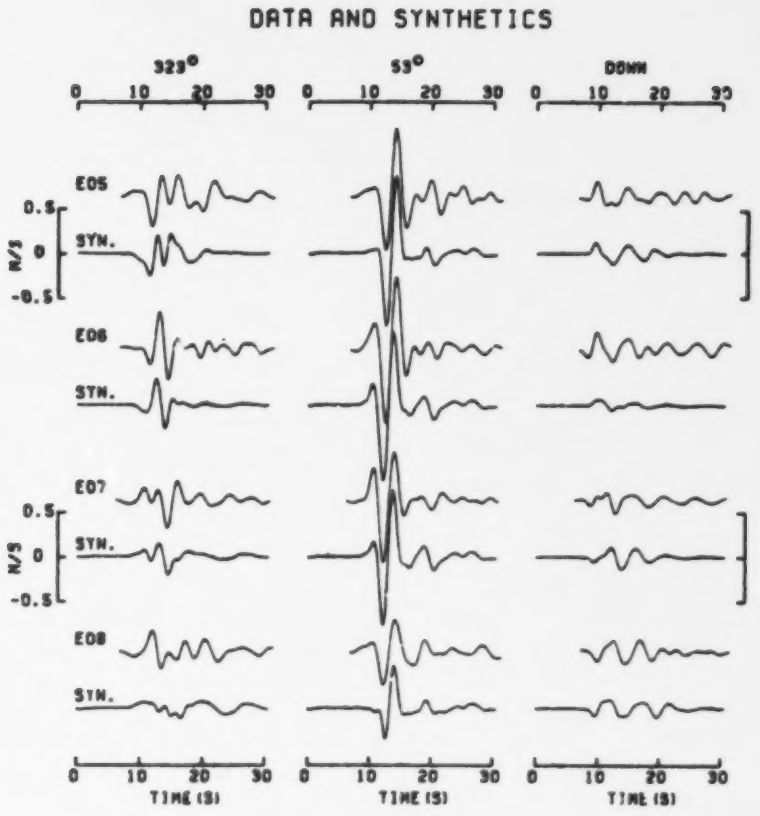

Fig. 5.2.8. Comparison of synthetic particle velocities and data at Stations 5, 6, 7 and 8 (Archuleta, 1984).

BEST COPY AVAILABLE

5.8 Conclusions.

Review of the simulation studies of near-source records obtained during the 1966 Parkfield and 1979 Imperial Valley earthquakes leads to the following conclusions:

1. The gross features of the near-source ground motion can be simulated by use of simple dislocation models involving fault slips, rupture velocities and rise times constant or slowly varying over the fault plane.

2. The simulation of details of the near-source ground motion requires the use of complex dislocation models involving spatially variable slips, rupture velocities and rise times.

3. To obtain an accurate relation between the amplitude of motion on the ground surface and the slip on the fault it is necessary to account for the layering in the vicinity of the fault.

4. Even in cases in which the rupture model is obtained by an inversion process applied to near-source data, the error of the synthetic near-source ground motion can be as high as a factor of two.

BEST COPY AVAILABLE

References

Parkfield 1966 Earthquake - Simulation Studies

Aki, K. (1968). Seismic displacements near a fault, *J. Geophys. Res. 73*, 5359-5376.

Haskell, N. A. (1969). Elastic displacements in the near field of a propagating fault, *Bull. Seism. Soc. Am. 59*, 865-908.

Boore. D. M., K. Aki and T. Todd (1971). A two-dimensional moving dislocation model for a strike slip fault, *Bull. Seism. Soc. Am. 61*, 177-194.

Tsai, Y. B. and H. J. Patton (1973). Near field small earthquakes-dislocation motion, Semi-Annual Report 1, Texas Instruments Inc. (prepared for Air Force Office of Scientific Research Contract F44620-72-C-0073).

Niazy, A. (1973). Elastic displacements caused by propagating crack in an infinite medium: an exact solution, *Bull. Seism. Soc. Am. 63*, 357-379.

Boore, D. M. and M. D. Zoback (1974). Near-field motions from kinematic models of propagating faults, *Bull. Seism. Soc. Am. 64*, 321-342.

Trifunac, M. D. and F. E. Udwadia (1974). Parkfield, California earthquake of June 27, 1966: a three-dimensional moving dislocation, *Bull. Seism. Soc. Am. 64*, 511-533.

Anderson, J. G. (1974). A dislocation model for the Parkfield earthquake, *Bull. Seism. Soc. Am. 64*, 671-686.

Kawasaki, I. (1975). On the dynamical process of the Parkfield earthquake of June 28, 1966, *J. Phys. Earth 23*, 127-144.

Levy, N. A. and A. K. Mal (1976). Calculation of ground motion in a three-dimensional model of the 1966 Parkfield earthquake, *Bull. Seism. Soc. Am. 66*, 405-423.

Hartzell, S. B., G. A. Frazier, and J. N. Brune (1978). Earthquake modeling in a homogeneous half-space, *Bull. Seism. Soc. Am. 68*, 301-316.

EST COPY AVAILABLE

_____ (1978). Simulation of earthquake ground motions for San Onofre Nuclear Generating Station Unit I, *Final Report, Del Mar Technical Associates/Tera Corporation*, May.

Bouchon, M. (1979). Predictability of ground displacement and velocity near an earthquake fault: an example: the Parkfield earthquake of 1966, *J. Geophys. Res. 84*, 6149-6156.

Archuleta, R. J. and S. M. Day (1980). Dynamic rupture in a layered medium: the 1966 Parkfield earthquake, *Bull. Seism. Soc. Am. 70*, 671-689.

Luco, J. E. and J. G. Anderson (1985). Near source earthquake groundmotion from kinematic fault models, in *Strong Ground Motion Simulation and Earthquake Engineering Applications*, R. E. Scholl and J. L. King (Eds.), Publication No. 85-02. EERI. 18-1/18-20.

Parkfield 1966 Earthquake - Basic Data and Other Studies

Allen, C. R. and S. W. Smith (1966). Parkfield earthquake of June 27-29, 1966, Pre-earthquake and post-earthquake surficial displacement, *Bull. Seism. Soc. Am. 56*, 955-967.

Algermissen, S. T. and S. T. Harding (1967). A note on the focal mechanism of the Parkfield, California earthquake of June 28, 1966, *Bull. Seism. Soc. Am. 57*, 1131-1141.

Cloud, W. K. and V. Perez (1967). Accelerograms - Parkfield earthquake, *Bull. Seism. Soc. Am. 57*, 1131-1141.

Filson, J. and T. V. McEvilly (1967). Love wave spectra and the mechanism of the 1966 Parkfield sequence, *Bull. Seism. Soc. Am. 57*, 1245-1257.

Housner, G. W. and M. D. Trifunac (967). Analysis of accelerograms - Parkfield earthquake, *Bull. Seism. Soc. Am. 57* 1193-1220.

Hudson, D. E. and W. K. Cloud (1967). An analysis of seismoscope data from the Parkfield earthquake of June 27, 1966, *Bull. Seism. Soc. Am. 57*, 1143-1159.

McEvilly, T. V., W. H. Bakum and K. B. Casaday (1967). The Parkfield, California earthquake of 1966, *Bull. Seism. Soc. Am. 57*, 1221-1244.

Murray, G. I. (1967). Note on strong motion records from the June 1966 Parkfield earthquake

BEST COPY AVAILABLE

sequences, *Bull. Seism. Soc. Am. 57*, 1259-1266.

Wu, F. T. (1968). Parkfield earthquake of June 28, 1966: magnitude and source mechanism, *Bull. Seism. Soc. Am. 58*, 689-709.

Smith, S. W. and M. Wyss (1968). Displacement on the San Andreas Fault subsequent to the 1966 Parkfield earthquake, *Bull. Seism. Soc. Am. 58*, 1955-1973.

Scholtz, C. H., M. Wyss and S. W. Smith (1969). Seismic and aseismic slip on the San Andreas fault, *J. Geophys. Res. 74*, 2049-2069.

Eaton. J. P., M. E. O'Neill and J. N. Murdock (1970). Aftershocks of the 1966 Parkfield-Cholame, California, earthquake: A detailed study, *Bull. Seism. Soc. Am. 60*, 1151-1197.

Trifunac, M. D. and D. E. Hudson (1970). Analysis of the Station No. 2 seismoscope record - 1966 Parkfield, California, earthquake, *Bull. Seism. Soc. Am. 60*, 785-794.

Murray, G. F. (1973). Dislocation mechanism - the Parkfield 1966 accelerograms, *Bull. Seism. Soc. Am. 63*, 1539-1555.

Bakum, W. H. and T. V. McEvilly (1979). Earthquakes near Parkfield, California, comparing the 1934 and 1966 sequences. *Science 205*, 1375-1377.

Aki, K. (1979). Characterization of barriers on an earthquake fault, *J. Geophys. Res. 84*, 6140-6148.

Borrego Mountain 1968 Earthquake

Heaton, T. H. and D. V. Helmberger (1977). A study of the strong ground motion of the Borrego Mountain, California, earthquake, *Bull. Seism.Soc. Am. 67*, 315-330.

Ebel, J. E. and D. V. Helmberger (1982). P-wave complexity and fault asperities: the Borrego Mountain, California, earthquake of 1968, *Bull. Seism. Soc. Am. 72*, 413-437.

San Fernando 1971 Earthquake

Mikumo, T. (1973). Faulting process of the San Fernando earthquake of February 9, 1979 inferred from static and dynamic near-field displacements, *Bull. Seism. Soc. Am. 63*, 249-

BEST COPY AVAILABLE

269.

Niazy, A. (1973). Elastic displacements caused by propagating crack in an infinite medium: an exact solution, *Bull. Seism. Soc. Am. 63*, 357-379.

Trifunac, M. D. (1974). A three-dimensional dislocation model for the San Fernando, California, earthquake of February 9, 1971, *Bull. Seism. Soc. Am. 64*, 149-172.

Boore, D. M. and M. D. Zoback (1974). Two-dimensional kinematic fault modeling of the Pacoima Dam strong-motion recordings of the February 9, 1971, San Fernando earthquake, *Bull. Seism. Soc. Am. 64*, 555-570.

Niazy, D. (1975). An exact solution for a finite, two-dimensional moving dislocation in an elastic half-space with application to the San Fernando earthquake of 1971, *Bull. Seism. Soc. Am. 65*, 1797-1826.

Bouchon, M. and K. Aki (1977). Discrete wave-number representation of seismic-source wave fields, *Buil. Seism. Soc. Am. 67*, 259-277.

Bouchon, M. (1978). A dynamic crack model for the San Fernando earthquake, *Bull. Seism. Soc. Am. 68*, 1555-1576.

Heaton, T. H. and D. V. Helmberger (1979). Generalized ray models of the San Fernando earthquake, *Bull. Seism. Soc. Am. 69.*, 1311-1341.

Heaton, T. H. (1982). The 1971 San Fernando earthquake: a double event? *Bull. Seism. Soc. Am. 72*, 2037-2062.

Imperial Valley 1979 Earthquake

McMechan, G. A. and W. D. Mooney (1980). Asymptotic ray theory and synthetic seismograms for laterally varying structures, theory and applications to the Imperial Valley earthquake, *Bull. Seism. Soc. Am. 70*, 2121-2135.

Archuleta, R. J. (1982). Analysis of near-source static and dynamic measurements from the 1979 Imperial Valley earthquake, *Bull. Seism. Soc. Am. 72*, 1927-1956.

Hartzell, S. H. and D. V. Helmberger (1982). Strong-motion modeling of the Imperial Valley

BEST COPY AVAILABLE

earthquake of 1979, *Bull. Seism. Soc. Am. 72*, 571-596.

Olson, A. H. (1982). Forward simulation and linear inversion of earthquake ground motions, *Ph.D. Thesis*, University of California, San Diego, La Jolla, CA.

Olson, A. H.and R. J. Apsel (1982). Finite faults and inverse theory with applications to the 1979 Imperial Valley earthquake, *Bull. Seism. Soc. Am. 72*, 1969-2001.

Hartzell, S. H. and T. H. Heaton (1983). Inversion of strong ground motion and teleseismic waveform data for the fault rupture history of the 1979 Imperial Valley, California, earthquake, *Bull. Seism. Soc. Am. 73*, 1553-1583.

Archuleta, R. J. (1984). A faulting model for the 1979 Imperial Valley earthquake, *J. Geophys. Res. 89*, 4559-4585.

Coyote Lake 1979 Earthquake

Bouchon, M. (1982). The rupture mechanism of the Coyote Lake earthquake of 6 August 1979 inferred from near-field data, *Bull. Seism. Soc. Am. 72*, 745-758.

Liu, H.-L. and D. V. Helmberger (1983). The near-source ground motion of the 6 August 1979 Coyote Lake, California, earthquake, *Bull. Seism. Soc. Am. 73*, 201-218.

1984 Morgan Hill Earthquake

Hartzell, S. H. and T. H. Heaton (1986). Rupture history of the 1984 Morgan Hill, California earthquake from inversion of strong motion records, *Bull. Seism. Soc. Am. 76*, 649-674.

Other General References

de Hoop, A. T. (1985). Representation theorems for the displacement in an elastic solid and their application to elastodynamic diffraction theory, Thesis, Techniche Hogeschool, Delft.

Maruyama, T. (1963). On force equivalents of dynamic elastic dislocations with reference to the earthquake mechanism, *Bull. Earthquake Res. Inst. Tokyo Univ. 41*, 467-486.

Ben-Menahem, A. (1961) Radiation of seismic surface waves from finite moving sources, *Bull.*

BEST COPY AVAILABLE

Seism. Soc. Am. 51, 401-435.

Haskell, N. A. (1964). Total energy and energy spectral density of elastic wave radiation from propagating faults, *Bull. Seism. Soc. Am. 54*, 1811-1841.

Johnson, L. R. (1974). Green's functions for Lamb's problem, *Geophys. J. Astr. Soc. 37*, 99-131.

BEST COPY AVAILABLE

6. CLOSURE

The solutions available for a number of dynamic dislocation fault models have been examined with the objective of describing some of the expected characteristics of the near-source earthquake ground motion at intermediate and low frequencies. Decompositions of the near source ground motion into starting, passage of rupture and stopping phases have been presented; and the characteristic pulse shapes, attenuation with distance and relative importance of these phases have been described. Two- and three-dimensional models have been employed to give a description of the geometrical patterns of the distribution of peak ground motion amplitudes in the vicinity of faults. The effects of modeling parameters such as rupture velocity, rise time and location of the fault with respect to the free surface on the synthetic ground motion have been described. The effects of layering and, in particular, the relation between the rupture velocity and the wave velocities on the softer layers and its effect on the amplitude of the calculated ground motion have been reviewed. Finally, a number of modelling studies for the Parkfield and Imperial Valley earthquakes have been used to illustrate the capabilities of dislocation models to synthesize near-source ground motion and to illustrate the complexity of the rupture models obtained by inversion of near-source data. Given this complexity, it is unlikely that simple dislocation models can be used to synthesize the high-frequency components of the near-source ground motion. For intermediate and low frequencies, however, simple dislocation models can be used to determine the gross features of motion in the vicinity of faults.

BEST COPY AVAILABLE

NRC FORM 335 (2-84) NRCM 1102, 3201, 3202

U.S. NUCLEAR REGULATORY COMMISSION

BIBLIOGRAPHIC DATA SHEET

SEE INSTRUCTIONS ON THE REVERSE

1 REPORT NUMBER (Assigned by TIDC, add Vol No., if any)

NUREG/CR-4903, Vol. 3

2. TITLE AND SUBTITLE

Selection of Earthquake Resistant Design Criteria for Nuclear Power Plants - Methodology and Technical Cases: Dislocation Models of Near-Source Earthquake Ground Motion - A Review

3 LEAVE BLANK

4. DATE REPORT COMPLETED

MONTH	YEAR
September	1986

5. AUTHOR(S)

J.E. Luco, University of California, San Diego

6. DATE REPORT ISSUED

MONTH	YEAR
May	1987

7. PERFORMING ORGANIZATION NAME AND MAILING ADDRESS (Include Zip Code)

Structural and Earthquake Engineering Consultants, Inc.
Arcadia, CA 91006

8 PROJECT/TASK/WORK UNIT NUMBER

9. FIN OR GRANT NUMBER

FIN B8298
NRC-04-83-022

10. SPONSORING ORGANIZATION NAME AND MAILING ADDRESS (Include Zip Code)

Division of Engineering
Office of Nuclear Regulatory Research
U.S. Nuclear Regulatory Commission
Washington, D.C. 20555

11a. TYPE OF REPORT

Technical

b. PERIOD COVERED (Inclusive dates)

1983 - 1986

12 SUPPLEMENTARY NOTES

13. ABSTRACT (200 words or less)

The solutions available for a number of theoretical fault models are examined in an attempt at establishing some of the expected characteristics of earthquake ground motion in the near-source region. In particular, solutions for two-dimensional anti-plane shear and plane-strain models as well as for three-dimensional fault models in full space, uniform half-space and layered half-space media are reviewed.

14 DOCUMENT ANALYSIS - a KEYWORDS/DESCRIPTORS

Earthquake Engineering
Strong Motion Seismology
Earthquake Ground Motion

b IDENTIFIERS/OPEN-ENDED TERMS

15 AVAILABILITY STATEMENT

Unlimited

16 SECURITY CLASSIFICATION

(This page)
Unclassified
(This report)
Unclassified

17 NUMBER OF PAGES

18 PRICE

*U.S. GOVERNMENT PRINTING OFFICE:1987-181-682:60113

BEST COPY AVAILABLE